

**TECHNISCHE  
UNIVERSITÄT  
WIEN**  
Vienna University of Technology

## DIPLOMARBEIT

# NANODIAMOND PARTICLES FOR DIAMOND MAGNETOMETRY IN BIOLOGICAL SYSTEMS

Ausgeführt am

Institut für Chemische Technologien und Analytik  
der Technischen Universität Wien

unter der Anleitung von

Ao.Univ.Prof. Dipl.-Ing. Dr.techn. Bernhard Lendl  
Assistant Prof. Dr. rer. nat. Romana Schirhagl

durch

Andreas Nagl, BSc

Resselstraße 1/25  
4400 Steyr

## Abstract

Diamond is a highly investigated material in materials science for its remarkable properties (e.g. its hardness or its unsurpassed thermal conductivity). Recently, fluorescent defects in diamond, particularly the negatively charged nitrogen-vacancy center (NV<sup>-</sup>-center), have gained much attention: Fluorescent nanodiamonds (FNDs) have been identified as a promising photostable, non-bleaching fluorescence label. The most remarkable property of the NV<sup>-</sup>-center, however, is the possibility to read out its spin properties by fluorescence. Therefore, these nanodiamonds (NDs) can be utilized as a sensor for magnetic fields as small as the field of a single electron spin.

The group aims to use NDs to detect magnetic resonance from reactive oxygen species (ROS) in biological cells with nanometer resolution. In this thesis, ND particles and their interactions with biological environments and ND modification (e.g. conjugation with biomolecules) for diamond magnetometry in mind are covered. NDs were characterized by dynamic light scattering (DLS), transmission electron microscopy (TEM) and x-ray photoelectron spectroscopy (XPS) as well as x-ray powder diffraction (XRD).

Aggregation of NDs in cellular medium was investigated for the first time: Interaction between medium (containing fetal bovine serum (FBS) as protein source) and NDs was studied. Surprisingly, nearly only sodium chloride was identified to be the inorganic compound responsible for the aggregation in DMEM medium. Analysis of the proteins involved in this process revealed a certain selectivity of NDs for other than the most abundant proteins in the serum. No correlation between protein adsorption and the (theoretical) isoelectric point or the molecular mass of the proteins could be established. However, several proteins known to bind to negatively charged compounds, also bind to NDs.

In order to influence the fate of NDs in cells and direct them to a biologically relevant target, conjugation with antibodies by physisorption was achieved. Experiments revealed that the adsorption of the antibody is stable in cellular media. Future experiments will thoroughly test if the biological function of the antibodies is sufficiently preserved.

A proof-of-concept showed that fast screening of the ND uptake by biological cells is principally possible for a concentration of approximately 1 ng/mL which corresponds to roughly 0.2 ND particles per cell (for NDs of 70 nm of size with approximately 300 NV<sup>-</sup>-centers per particle). After implementation of this method, a fast screening of NDs with various antibodies and other proteins is possible, thus allowing fast selection of ideal ND uptake conditions (and targeting of biologically relevant areas in cells such as mitochondria or the nucleus).

## Kurzzusammenfassung

Wegen seiner außergewöhnlichen Eigenschaften (wie z.B. die Härte oder seine unerreichte thermische Leitfähigkeit) ist Diamant ein vielbeachtetes Material in den Materialwissenschaften. In letzter Zeit erlangten fluoreszierende Defekte in Diamant, speziell das Stickstoff-Fehlstellen-Zentrum (NV-center), viel Aufmerksamkeit: Fluoreszierende Nanodiamanten (FNDs) wurden als vielversprechende photostabile und nicht bleichende Labels identifiziert. Das herausragendste Merkmal des NV-Centers, jedoch, ist die Möglichkeit seinen Spin-Zustand mittels Fluoreszenz auszulesen. Daher können diese Nanodiamanten (NDs) als Sensor für sehr kleine magnetische Fehler, bis hin zu einem einzelnen Elektronenspin, verwendet werden.

Die Gruppe hat das als Ziel, Nanodiamanten zur Detektion von magnetischen Resonanzen von reaktiven Sauerstoffspezies (ROS) in biologischen Zellen mit Nanometer-Auflösung zu messen. In dieser Arbeit wurden Nanodiamant-Partikel und deren Interaktion mit biologischen System sowie Nanodiamant-Modifikation (z.B. Konjugation mit Biomolekülen) für Magnetometrie im Sinn, untersucht. Nanodiamanten wurden mit dynamischer Lichtstreuung (DLS), Transmissionselektronenmikroskopie (TEM), Röntgenphotoelektronenspektroskopie (XPS) und Röntgenpulverdiffraktion (XRD) charakterisiert.

Aggregation von Nanodiamanten in Zellmedium wurde das erste Mal untersucht: Die Wechselwirkungen zwischen Medium (mit fetalem Kälberserum (FBS)) und Nanodiamanten wurden analysiert. Überraschenderweise war Natriumchlorid die anorganische Komponente, welche fast ausschließlich für die Aggregation in DMEM Medium verantwortlich war. Die Analyse der Proteine in diesem Prozess zeigte eine gewisse Selektivität für Proteine im Serum, welche nicht denen mit der höchsten Konzentration zuzuordnen sind. Während keine Korrelation zwischen dem (theoretischen) isoelektrischen Punkt oder der molekularen Masse und der Proteinadsorption an den Nanopartikeln hergestellt werden konnte, sind für einige der identifizierten Proteine Affinitäten zu negativ geladenen Komponenten bekannt.

Um das Schicksal der Nanodiamanten in Zellen zu beeinflussen, und sie zu biologisch relevanten Zielen zu dirigieren, wurden Antikörper mittels Physisorption an den Nanodiamanten gebunden. Die Experimente zeigten, dass die Adsorption der Antikörper in Zellmedium stabil ist. Zukünftige Experimente werden zeigen, ob die biologische Funktion der Antikörper in ausreichendem Maße erhalten bleibt.

Es wurde gezeigt, dass ein schnelles Screening der Nanodiamant-Aufnahme in biologische Zellen prinzipiell bis zu einer Konzentration von 1 ng/mL möglich ist, was in etwa 0,2 Nanodiamant-Partikel pro Zelle entspricht (für Nanodiamanten mit 70 nm Größe und ca. 300 NV-Center pro Partikel). Nach

der Implementierung dieser Methode ist ein schnelles Screening der Nanodiamanten mit verschiedenen Antikörpern und anderen Proteinen möglich, was eine schnelle Selektion der Bedingungen für ideale Nanodiamant-Aufnahme (und Targeting von biologisch relevanten Bereichen in Zellen wie z.B. Mitochondrien oder den Zellkern) erlaubt.

## Inhalt

|       |  |    |
|-------|--|----|
| 1.    | Introduction.....  | 7  |
| 1.1   | Motivation.....  | 7  |
| 1.2   | Diamond Magnetometry.....  | 8  |
| 1.3   | Nanodiamond Aggregation: Protein Corona.....                                   | 11 |
| 1.4   | Project Goal.....  | 12 |
| 2.    | Experimental Section.....  | 13 |
| 2.1   | Nanodiamond Characterization.....  | 13 |
| 2.1.1 | Chemicals and Materials.....   | 13 |
| 2.1.2 | Transmission Electron Microscopy (TEM) and X-ray Powder Diffraction (XRD)..... | 14 |
| 2.1.3 | Dynamic Light Scattering (DLS) Measurements.....                               | 15 |
| 2.1.4 | X-ray photoelectron spectroscopy (XPS).....                                    | 16 |
| 2.2   | Nanodiamond Aggregation.....   | 16 |
| 2.2.1 | Chemicals and Materials.....   | 16 |
| 2.2.2 | Dynamic Light Scattering (DLS) Measurements.....                               | 17 |
| 2.2.3 | X-ray photoelectron spectroscopy (XPS).....                                    | 18 |
| 2.2.4 | Transmission Electron Microscopy (TEM) Measurements.....                       | 18 |
| 2.2.5 | Analysis of the Protein Corona (MALDI-TOF-MS and nanoLC-MS/MS).....            | 18 |
| 2.3   | Nanodiamond Modification.....  | 20 |
| 2.4   | Quantification of ND Uptake in Cells.....                                      | 22 |
| 3.    | Results and Discussion.....  | 23 |
| 3.1   | Nanodiamond Characterization.....  | 23 |
| 3.1.1 | Dynamic Light Scattering (DLS) Measurements.....                               | 23 |
| 3.1.2 | Shape Considerations.....  | 26 |
| 3.1.3 | X-ray photoelectron spectroscopy (XPS).....                                    | 29 |
| 3.1.4 | Conclusion.....  | 31 |
| 3.2   | Nanodiamond Aggregation.....   | 32 |
| 3.2.1 | Dynamic Light Scattering (DLS) Measurements.....                               | 32 |

## Introduction

|   |     |
|---|-----|
| 3.2.2 X-ray photoelectron spectroscopy (XPS).....                         | 35  |
| 3.2.3 Transmission Electron Microscopy (TEM) Measurements.....            | 40  |
| 3.2.4 Analysis of the Protein Corona (MALDI-TOF-MS and nanoLC-MS/MS)..... | 42  |
| 3.2.5 Conclusion .....  | 48  |
| 3.3 Nanodiamond Modification .....  | 48  |
| 3.4 Quantification of ND Uptake in Cells.....                             | 52  |
| 4. Conclusion and Outlook .....   | 57  |
| 5. References.....  | 60  |
| 6. Annex.....   | 63  |
| 5.1 Medium Compositions .....   | 63  |
| 5.2 X-ray Powder Diffraction (XRD).....                                   | 66  |
| 5.3 X-ray photoelectron spectroscopy (XPS).....                           | 72  |
| 5.3 Proteins Identified by nLC-MS/MS .....                                | 87  |
| 5.4 ND Modification .....   | 104 |
| 6. List of Figures.....   | 105 |
| 7. List of Tables.....  | 108 |
| 8. Acknowledgements .....   | 110 |

# 1. Introduction

## 1.1 Motivation

Reactive oxygen species (ROS) are a class chemical compounds of utmost significance in biochemistry<sup>[1]</sup>. They include superoxide, hydrogen peroxide, singlet oxygen, ozone, hypohalous acids and organic peroxides<sup>[1]</sup>. Striking findings in ROS research include the production of H<sub>2</sub>O<sub>2</sub> by human tumor cell lines (leading to hypothesizes on the role of ROS in oncogenesis and cancer progression) or antibiotics killing bacteria partly because of inducing ROS in bacteria<sup>[1]</sup>.

Smoke, air pollutants, ultraviolet radiation,  $\gamma$ -irradiation and several drugs have long been known as exogenous ROS sources that can lead to oxidative stress, potentially leading to cell death or malignant transformation<sup>[1]</sup>. However in recent years only have scientists began to gain a more complete picture of the role of ROS in biology. Endogenous sources of ROS, regulation of ROS production, its catabolism as well as its role within the immune system, inflammation and cell signaling have been investigated<sup>[1]</sup>. Rather specific targets of ROS have been identified: "Atomic" targets (ROS react with sulphur, especially in the side chains of cysteine or methionine residues in peptides or proteins) and molecular targets such as proteins and DNA<sup>[1]</sup>.

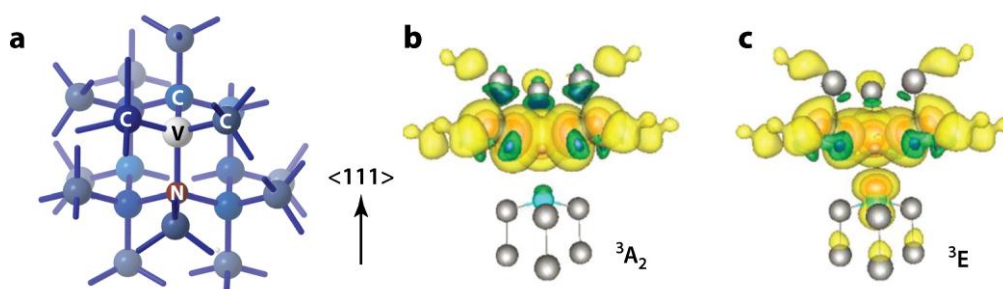
Further advances in ROS biology and its integration in systems biology critically depend on tools that "identify ROS and their subcellular localization and to quantify them at the level of single cells and single molecular species in real time"<sup>[1]</sup>. At this point, ROS remain difficult to distinguish from each other by specific assays and are challenging to quantify (current methods include fluorescent probes, nanotubes, peroxalate micelles and genetically encoded redox-sensitive fluorescent proteins)<sup>[1]</sup>. The need for real time information as well as determining the extent of oxidation of specific targets (especially on the single molecule level) complicate this challenge<sup>[1]</sup>.

Chemically, many of the ROS (e.g. hydroxyl radical OH<sup>\*</sup>, superoxide O<sup>2\*</sup> <sup>-</sup>) as well as nitric oxide (NO<sup>\*</sup>) and NO<sub>2</sub><sup>\*</sup>, both of which are belonging to the group of reactive nitrogen species (RNS), are radicals and therefore have a permanent magnetic moment (paramagnetism). Thus, they are a target of interest for optically detected magnetic resonance (ODMR) measurements, a method for electron spin resonance (ESR) or nuclear magnetic resonance (NMR), taking advantage of the nitrogen-vacancy (NV) centers in diamond (so called diamond magnetometry). This project focuses on the characterization and modification of NDs designated for (later) the real-time measurement of ROS in biomedical applications using diamond magnetometry, a novel method first proposed<sup>[2,3]</sup> and first realized in 2008<sup>[4]</sup> aiming at producing a spectrum of selected ROS present in a cell simultaneously. This is indeed

the aim of the research group: Applying diamond magnetometry, a new technique which emerged recently from the quantum information field, to biological samples.

## 1.2 Diamond Magnetometry

Diamond magnetometry is a novel method taking advantage of the spin properties of a fluorescent crystal defect, the so-called NV-centers, to detect external spins (magnetic fields, reactive oxygen species in this case)<sup>[5,6]</sup>. The NV-center emits stable, non-bleaching fluorescence. Its electronic structure (see Figure 1) involves six electrons, two of them provided by the nitrogen atom, another three from dangling bonds from the surrounding carbons and the sixth electron from the lattice (typically, nitrogen donors)<sup>[5]</sup>. The resulting negative charge is crucial for magnetometry as neither the neutral  $NV^0$ , nor the positively charged  $NV^+$  are magneto-optically active (indeed, preventing the conversion to the neutral  $NV^0$  is a major challenge in the use of very shallow, typically  $<10$  nm, NV centers)<sup>[5]</sup>. As depicted in Figure 1, the electron density is mostly located in a plane vertical to the main NV axis, with the highest density on the three carbon atoms and the vacant site<sup>[5]</sup>.




 Schirhagl R, et al. 2014.  
Annu. Rev. Phys. Chem. 65:83–105

Figure 1 (a) Lattice structure of the NV center. (b, c) Three-dimensional electron density of the  $^3A_2$  electronic ground state and the  $^3E$  excited state. Reprinted with permission from<sup>[5]</sup>.

The NV-center's main axis is along the (111) crystal axis<sup>[5]</sup>, which is relevant for the shape considerations of nanodiamonds (NDs) in the section 3.1.2 of this work. Indeed, while diamond magnetometry can be performed using both bulk diamond and nanodiamonds, this work focuses on NDs (sometimes referred to as fluorescent nanodiamonds, FNDs) that can be taken up by biological cells and thus give a signal from inside the cell.

Figure 2 explains the basic principle of diamond magnetometry: Two triplet states split into three spin sublevels ( $m_s = \pm 1$  states are degenerate, and the  $m_s = 0$  state is energetically lower)<sup>[5]</sup>. The energy difference between the spin sublevels is  $D = 2.87$  GHz for the ground state and  $D = 1.42$  GHz for the excited state and called zero-field splitting<sup>[5]</sup>. "The transition rate between  $m_s=0$  and  $m_s = \pm 1$  sublevels



is given by the spin-lattice relaxation time  $T_1$  (longitudinal relaxation time) and is a few milliseconds at room temperature”<sup>[5]</sup>. Using a magnetic field, the degeneracy can be lifted, which cause the  $m_s = \pm 1$  levels to shift in opposite directions (this is the basis for all magnetometry applications)<sup>[5]</sup>.

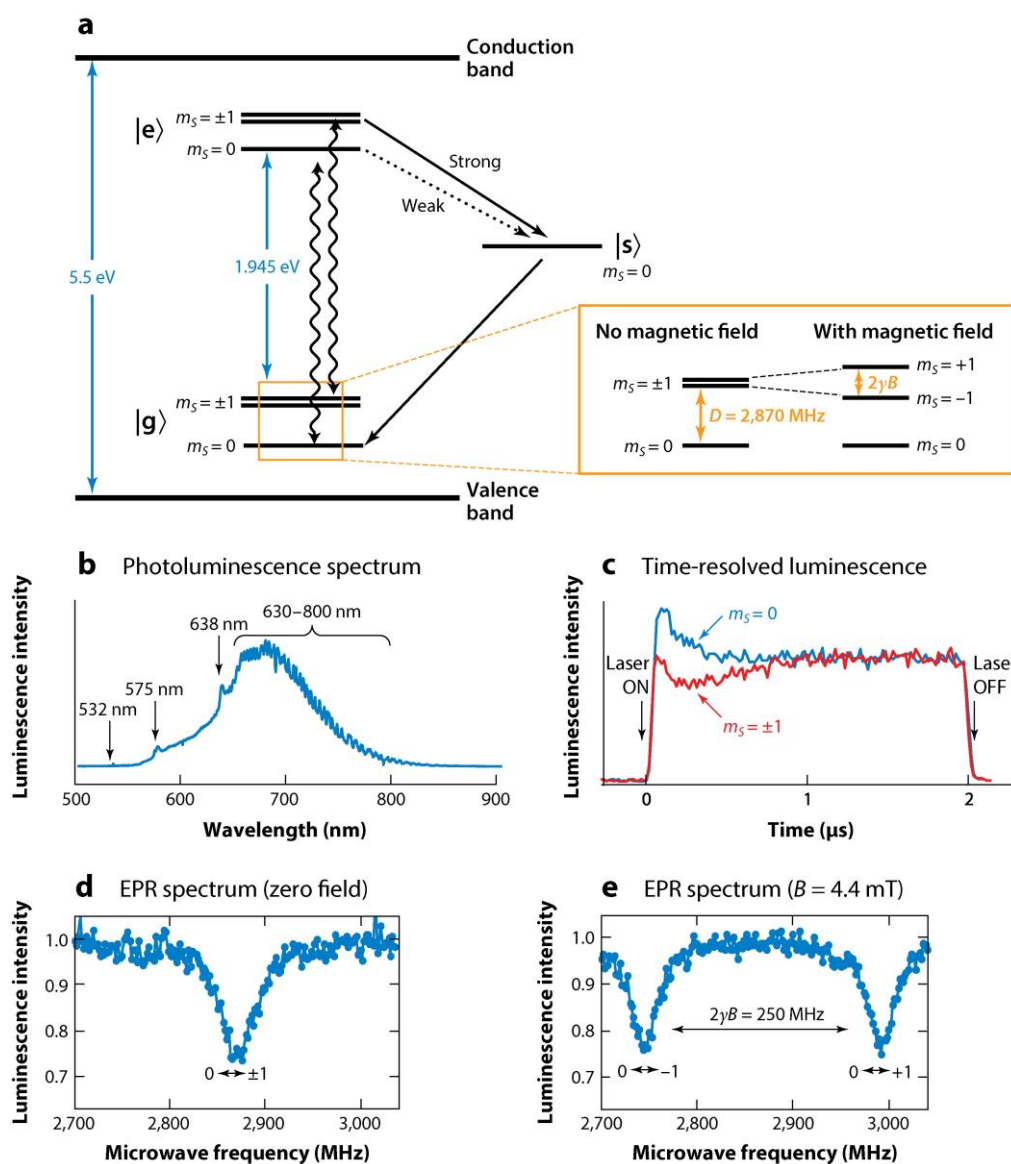
As the optical transitions are strongly spin preserving, and because of different crossover rates between the  $|e, m_s = \pm 1\rangle$  (“dark state”) state and the  $|e, m_s = 0\rangle$  state to the long-lived singlet state  $|s\rangle$  there is an optical contrast between the  $m_s = 0$  and  $m_s = \pm 1$  states of approximately 30% (which disappears due to the repumping of the electron to  $m_s = 0$  via the  $|s\rangle$  singlet state after some time) <sup>[5]</sup>. Therefore, the spin state can be read out using fluorescence spectroscopy, which is the basis for the so-called “optically detected magnetic resonance” (ODMR). “ODMR experiments can be carried out under both continuous illumination and microwave excitation, or in pump-probe experiments”<sup>[5]</sup>.

While this work itself is not about ESR measurements, the two planned ways of measurements in the research group play an important role as they have grave implications (covered in detail in section 1.4) on the demands in regards to the NDs, especially their surface chemistry and their biofunctionalization (which is why, of course, the magnetometry application has to be kept in mind): More detailed information about this can be found in the review of Nagl et al<sup>[10]</sup>.

Firstly, the longitudinal relaxation time  $T_1$  can be directly linked to the spin bath (the ROS as analytes of interest as well as noise such as surrounding  $^{13}\text{C}$  in the diamond lattice) surrounding the NV<sup>-</sup>-center as the spin flip rate of the electron spin in the NV<sup>-</sup>-center is proportional to the fluctuating magnetic field of the external spins (the  $T_1$  is therefore decreasing in the presence of spins)<sup>[7-9]</sup>. This methods has the advantage of not needing microwaves.

The second possibility is double electron-electron resonance (DEER)<sup>[11,12]</sup>, an adaption of the well-known Hahn echo<sup>[13]</sup> with NV<sup>-</sup>-centers: Here, a microwave pulse (in the MHz range) is used to excite the external spins at their Larmor frequency (therefore, the choice of the frequency determines the spins observed). A microwave pulse (in the GHz range) is also applied to the NV<sup>-</sup>-center. Thus, the resonance of the external spin is synchronized with the resonance of the NV<sup>-</sup>-center. By sweeping through the microwave frequencies (for the external spins) of interest, a spectrum of the external spins (e.g. ROS) can be obtained.

Both methods are extremely depending on the surface chemistry of the ND as well as the spin bath around the NDs.



**AR** Schirhagl R, et al. 2014.  
Annu. Rev. Phys. Chem. 65:83–105

Figure 2 (a) Simplified energy diagram of the  $\text{NV}^-$ -center: After excitation with a green laser (532 nm in the equipment of the group) fluorescence in the red spectral region is emitted<sup>[5]</sup>.  $|g\rangle$  marks the electronic ground state,  $|e\rangle$  the electronic excited state, and  $|s\rangle$  the metastable singlet state. Wiggly arrows indicate the radiative transition, and black arrows indicate strong and weak nonradiative decay via the singlet state<sup>[5]</sup>. As the process is strongly spin-preserving and there are differing cross-over rates depending on the spin state (The three spin sublevels are shown in the yellow box:  $m_s = 0$  and  $m_s = \pm 1$  at zero and nonzero magnetic field  $B$ .  $D$  is the zero-field splitting and  $2\gamma B$  is the Zeeman splitting, where  $\gamma$  is the electron gyromagnetic ratio.), an optical contrast between  $m_s = 0$  and  $m_s = \pm 1$  states of approximately 30% is achieved: The spin state can be read out by fluorescence (basis of the “Optically Detected Magnetic Resonance”, ODMR)<sup>[5]</sup>. (b) The photoluminescence spectrum (used for the quantification of diamond in this work) with the  $\text{NV}^0$  zero phonon line (575 nm), the  $\text{NV}^-$  zero phonon line (638 nm), and  $\text{NV}^-$  vibrational side bands (630–800 nm). (c) The optical contrast between the spin states is for 2- $\mu\text{s}$  laser pulse that disappears after some time (due to the repumping of the electron to  $m_s = 0$  via the  $|s\rangle$  singlet state).<sup>[5]</sup> (d,e) Electron paramagnetic resonance (EPR) spectrum of a single  $\text{NV}^-$  center at zero and nonzero magnetic field (measured using ODMR). Reprinted with permission from<sup>[5]</sup>

### 1.3 Nanodiamond Aggregation: Protein Corona

With nanobiotechnology as emerging interdisciplinary field, the interaction of nanoparticles with the biological environment gets into focus. The so-called “protein corona”, a new interface, is formed by medium components, proteins in particular, as they compete for binding to the nanoparticle’s surface<sup>[14,15]</sup>. It determines the nanoparticle’s physicochemical properties, including hydrodynamic size, surface charge, and aggregation behavior<sup>[16]</sup>. The latter is of special interest as previous experiments of our research group revealed the formation of nearly micron sized aggregates of nanodiamonds in cell culture medium, which are unfavorable due to the fact that endocytosis of nanoparticles is size dependent<sup>[17]</sup>.

Furthermore, the interaction with cell membranes and the mechanism of cellular uptake is controlled by the proteins adsorbed to nanoparticles<sup>[15,16]</sup>. Also the cytotoxicity is influenced by the protein corona<sup>[16]</sup>. Formation of the protein corona is a complex and time-depending process driven by various parameters such as protein concentration, pH, ionic strength, and the presence of other biomolecules such as enzymes<sup>[14,18]</sup>. The average composition of the protein corona does not necessarily reflect the relative abundance of proteins in the medium<sup>[14]</sup>. Consequently, the most abundant proteins do not necessarily have the most profound effect as a less abundant protein with higher affinity and specificity for a particular receptor may be extremely important<sup>[14]</sup>.

Existing studies have been distinguishing between the so-called “hard” corona (the fraction of proteins which are bound to the surface) and the “soft” corona (the proteins which are in exchange with surrounding proteins from the biological environment)<sup>[15,19]</sup>. Protein corona formation is a dynamic process involving a continuous adsorption/desorption equilibrium of proteins<sup>[20]</sup>. Proteins on the surface may be displaced by proteins with a lower concentration, lower exchange rate, but higher affinity, resulting in the formation of the hard corona<sup>[14,20]</sup>. Therefore, the protein corona can be categorized as “hard” corona composed of proteins with high affinity or “soft” corona composed of proteins with low affinity<sup>[20]</sup>.

Conformational changes of the proteins adsorbed may occur during adsorption on the nanoparticle<sup>[20,21]</sup> and, even exposition of unknown epitopes and subsequently activation of undesired signaling pathways may happen<sup>[20]</sup>.

Cellular uptake can be energy dependent (intake) and energy independent (insertion, also known as endocytosis)<sup>[20]</sup>. Endocytosis likely involves two steps: absorption to the cell surface and internalization into cells, a slow-rate step and a rapid-rate step<sup>[20]</sup>. This results in a different cellular uptake for nanoparticles with a protein corona and for bare nanoparticles. Even different uptake mechanisms could be observed for serum free medium and serum containing medium<sup>[20]</sup>. To further complicate this

complex process, for the same nanoparticles, different uptake pathways are present in different cell types<sup>[20]</sup>. For NDs, this has not been investigated so far.

Importantly, the protein corona plays an important role once the nanodiamonds are taken up by cells: Bare nanodiamonds are able to damage lysosomal membranes (possibly inducing cell death)<sup>[20]</sup>. The protein corona can undergo a dynamic change and the corona partially displaces intracellular biomolecules, affecting intracellular organelles<sup>[20]</sup>. The detailed fate of the original corona, as it passes through membranes and barriers and interacts with the extracellular matrix, remains unknown<sup>[15]</sup>. As scarce the current knowledge is, findings on other (than ND) nanoparticles suggest that at least parts of the original corona may be carried into the cell<sup>[15]</sup>.

Proteins show a high affinity for (oxygen-terminated) nanodiamonds based on the electrostatic interaction between the surface-terminating anionic groups (-COO-) and the positively charged amino groups (-NH<sub>3</sub><sup>+</sup>) of the biomolecules<sup>[22]</sup>. Unlike detonation nanodiamonds that are well-known to aggregate<sup>[23,24]</sup>, FNDs produced by HPHT (high-pressure, high-temperature) are stable as suspensions and commercially available.

So far, the protein corona of nanodiamonds has not been investigated and therefore the behavior of FNDs in biological environment is poorly understood. Aggregation of FNDs under physiological salt concentrations has been observed<sup>[25]</sup>, however the complex coaction of salts and serum proteins as present in cell culture medium is not yet studied. In human serum about 3700 different proteins with concentrations up to 70 mg ml<sup>-1</sup>, in which the most abundant proteins represent 97% of the total protein content<sup>[21]</sup> (which limits the dynamic range of measurements and therefore makes depletion of the most abundant proteins, e.g. using a molecular weight cutoff centrifugal filters, necessary<sup>[26]</sup>). Thus, identification of the proteins in FBS (fetal bovine serum) as used in the cell culture medium is a challenging task involving proteomic techniques.

### 1.4 Project Goal

The goal of this project was to find the optimal NDs to perform diamond magnetometry within (living) cells. Requirements regarding the physics as well as from (cell) biology had to be taken into account.

From the physical point of view, it is important to have the external spins of interest (the ROS) as close as possible to the ND's surface: The "sensing radius" of an NV<sup>-</sup>-center was found by Sushkov et al. to be approximately 12 nm<sup>[9]</sup> (although different values can be found in literature for NDs or bulk diamond and depending on the measuring protocol). Fluorescent background in the spectral region between approx. 550 – 800 nm (the emission of the NV<sup>-</sup>-center) is to be avoided.

On the other hand, from the biological point of view, the biocompatibility of the NDs has to be kept in mind: Oxidative stress should be measured inside of cells, without inducing it (for example, fluorine terminated diamonds, which would be favorable for the stability of the NV-center<sup>[10]</sup>, could react entirely differently from this point of view than oxygen-terminated NDs). The effect of ND aggregation in cellular medium, a completely uninvestigated phenomenon, needed to be solved in order to allow optimum uptake in cell culture as well as to allow spins to come into the “sensing radius” of the ND.

Therefore, this work is organized as follows: Firstly, ND characterization in order to understand the properties of the NDs in use, followed by a thorough investigation of the aggregation phenomenon in cellular media (Some of the results later sorted into the ND characterization section, such as the shape considerations in section 3.1.2, where indeed “side products” – nevertheless important for both physics and biology – of this.).

The next step was the modification of the NDs with biomolecules to control the fate of the diamond in the biological environment: Amongst the various opportunities considered and published as review<sup>[10]</sup> the simplest, physical adsorption of antibodies (ABs) was chosen. Main reasons for this decision were: (1) Simplicity of the procedure requiring only few steps. (2) Applicability for a broad range of proteins. (3) The hope of “killing two birds with one stone”: As the formation of a protein corona of nanoparticles in a biological medium is inevitable, it could be possible to tailor it to biological needs (e.g. low cytotoxicity, maximum uptake, promoted endosomal escape and guide the ND to its desired destination). The stability of these antibody-conjugated NDs was explored in various media.

Finally as current methods for the quantification of ND uptake utilizing confocal fluorescence microscopy are time consuming (and therefore allow only a limited number of cells examined) and plate readers are often not sensitive, a method based on fluorescence and cell counting techniques was developed to allow faster screening.

## 2. Experimental Section

### 2.1 Nanodiamond Characterization

#### 2.1.1 Chemicals and Materials

Commercially available ND particles of type Ib produced by HPHT (high-pressure, high-temperature) synthesis, available as slurries in DI water, were used. An overview of the ND particles is given in Table 1 (non-fluorescent NDs with maximum 1 NV-center per particle acquired from Microdiamant AG, Lengwil, Switzerland) and Table 2 (FNDs acquired from Adámas Nanotechnologies, Raleigh, United States). NDs of both suppliers are oxygen-terminated. In particular with ND modification (e.g.

conjugation with biomolecules) in mind, the ND particles were characterized by dynamic light scattering (DLS), transmission electron microscopy (TEM), X-ray photoelectron spectroscopy (XPS) (for 25 nm NDs only, mainly as reference for the aggregation phenomenon covered in section 2.2) and x-ray powder diffraction (XRD). Diamond slurries purchased from Microdiamant AG were also tested for suitability as a model system: Analysis methods with higher requirements in regards to the minimum sample amount needed were to be avoided with the significantly more expensive Adámas slurries.

Table 1 NDs from Microdiamant AG

| Product   | Size [nm]         |
|---|-------------------|
| <b>Microdiamant Liquid Diamond Monocrystalline MSY 0-0.05 micron GAF</b><br><b>Conc. 100 cts/kg (= 20g/kg <math>\approx</math> 20 mg/mL), Lot L11033, Ref 129578</b>  | 25 (median, D50)  |
| <b>Microdiamant Liquid Diamond Monocrystalline MSY 0-0.15 micron GAF</b><br><b>Conc. 100 cts/kg (= 20g/kg <math>\approx</math> 20 mg/mL), Lot L11004, Ref 131179</b>  | 75 (median, D50)  |
| <b>Microdiamant Liquid Diamond Monocrystalline MSY 0-0.25 micron GAF</b><br><b>Conc. 500 cts/kg (= 20g/kg <math>\approx</math> 100 mg/mL), Lot L11004, Ref 131179</b> | 125 (median, D50) |

Table 2 FNDs from Adámas Technologies

| Product   | Size [nm]  |
|---|--|
| <b>ND-NV-120nm-W</b><br><b>0.1% 10 mL, PL: &gt;900 NV/Particle<sup>1</sup>; Polyfunctional <math>\zeta</math> = .35 mV</b><br><b>Batch: 1-E3/E4-#2F-K</b> | 120 (average particle size according to volume distribution) |
| <b>ND-NV-70nm-W</b><br><b>0.1% 10 mL, PL: &gt;300 NV/Particle<sup>1</sup>; Polyfunctional <math>\zeta</math> = .35 mV</b><br><b>Batch: 1-E3/E4-#2F-K</b>  | 70 (average particle size according to volume distribution)  |

### 2.1.2 Transmission Electron Microscopy (TEM) and X-ray Powder Diffraction (XRD)

TEM measurements have been performed using a Philips CM12 (Philips, Eindhoven, The Netherlands) operating at 120 kV. Images were recorded on a slow scan CCD camera. NDs of 25 nm median size (Microdiamant AG) were imaged on glow discharged plain carbon coated 400 mesh copper grids. Samples were directly applied on the grids with a diamond concentration of 1  $\mu$ g/mL in DI water.

For the XRD analysis of diamond powder with a median size of 25 nm, the diamond powder Microdiamant (Microdiamant AG, Lengwil, Switzerland) Monocrystalline Diamond Powder MSY 0-0.05 micron (Lot L11026, Ref 125132) was used. For median sizes of 75 nm and 125 nm, the powder for the XRD analysis was obtained by evaporation of the corresponding ND slurries in Table 1 (see section 2.1.1). Quantitative analysis was performed using the Rietveld method. The measurements were

<sup>1</sup> According to Adámas Nanotechnologies the number of NV<sup>-</sup>-centers must be considered as a rough estimate (based on a spectroscopic comparison with a reference nanodiamond powder).

carried out in cooperation with Frank Kubel (Institute of Chemical Technologies and Analytics, Vienna University of Technology, Vienna, Austria).

### 2.1.3 Dynamic Light Scattering (DLS) Measurements

The hydrodynamic diameter as well as the zeta potential of the diamond particles were measured using dynamic light scattering (DLS). For this, a Zetasizer Nano ZS system (Malvern Instruments Ltd, Malvern, UK) equipped with a He-Ne-Laser ( $\lambda = 633 \text{ nm}$ ) was used. Evaluation of the data was performed using ZetaSizer Software version 7.1 (Malvern Instruments Ltd.). For both size and zeta potential measurements, disposable folded capillary cells were used (with multiple use after cleaning with DI water instead of disposal).

The instrument parameters for the size measurements were set as follows:

*Table 3 DLS settings for size measurements*

| <b>Setting</b>               | <b>Value</b>  |
|------------------------------|---|
| <b>Refractive Index (RI)</b> | 2.419 (bulk diamond)                                |
| <b>Absorption</b>            | 0.010 default setting                               |
| <b>Temperature</b>           | 25.0 °C (with not equilibration time)               |
| <b>Viscosity</b>             | 0.8872 cP   |
| <b>Dispersant</b>            | Water   |
| <b>Dispersant RI</b>         | 1.330   |
| <b>Measurement angle</b>     | 173° backscatter (Non-. Invasive Backscatter, NIBS) |

Further instrument settings: Logarithmic baseline: symmetric; Positioning method: Seek for optimum position; Automatic Attenuator Selection: Yes; Analysis Mode: General purpose (Cumulants analysis with the order of fit set to 3 and a quadratic weighting scheme. Result transformation according to Mie theory.). If not explicitly specified, all the other settings were set to the default values of the instrument.

The measurement duration was set to 15 or 25 runs (specified in the results section), each of them taking 10 seconds. The measurement was started 3-5 minutes after insertion into the instrument to reduce movement of particles due to movement of the cuvette. ND concentrations of the measured solutions are specified in the Results and Discussion section 3.1.

As important parameter for the stability of suspensions, the zeta potential was determined. The same parameters were chosen as for the size measurement (see Table 3) with the number of runs manually set to 15.

The Smoluchowski approximation for sufficiently thin double layers was chosen. Further parameters: Lower limit - 150 V; Higher limit: 150 V; Filtering: Zeta Analysis Version 5.1; Automatic Attenuator Selection: Yes; Automatic Voltage Selection: Yes (based on the measured conductivity of the sample, which was in all measured samples below 25 mS/cm, which is the condition for the Result type setting of General purpose). Also in this case, if not explicitly specified, all the other settings were set to the default values of the instrument. The measurement was started 3-5 minutes after insertion into the instrument to reduce movement of particles due to movement of the cuvette. ND concentrations of the measured solutions are specified in the Results and Discussion section 3.1.

Dilutions – also in all other parts of this work – were prepared with deionized water from a Sartorius arium 611 DI system (Sartorius, Göttingen, Germany).

### 2.1.4 X-ray photoelectron spectroscopy (XPS)

NDs of 25 nm size (Microdiamant AG) were analyzed by X-ray photoelectron spectroscopy (XPS): An S-Probe (Surface Science Instruments, Scienta Scientific, Uppsala, Sweden) instrument was used with the following settings:

- X-ray production (10 kV, 22 mA) with a spot size of 250 × 1000 μm using an Al anode
- Wide scans with an energy range of 0 to 1200 eV at low resolution (pass energy: 150 eV)
- The area under each peak, after Shirley background subtraction, was used to calculate peak intensities, yielding elemental surface concentration ratios for nitrogen (N), oxygen (O), and phosphorus (P) to carbon (C).
- Narrow scans for C, O and N were made at a pass energy of 50 eV, these were used for peak fitting of the carbon and oxygen peak.

The carbon peak was scaled to 284.6 eV and 284.8 eV (for measurements after 1st July 2015 as a result of an instrument upgrade where more recent recommendations for the instrument were taken into account) in the peak fitting process. Measurements were carried out in cooperation with Joop de Vries (Dep. of Biomedical Engineering, Faculty of Medical Sciences, University of Groningen).

## 2.2 Nanodiamond Aggregation

### 2.2.1 Chemicals and Materials

The phenomenon of ND aggregation as described in section 1.3 was investigated for two different cellular media types:



1. DMEM complete medium (DMEM (Dulbecco's Modified Eagle Medium) + Glutamax (1%) + and penicillin/streptomycin (1%) + Fetal bovine serum (FBS) (10%), Gibco Life Technologies, Bleiswijk, The Netherlands). The exact composition of DMEM can be found in the annex.
2. Yeast medium base without amino acids (Formedium™, King's Lynn, United Kingdom) for yeast cells that are used in cooperation with ERIBA (European Research Institute for the Biology of Ageing, Groningen, The Netherlands). 6.7 g/L of yeast medium base without amino acids (abbreviated as YMB) were in DI water. The exact composition can be found in the annex (it is important to note that in this case no proteins are part of the investigated medium).

For investigating the aggregation process, only NDs of 25 nm median size (Microdiamant AG) were used. However, the aggregation phenomenon – less severely – occurs also with larger NDs.

### 2.2.2 Dynamic Light Scattering (DLS) Measurements

The aggregation behavior was assessed by DLS measurements using the instrument settings as described above in section 2.1 (for both size and zeta potential measurements). Size measurements were performed twice using (single-use) disposable sizing cuvettes as well as disposable folded capillary cells (usable for zeta potential measurements). The following samples have been prepared and measured:

- 10% FBS (in DI water) as a control sample
- ND of 25 nm of median size (Microdiamant AG) in 10% FBS
- ND of 25 nm of median size (Microdiamant AG) in 10% FBS (washed): After centrifugation and discarding the supernatant, DI water was added in which it was measured (the same procedure was applied to the other washed samples).
- ND of 25 nm of median size (Microdiamant AG) in DMEM with 10% FBS
- ND of 25 nm of median size (Microdiamant AG) in DMEM with 10% FBS (washed)
- ND of 25 nm of median size (Microdiamant AG) in DMEM (no FBS)
- ND of 25 nm of median size (Microdiamant AG) in DMEM (no FBS) (washed)

For all the samples, the ND concentration was 200 µg/mL. In order to investigate ways to avoid (or significantly mitigate) the formation of aggregates, ND of 25 nm of median size were also measured in 100% FBS (including a 100% FBS control sample) and adding diamonds to 100% FBS prior to adding them to DMEM (resulting in 10% FBS in DMEM). For these samples, for simplicity, no zeta potential was measured.

For the YMB, samples with a ND concentration of 200  $\mu\text{g}/\text{mL}$  were measured using disposable folded capillary cells.

### 2.2.3 X-ray photoelectron spectroscopy (XPS)

(Inorganic) elements involved in the aggregation process were determined using X-ray photoelectron spectroscopy (XPS). The same parameters were used as for the analysis of pure NDs as described in section 2.1.4.

For both types of medium, 10  $\mu\text{L}$  of NDs with 25 nm median size (from Microdiamant AG) were added per mL medium (this results in a ND concentration of 200  $\mu\text{g}/\text{mL}$ ), followed by centrifugation and freeze-drying of the samples. The following samples have been measured:

1. NDs of 25 nm of median size (Microdiamant AG) in DMEM with 10% FBS
2. NDs of 25 nm of median size (Microdiamant AG) in DMEM (without FBS)
3. NDs of 25 nm of median size (Microdiamant AG) in yeast medium base without amino acids

Sample 1 was previously measured in the group and only the evaluation was part of this work. Sample 2 and Sample 3 were measured at several spots (specified in detail in the results section). Measurements were carried out in cooperation with Joop de Vries (Dep. of Biomedical Engineering, Faculty of Medical Sciences, University of Groningen).

### 2.2.4 Transmission Electron Microscopy (TEM) Measurements

Visualization of the aggregation was achieved by TEM measurements, which have been performed using a Philips CM12 (Philips, Eindhoven, The Netherlands) operating at 120 kV. Images were recorded on a slow scan CCD camera.

Aggregates were imaged utilizing holey carbon coated grids (Quantifoil 1.2/1.3, Quantifoil, Jena, Germany). Samples were directly applied on the grids with a diamond concentration of 1  $\mu\text{g}/\text{mL}$  in medium (total sample amount 1  $\mu\text{L}$ ). In case of samples in medium, a washing step followed with 1  $\mu\text{L}$  DI water.

### 2.2.5 Analysis of the Protein Corona (MALDI-TOF-MS and nanoLC-MS/MS)

The MALDI-TOF-MS measurement was inspired by Kong et al.<sup>[27]</sup> With an AB SCIEX Voyager DE Pro MALDI-TOF system (SCIEX, Framingham, United States) equipped with a Nd-YaG laser, a fingerprint of the proteins associated with the diamond nanoparticles upon contact with medium was made: Sample

preparation consisted of mixing 10  $\mu\text{L}$  25 nm ND slurry (Microdiamant AG) with per mL DMEM medium (final ND concentration: 200 $\mu\text{g}/\text{mL}$ ), followed by centrifugation and washing of the precipitated aggregates with DI water. After centrifugation and discarding the supernatant, the aggregates were freeze-dried. 5 mg/mL alpha-cyanohydroxycinnamic acid in 50/50/0.1 DI water/acetonitrile/trifluoroacetic acid (TFA) was used as matrix. A few particles were suspended in 3  $\mu\text{L}$  matrix and spotted on the MALDI plate. Measurements were in positive, linear mode. The mass range measured was 500 – 5000 Da. The analysis was performed in cooperation with Annie van Dam (Mass Spectrometry Core Facility, Groningen Research Institute of Pharmacy, University of Groningen, Groningen, The Netherlands).

For the analysis with nanoLC–MS/MS, a more sophisticated approach involving a trypsin digest with the following five samples was undertaken:

1. Pure FBS as control sample.
2. 10% FBS in DI water with 25 nm-diamond slurry (10  $\mu\text{L}$  per mL)
3. 10% FBS in DI water with 25 nm-diamond slurry (10  $\mu\text{L}$  per mL), 1x washed with DI water
4. DMEM with 10% FBS and 25 nm-diamond slurry (10  $\mu\text{L}$  per mL)
5. DMEM with 10% FBS and 25 nm-diamond slurry (10  $\mu\text{L}$  per mL), 1x washed with DI water

Samples 2-5 were freeze-dried (after centrifugation and discarding of the supernatant), whereas sample 1 was the pure FBS solution as provided by the supplier.

Small amounts of the freeze dried sample (and a few microliters of sample 1, respectively) were first treated with 20  $\mu\text{L}$  freshly prepared 10 mM dithiothreitol (DTT) in 100 mM  $\text{NH}_4\text{HCO}_3$  to reduce the protein. This was followed by an incubation step at 55-60°C for 30 minutes. The alkylation of the cysteines was achieved by adding 10  $\mu\text{L}$  iodoacetamide in 100 mM  $\text{NH}_4\text{HCO}_3$  (incubation for 45 minutes). Subsequently a second treatment with DTT followed for 30 minutes (to get rid of the unreacted iodoacetamide).

A trypsin digest followed by adding 20  $\mu\text{L}$  solution with 10 ng/ $\mu\text{L}$  trypsin (sequencing grade, Promega, Madison, United States). An overnight incubation followed at 37°C. A clean-up using SPE with C-18 cartridges followed using a 70/30/0.1 acetonitrile/water/formic acid mixture for elution.

The samples were analyzed by nanoLC–MS/MS on an Ultimate 3000 system (Dionex, Amsterdam, The Netherlands) interfaced on-line with a Q-ExactivePlus (Orbitrap) mass spectrometer (Thermo Fisher Scientific Inc., Waltham, Massachusetts, United States). Peptide mixtures were loaded onto a 5 mm  $\times$  300  $\mu\text{m}$  i.d. trapping micro column packed with C18 PepMAP100 5  $\mu\text{m}$  particles (Dionex) in 2% acetonitrile in 0.1% formic acid at the flow rate of 20  $\mu\text{L}/\text{min}$ . After loading and washing for 3 minutes, peptides were back-flush eluted onto a 15 cm  $\times$  75  $\mu\text{m}$  i.d. nanocolumn, packed with C18 PepMAP100

1.8  $\mu\text{m}$  particles (Dionex). The following mobile phase gradient (total run time: 75 minutes) was delivered at the flow rate of 300 nL/min: 2–50% of solvent B in 60 min; 50–90% B in 1 min; 90% B during 13 min, and back to 2% B in 1 min (held for 15 minutes). Solvent A was 100:0 H<sub>2</sub>O/acetonitrile (v/v) with 0.1% formic acid and solvent B was 0:100 H<sub>2</sub>O/acetonitrile (v/v) with 0.1% formic acid.

Peptides were infused into the mass spectrometer via dynamic nanospray probe (Thermo Fisher Scientific Inc.) with a stainless steel emitter (Thermo Fisher Scientific Inc.). Typical spray voltage was 1.8 kV with no sheath and auxiliary gas flow; ion transfer tube temperature was 275°C. Mass spectrometer was operated in data-dependent mode. DDA cycle consisted of the survey scan within  $m/z$  300–1650 at the Orbitrap analyzer with target mass resolution of 70,000 (FWHM, full width at half maximum at  $m/z$  200) followed by MS/MS fragmentations of the top 10 precursor ions. Singly charged ions were excluded from MS/MS experiments and  $m/z$  of fragmented precursor ions were dynamically excluded for further 20 s. The nanoLC–MS/MS including the sample preparation was performed in cooperation with Marcel de Vries (Mass Spectrometry Core Facility, Groningen Research Institute of Pharmacy, University of Groningen, Groningen, The Netherlands).

Data processing was performed as follows: The software PEAKS Studio version 7 (Bioinformatics Solutions Inc., Waterloo, Canada) was applied to the spectra generated by the Q-exactive plus mass spectrometer to search against either the protein sequence database UniProtKB/Trembl of the UniProt Knowledgebase (UniProtKB), limited to protein sequences of *Bos Taurus* (a search including the whole database was performed as well in order to rule out the relevance of possible contaminations). Searching for the fixed modification carbamidomethylation of cysteine and the variable post translational modifications oxidation of methionine was done with a maximum of 5 posttranslational modifications per peptide at a parent mass error tolerance of 10 ppm and a fragment mass tolerance of 0.02 Da. False discovery rate was set at 0.1%.

### 2.3 Nanodiamond Modification

In order to change the fate of the diamonds in the biological environment, NDs were modified with biomolecules. As described in section 1.4, physical adsorption as straightforward method to attach biomolecules. Antibodies have been chosen as they have specific interaction with their target and they are easily commercially available (also with fluorescent labelling). While the affinity of NDs to proteins was discussed in section 1.3, the practical application of the physisorption has been shown by Vermeeren et al.<sup>[28]</sup> and Siddiqui et al.<sup>[29]</sup> (both for hydrogen-terminated diamond surfaces). For this work, however, oxygen-terminated fluorescent NDs of 70 nm size (Adámas Nanotechnologies) were used. For initial experiments also FNDs of 120 nm size were utilized, but as the NDs with 70 nm of size

were perfectly visible in the confocal microscope, the latter were preferred (generally, smaller diamonds are preferred in the biological environment).

Fluorescent FNDs have been conjugated with FITC-labelled antibodies (later, the use of non-labelled antibodies specific to the desired target shall be used) based on the following protocol<sup>2</sup>: Fluorescein (FITC) AffiniPure Goat Anti-Mouse IgG (H+L) (Jackson ImmunoResearch Inc., United States)<sup>3</sup> with a concentration of 1.5 mg in 2.2 mL was diluted by 1:10. 1.5  $\mu$ L of the solution was added to 5  $\mu$ L FND stock solution (concentration: 1 mg/mL). The mixture was incubated overnight at 37°C and then medium of interest was added (control samples were always prepared with water) to a final volume of 50  $\mu$ L. To test the stability of the antibodies adsorbed in biologically relevant media the double amounts were used in order to have a higher ratio of the medium. Stability was tested following media were tested:

- Phosphate buffered saline, PBS
- FBS
- 10% FBS
- DMEM + 10% FBS

1.5  $\mu$ L were spin-coated on a cover glass using a Spin150 spin coater (SPS-Europe B.V., Putten, The Netherlands) using the following settings: 2500 rpm for 30 seconds (for DMEM and PBS 2x 30 seconds was necessary to avoid the formation of salt crystals) with an acceleration of 1000 rpm/second.

The adsorption process was evaluated using confocal fluorescence microscopy by checking the co-localization of the ND signal with the FITC signal of the labelled antibodies. Preliminary tests were performed using a Leica SP2 confocal microscope (Leica Microsystems, Wetzlar, Germany). As the sensitivity turned out to be too low, all further images were made by a Zeiss LSM 780 confocal microscope (Carl Zeiss AG, Jena, Germany). The parameters were set as follows:

For the FITC-labelled antibodies, the 488 nm Ar laser with 2.0% power (for selected samples specified in the results only 0.5%). For the samples prepared in water (measurement always happened in the dry form after spin coating), acquisition was performed between 508 – 597 nm and for samples in PBS, FBS or DMEM (with 10% FBS) from 508 – 561 nm (to guarantee that there is no overlap with the spectrum of the NV<sup>-</sup>center as FITC emits till approx. 650 nm). The NDs were imaged using a 561 nm DPSS laser collecting photons from 606 – 694 nm.

---

<sup>2</sup> This protocol is the final, already optimized, version. Initial experiments were performed with an (approximate, assuming that all the NDs have the same size of 75 nm) ND to antibody (molar) ratio of 1:1. However, for detecting one antibody per ND, the confocal fluorescent microscope used was not sensitive enough.

<sup>3</sup> For the detailed description of the antibody see the annex.

The identity of NDs and FITC was confirmed by measuring spectra in the instrument's lambda mode.

## 2.4 Quantification of ND Uptake in Cells

Quantification of the nanoparticle uptake by cells, particularly at the cellular and sub-cellular level remains a less explored problem in the application of nanodiamonds<sup>[30]</sup>. Confocal microscopy remains a time-consuming method with poor statistics. To address this issue, a method based on Raman spectroscopy or fluorescence spectroscopy (relying on the emission of the NV-centers in FNDs) on bulk cell suspensions (as opposed to single cells on a microscopy slide) was utilized. This was combined with cell counting methods (in order to quantify the overall diamond amount and set it in relation to the number of biological cells).

Detection of the diamond Raman band at a Raman shift of  $1332\text{ cm}^{-1}$  has been reported in literature for several laser wavelengths, including  $785\text{ nm}$ <sup>[31]</sup>,  $532\text{ nm}$ <sup>[32]</sup>, both of which we were using. Additionally, the use  $355\text{ nm}$  and  $473\text{ nm}$  lasers has been evaluated. However, due to the low concentrations expected in cell uptake studies ( $10\text{ }\mu\text{g/mL}$  –  $0.1\text{ ng/mL}$ ), no Raman signal could be observed.

Therefore, the well-known fluorescence signal from NV-centers<sup>[33]</sup> in FNDs using the  $532\text{ nm}$  laser as excitation source was used. While with the  $473\text{ nm}$  laser also a good fluorescence signal could be obtained, the  $532\text{ nm}$  source was preferred as lasers of this wavelength were easily available in the research group (for the diamond magnetometry setup) and therefore an easy transfer of the method is possible. Standards with  $70\text{ nm}$  FNDs from Adámas in DI water with the concentrations  $10\text{ }\mu\text{g/mL}$ ,  $1\text{ }\mu\text{g/mL}$ ,  $0.1\text{ }\mu\text{g/mL}$ ,  $10\text{ ng/mL}$ ,  $1\text{ ng/mL}$  and  $0.1\text{ ng/mL}$  have been measured. Furthermore, cell lysate samples (J774 cells lysated in RIPA buffer consisting of  $50\text{ mM}$  Tris-HCl,  $1\%$  NP-40,  $0.5\%$  Na-deoxycholate,  $0.1\%$  SDS,  $150\text{ mM}$  NaCl,  $2\text{ mM}$  EDTA,  $50\text{ mM}$  NaF) spiked with NDs yielding concentrations  $10\text{ }\mu\text{g/mL}$ ,  $1\text{ }\mu\text{g/mL}$ ,  $0.1\text{ }\mu\text{g/mL}$ ,  $10\text{ ng/mL}$  and  $1\text{ ng/mL}$  were measured. For all samples, FNDs of  $70\text{ nm}$  average size (Adámas Technologies) incorporating approximately 300 NV-centers per particle were used.

Emission spectra were recorded by excitation at  $532\text{ nm}$  ( $25\text{ mW}$  CW DPSS laser, Cobolt AB, Solna, Sweden) via an Olympus BX51 microscope (Olympus K.K., Shinjuku, Japan) modified with a macro sampling unit (Ventacon UK, Godalming, United Kingdom). A laser line clean up filter,  $450\text{ nm}$  dichroic and steep edge long pass filter (Semrock, New York, United States) were used for excitation delivery and emission collection. The emitted light was passed via a fibre optic (round to line configuration) to a Shamrock163 spectrograph (Andor Technology, Belfast, United Kingdom) with a  $300\text{ l/mm}$  grating blazed at  $500\text{ nm}$  with an Andor iDUS-420-OE CCD camera operating in full vertical binning mode.

Spectral acquisition was carried out using Andor Solis (Andor Technology). The exact parameters varied for several measurements, which is why they are given in the results section.

Peak integration and data evaluation was performed using OriginPro 2015G (OriginLab Corporation, Northampton, United States)

### 3. Results and Discussion

#### 3.1 Nanodiamond Characterization

##### 3.1.1 Dynamic Light Scattering (DLS) Measurements

DLS measurements of the diamond slurries of the suppliers listed in section 2.1 resulted in similar size distributions. Furthermore, suspensions with different diamond concentrations have been measured (measurement duration was set to 25 runs, each of them taking 10 seconds) as displayed in Table 4. There, according to the International Standard on Dynamic Light Scattering ISO13321 (1996) and ISO22412 (2008), “z-Average” refers to the intensity-weighted mean diameter derived from the cumulants analysis while “Pdl” refers to the polydispersity index giving an estimate of the width of the distribution. The number mean is automatically calculated by the software of the instrument using the Mie scattering theory. The Rayleigh theory is applicable for small particles and molecules whose diameters are less than  $1/10^{\text{th}}$  of the laser wavelength. For the He-Ne-Laser ( $\lambda = 633 \text{ nm}$ ), this means around particle diameters of about 60 nm.

Table 4 DLS Measurements with Different Diamond Concentrations

| Sample  | z-Average [nm] | Pdl   | Number Mean [nm] |
|---|----------------|-------|------------------|
| 25 nm Microdiamant 1 $\mu\text{g}/\text{mL}$    | 62.31          | 0.269 | 26.09            |
| 25 nm Microdiamant 100 $\mu\text{g}/\text{mL}$  | 51.67          | 0.125 | 33.44            |
| 25 nm Microdiamant 20 $\text{mg}/\text{mL}$     | 46.42          | 0.178 | 27.65            |
| 70 nm Adámas 1 $\mu\text{g}/\text{mL}$          | 136.0          | 0.209 | 70.67            |
| 70 nm Adámas 10 $\mu\text{g}/\text{mL}$         | 117.3          | 0.118 | 74.71            |
| 75 nm Microdiamant 1 $\mu\text{g}/\text{mL}$    | 168.9          | 0.275 | 78.13            |
| 75 nm Microdiamant 100 $\mu\text{g}/\text{mL}$  | 129.1          | 0.103 | 85.16            |
| 120 nm Adámas 1 $\mu\text{g}/\text{mL}$         | 161.9          | 0.078 | 118.0            |
| 125 nm Microdiamant 1 $\mu\text{g}/\text{mL}$   | 137.7          | 0.170 | 74.52            |
| 125 nm Microdiamant 100 $\mu\text{g}/\text{mL}$ | 132.9          | 0.116 | 86.62            |

Measurements of the Microdiamant stock solutions (as purchased with a concentration of 20  $\text{mg}/\text{mL}$  and 100  $\text{mg}/\text{mL}$ ) with diamonds of 75 nm and 125 nm median size were not possible (too much scattering at that concentration and therefore sample out of the measurement range of the

instrument). For all the other samples, no significant concentration dependent effects (due to multiple scattering or particle interactions) could be observed.

A detailed comparison of the diamond slurries (including multiple measurements of the same sample) can be found in Table 5 (practical measurement according to the developed protocol/method was performed in cooperation with Melissa Monzerrat Rodriguez Garcia). Each sample with a diamond concentration of 10 µg/mL was measured 3 times. The measurement duration was set to 15 runs, each of them taking 10 seconds.

Table 5 DLS Measurements of the Diamond Slurries with a Concentration of 10 µg/mL

| Sample                     | Z-Average ± Std. Dev [nm] | Rel. Std. Dev [%] | Pdl ± Std. Dev. | Rel. Std. Dev [%] | Number Mean ± Std. Dev [nm] | Rel. Std. Dev [%] |
|----------------------------|---------------------------|-------------------|-----------------|-------------------|-----------------------------|-------------------|
| <b>70 nm Adámas</b>        | 121.3 ± 0.2               | 0.2               | 0.10 ± 0.01     | 11.51             | 80.2 ± 2.4                  | 3.0               |
| <b>120 nm Adámas</b>       | 164.9 ± 0.0               | 0.0               | 0.06 ± 0.02     | 30.25             | 127.7 ± 5.0                 | 3.9               |
| <b>25 nm Microdiamant</b>  | 55.6 ± 0.6                | 1.0               | 0.15 ± 0.00     | 2.12              | 34.1 ± 1.2                  | 3.5               |
| <b>75 nm Microdiamant</b>  | 133.2 ± 3.0               | 2.3               | 0.11 ± 0.02     | 16.96             | 87.2 ± 1.6                  | 1.9               |
| <b>125 nm Microdiamant</b> | 157.9 ± 0.7               | 0.5               | 0.10 ± 0.01     | 11.89             | 110.2 ± 5.5                 | 5.0               |

While multiple measurements of the same sample yield low relative standard deviations, an increasing relative standard deviations can be observed with increasing particle size. Also, changing the number of measurement runs from 25 to 15 results in smaller particle sizes (see Table 4 as a comparison). Here also factors such as sedimentation of bigger particles could play a role (Waiting 3-5 minutes after inserting the sample into the instruments results in values closer to the supplier information. This has been done for all measurements.).

However, no more efforts have been made to perfect the measuring conditions as absolute values are not as relevant for the following work as the comparison between the two suppliers (Microdiamant AG and Adámas Nanotechnologies) as shown in Figure 3 and Figure 4. The 25 nm Microdiamant NDs have not been compared with other slurries as no other diamonds of that size from other suppliers were in use.

Figure 3 shows a slight difference between the 70 nm Adámas NDs and the 75 nm Microdiamant NDs, respectively. In Figure 4 we can see that the deviation between individual measurements is even bigger than the difference between the slurries of the two suppliers. Therefore, we consider the 75 nm and 125 nm Microdiamant NDs (slurries with NDs of 70 nm and 120 nm median size were not available from Microdiamant) as a suitable model system for the FNDs from Adámas Technologies.



## Results and Discussion

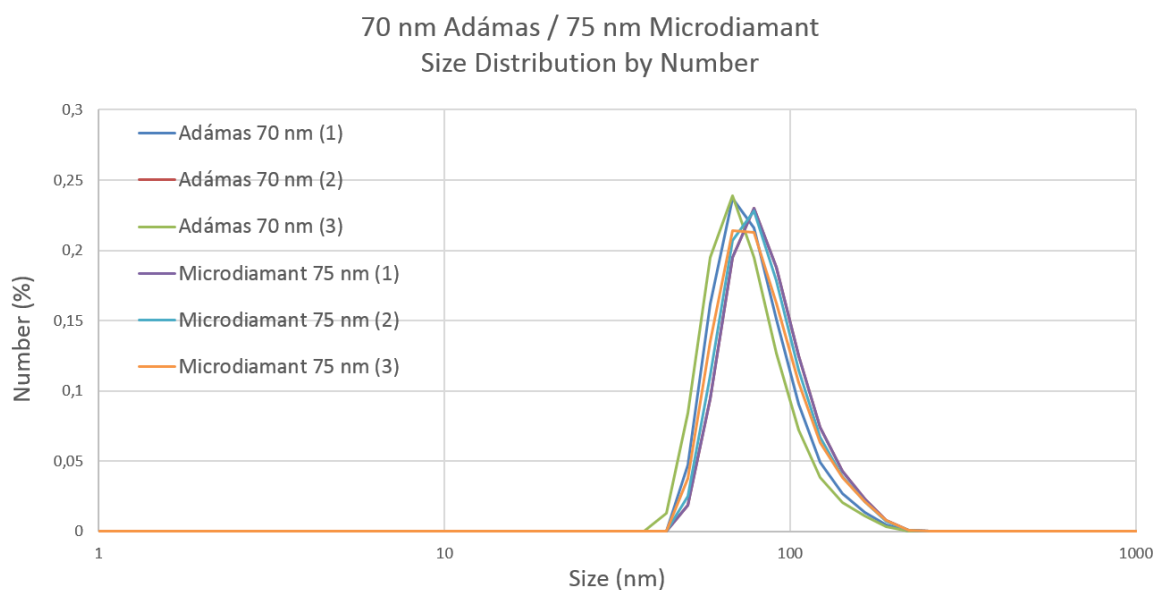


Figure 3 Comparison of 70 nm Adámas Diamonds with 75 nm Microdiamant Diamonds based on the Size Distribution by Number.

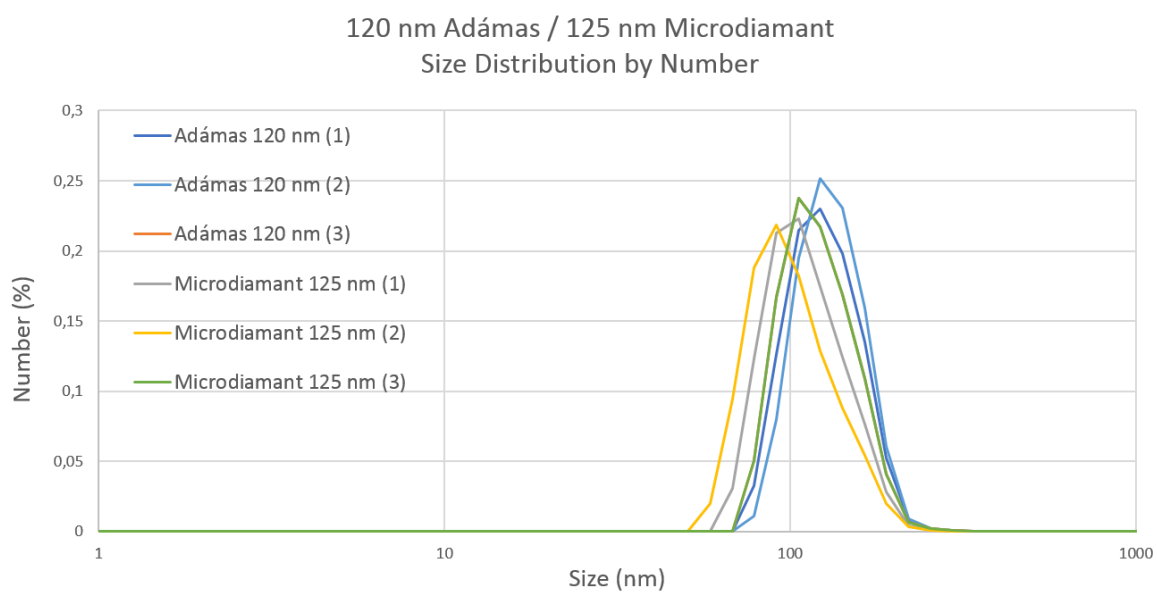


Figure 4 Comparison of 120 nm Adámas Diamonds with 125 nm Microdiamant Diamonds based on the Size Distribution by Number.

The zeta potentials measured at a concentration of 10  $\mu\text{g}/\text{mL}$  are given in Table 6 and those measured at a concentration of 1  $\mu\text{g}/\text{mL}$  in Table 7. Information from the supplier about the zeta potential was only available for diamonds purchased from Adámas: - 35 mV.

Table 6 Zeta potentials measured for the ND suspensions with a concentration of 10 µg/mL

| Sample              | Zeta potential ± Std. Dev [mV] | Rel. Std. Dev [%] |
|---------------------|--------------------------------|-------------------|
| 70 nm Adámas        | -40.27 ± 0.91                  | 2.25              |
| 120 nm Adámas       | -19.70 ± 0.82                  | 4.16              |
| 25 nm Microdiamant  | -20.33 ± 1.88                  | 9.23              |
| 75 nm Microdiamant  | -21.13 ± 2.97                  | 14.07             |
| 125 nm Microdiamant | -22.60 ± 0.60                  | 2.65              |

Table 7 Zeta potentials measured for the ND suspensions with a concentration of 1 µg/mL

| Sample              | Zeta potential ± Std. Dev [mV] | Rel. Std. Dev [%] |
|---------------------|--------------------------------|-------------------|
| 70 nm Adámas        | -30.60 ± 0.44                  | 1.42              |
| 120 nm Adámas       | -30.43 ± 0.35                  | 1.15              |
| 25 nm Microdiamant  | -22.20 ± 3.44                  | 15.49             |
| 75 nm Microdiamant  | -21.53 ± 0.64                  | 2.99              |
| 125 nm Microdiamant | -9.19 ± 1.38                   | 15.02             |

As with the sizes values, also the absolute values of zeta potential are not as relevant as the relative changes, especially in connection with the ND aggregation phenomenon covered in section 3.2. However, the values obtained for the Adámas NDs are close to the supplier's information. Adámas NDs have a lower zeta potential, meaning that the suspensions have a higher stability. The reason for the difference between the two suppliers is possibly found in a (slightly) different surface chemistry, (trace) contaminations and impurities (partly due to production).

It must be noted that the zeta potential is also depending on the particle concentration as well as the ionic strength of the suspension. The latter is indeed relevant for the ND aggregation in cellular medium with a high ion concentration. In fact, the empirical Schulze-Hardy rule deals with the flocculation of colloids with ions of opposite charge.

### 3.1.2 Shape Considerations

Current theoretical models regarding the spin properties of the NV center rely on an assumed spherical shape of the NDs<sup>[7]</sup>. However, according to Microdiamant AG's information, NDs have a rather blocky shape. TEM pictures of the 25 nm ND particles (Microdiamant AG) confirm this non-spherical shape (only 25 nm NDs have been considered for the shape and the outcomes are not necessarily applicable to larger NDs) with sharp edges (see Figure 5).

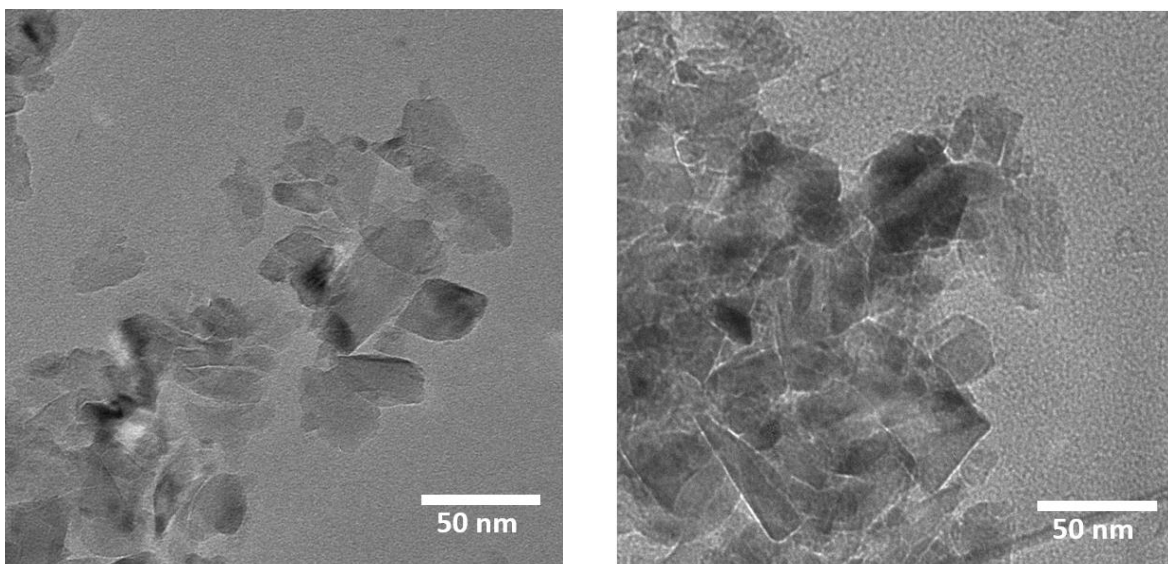


Figure 5 25 nm NDs on glow discharged plain carbon coated 400 mesh copper grids at different spots.

Selected area electron diffraction (SAED) was done on selected spots (with and without a protein corona). In all cases, the 111 plane was clearly visible as exemplarily shown with the spot in Figure 6 (the same picture is shown in Figure 17 to illustrate the protein corona) with the hexagonal diffraction pattern of the 111 plane displayed in Figure 7.

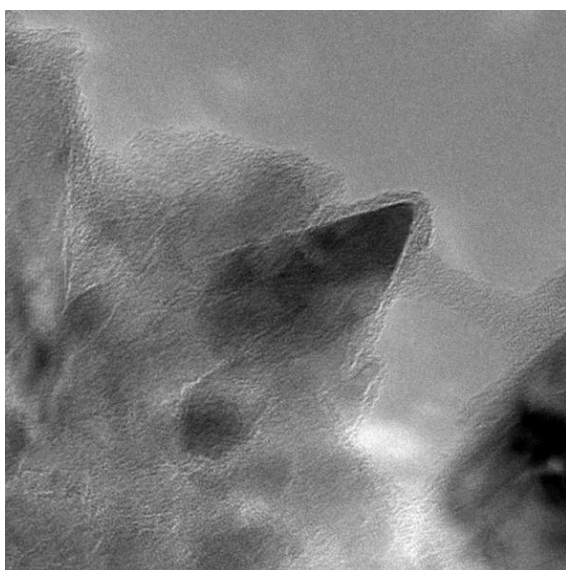


Figure 6 25 nm NDs on holey carbon coated grids. The big dark diamond in the middle of the picture marks de center where SAED was done.

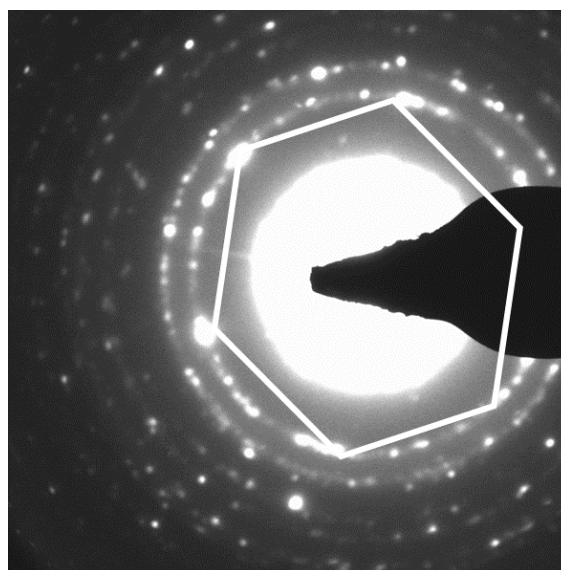


Figure 7 Hexagonal structure of the diamond 111 plane. This points to 111 texturation of the NDs.

This lead to the idea of a possible 111 texturation of the NDs. The initially with XRD established 111 texturation NDs of 25 nm size could not be confirmed (also for the 25 nm diamonds) after measuring NDs of 75 nm and 125 nm size (based on the better refinement of the data because of the correlation of the vibrational modes of the atoms with a 111 texturation). However, while this does not confirm a

111 texturation it also does not exclude it: Indeed, based on this TEM measurements and prior AFM and SEM measurements of NDs, a flat, flake-like structure of the NDs could be assumed. For the orientation of the NV<sup>-</sup>-center this would have quite relevant implications (see Figure 1 in section 1.2) illustrated in Figure 8 (the blue arrow marks the NV<sup>-</sup>-center while the red arrows represent external spins of interest). This however, has to be confirmed by future AFM and SEM measurements (preferably on the same spot, using AFM for the xy-parameter and SEM for the z-parameter). Existing models<sup>[7]</sup> could be further improved.



Figure 8 Schematic image of the implications of a flat, flake-like shape of the NDs with an assumed 111 texturation (with the NV<sup>-</sup>-center's main axis along the (111) crystal axis). The blue arrow marks the NV<sup>-</sup>-center while the red arrows represent external spins of interest (e.g. ROS).

While literature on the shape of NDs is scarce, the {111} planes are known as the planes of the lowest cleavage energy and strength in diamond<sup>[34,35]</sup>. Thus, cleavage occurs preferentially at (111) plane<sup>[36]</sup>.

The obtained crystallite sizes (using the Rietveld method) and the lattice parameters obtained by XRD can be found in Table 8 (for the full analysis report see the annex):

Table 8 Crystallite sizes and lattice parameters obtained by XRD

| Diamond                         | Crystallite Size [nm] | Lattice Parameters [Å] |
|---------------------------------|-----------------------|------------------------|
| <b>25 nm (Microdiamant AG)</b>  | 13.8 (1)              | 3.5652828(1)           |
| <b>75 nm (Microdiamant AG)</b>  | 38.54(26)             | 3.56675(15)            |
| <b>125 nm (Microdiamant AG)</b> | 44.59(23)             | 3.56663(11)            |

These values are in alignment with the DLS measurements: Smaller crystallite sizes are expected (especially for nanoparticles) due to the fact that with XRD, we can only observe “perfect” crystals. For the 75 nm ND sample, also SiC (likely as contamination from the production process) could be observed (indeed, Si was observed by XPS as covered in section 3.1.3). For the biggest NDs of 125 nm median size, NaHCO<sub>3</sub> was found (likely also contamination).

Considering the shape of NDs is therefore essential: Not only has it important implications on magnetometry, but it might also have impact on the biocompatibility (e.g. for Ag nanoparticles shape-dependent toxicity has been found<sup>[37]</sup>). The (surface) curvature, being a parameter for the protein corona of nanoparticles<sup>[14,15,19–21,38]</sup>. This underlines how the understanding of the bare NDs is interconnected with the understanding of phenomena such as the protein corona formation or the cellular uptake.

## 3.1.3 X-ray photoelectron spectroscopy (XPS)

The NDs of 25 nm size (Microdiamant AG) were measured on 3 different spots with XPS. Exemplarily, the spectrum for the first spot is shown in Figure 9. The full measurement information including the peak fittings for the elements of interest for all 3 spots are to be found in the annex. In Table 9 till Table 11 the element information is summarized. Even though very similar results could be obtained for the three spots, there are significant differences: Phosphorus (clearly a contamination) was only found in the first spot. Si could be found in every spot and is most probably present in the form of SiC (as already found by XRD in the 75 nm ND sample). Sodium in spot 3 could be present as NaHCO<sub>3</sub> (see XRD results in section 3.1.2). Because of these differences, the results are listed separately for each spot and not summarized in one table (likewise, no standard deviation was calculated for the atom ratios). Furthermore, relevant amounts of nitrogen were found.

Table 9 XPS results for NDs of 25 nm of median size (Microdiamant AG) – Spot 1. For more details see the annex.

| XPS   | B.E. [eV] | Atom [%] |
|-------|-----------|----------|
| P 2p  | 135.9     | 0.18     |
| N 1s  | 401.7     | 0.45     |
| Si 2p | 104.9     | 1.65     |
| C 1s  | 287.4     | 86.07    |
| O 1s  | 534.4     | 11.65    |

Table 10 XPS results for NDs of 25 nm of median size (Microdiamant AG) – Spot 2. For more details see the annex.

| XPS   | B.E. [eV] | Atom [%] |
|-------|-----------|----------|
| N 1s  | 400.3     | 0.40     |
| Si 2p | 105.5     | 4.69     |
| Si 2s | 155.8     | 4.60     |
| C 1s  | 287.4     | 74.62    |
| O 1s  | 534.7     | 15.69    |

Table 11 XPS results for NDs of 25 nm of median size (Microdiamant AG) – Spot 3. For more details see the annex.

| XPS   | B.E. [eV] | Atom [%] |
|-------|-----------|----------|
| N 1s  | 401.8     | 0.35     |
| Si 2p | 106.3     | 5.21     |
| C 1s  | 287.8     | 76.39    |
| O 1s  | 534.9     | 17.13    |
| Na 1s | 1074.8    | 0.92     |

Usually, XPS is known to be surface relevant method giving information typically from the top 10 nm of the sample. For NDs of 25 nm size, however, this means the core of the nanoparticles (the word “bulk” is avoided on purpose as we speak of relatively small nanoparticles).

Still, the peak fittings of carbon 1s peak are of major interest as summarized in Table 12:

Table 12 Summary of the peak fitting of carbon (1s) of all the 3 spots measured (NDs of 25 nm of median size, Microdiamant AG).

| Peak ID                     | Avg. Group% [%] | Std. Dev. [%] | Rel. Std. Dev. [%] |
|-----------------------------|-----------------|---------------|--------------------|
| <b>Carboxylate ("Pk03")</b> | 0.00            | -             | -                  |
| <b>Alcohol ("Pk02")</b>     | 78.90           | 0.92          | 1.17               |
| <b>Alkyl ("Pk01")</b>       | 21.10           | 0.92          | 4.37               |

Here, "Pk01" refers to carbon in alkyl groups (in this case, this means mostly  $sp^3$  hybridized carbon of the diamond core of the nanoparticle) while "Pk02" refers to alcohol groups (probably from the oxygen-terminated surface) or amine/amide groups (not likely to be present in the sample)<sup>4</sup>. The "Pk03" peak fitted into the carbon peak means (amongst others possibilities such as amide and (hemi)acetale groups) aldehyde and carboxylate groups: These are not present in the sample (see appendix for more details). Differentiation between  $sp^3$  carbon from the "bulk" diamond and  $sp^3$  carbon due with a more sophisticated peak fitting was not undertaken (and is possibly very difficult due to the too low resolution of the spectrum). Even though the spectra are scaled to C-C ("Pk01") = 284.8 eV, for some samples, the binding energy is 287.4 which is the highest point of the carbon peak and refers to 287.4 ("Pk02"), C-O and C-N (see Table 9 till Table 11 and Figure 9).

This is why the results of the oxygen peak fitting (oxygen 1s) are even more relevant, as the oxygen signal can be expected to originate from the oxygen-terminated surface of the diamond only (at least with good enough approximation):

Table 13 Summary of the peak fitting of oxygen (1s) of all the 3 spots measured (NDs of 25 nm of median size, Microdiamant AG).

| Peak ID                                      | Avg. Group% [%] | Std. Dev. [%] | Rel. Std. Dev. [%] |
|--|-----------------|---------------|--------------------|
| <b>Carboxylic Acid ("Pk02")</b>              | 74.27           | 27.11         | 36.60              |
| <b>Carboxylate/ Carboxylic Acid ("Pk01")</b> | 25.73           | 27.11         | 1.05               |

Here, "Pk01" stands for carboxylate groups ( $\text{COO}^-$ ) as well as amide (not likely to be present in the sample) and one of the oxygen atoms in the carboxylic acid ( $\text{O}=\text{C}-\text{OH}$ ) and "Pk02" refers to the other oxygen in the carboxylic acid ( $\text{O}=\text{C}-\text{O}-\text{H}$ ). This is of course well in alignment with the expectations when measuring an oxygen-terminated surface.

<sup>4</sup> The nomenclature was kept in order to remain compatible with the full analysis reports in the annex.

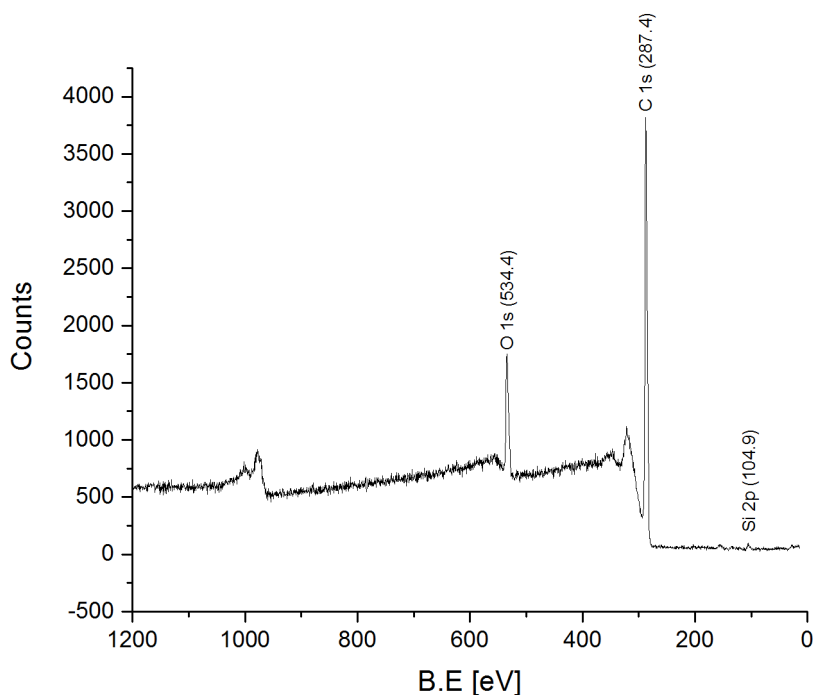


Figure 9 XPS spectrum of the NDs of 25 nm size (Microdiamant AG). Exemplarily shown for the measurement at the first spot. The complete measurement information including the peak fittings for the elements for this spot as well as for the other three spots measured can be found in the annex.

### 3.1.4 Conclusion

Diamond slurries from Microdiamant AG with 75 nm and 125 nm median size have a size distribution that is not significantly different from those of the NDs from Adámas Technologies of 70 nm and 120 nm size. Rather than a spherical shape assumed in current models<sup>[7]</sup>, a blocky shape and even a flat, flake-like structure can be assumed. This has to be confirmed by future AFM and SEM measurements (preferably on the same spot, using AFM for the xy-parameter and SEM for the z-parameter).

Considerable effects of the shape are expected to go beyond magnetometry related questions. Cell uptake and biocompatibility can be expected to be shape-dependent too. Therefore understanding the shape is of crucial importance for the biological application of the nanoparticles.

The surface chemistry, as revealed by XPS is characteristic for an oxygen-terminated surface. For NDs as small as 25 nm, however, the XPS spectra contain also information from the ND bulk (typically, XPS gives information of 10 nm depth). Future work could yield better results by an enhanced peak fitting procedure, fitting a diamond peak beneath the C 1s peak instead of an alkyl peak as done in this thesis.

Possibly – with high enough resolution – it is possible to distinguish between carbon at the surface of the diamond and carbon from the ND bulk.

## 3.2 Nanodiamond Aggregation

### 3.2.1 Dynamic Light Scattering (DLS) Measurements

DLS measurements undertaken to investigate the aggregation are summarized in Table 14 (with disposable sizing cuvettes) and Table 15 (with disposable folded capillary cells). For simplicity, ND of 25 nm of median size (Microdiamant AG) are referred to as “diamonds”. NDs in 10% FBS show only a slight increase of the hydrodynamic diameter (measured number mean from section 3.1:  $34.1 \pm 1.2$  nm). This in accordance with the fact that for the unwashed sample in 10% FBS, hardly any precipitation is visible with bare eyes while for the washed sample even no immediate precipitation can be observed. The situation after 24 hours is shown in the picture in Figure 10.

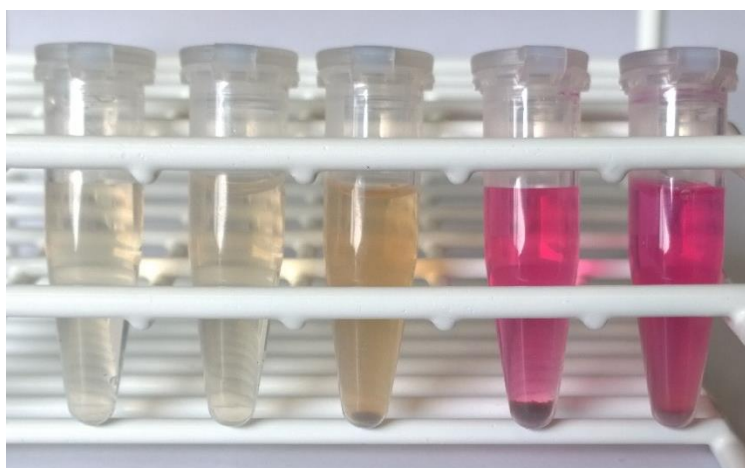


*Figure 10 Precipitation with NDs of 25 nm median size after 24 hours. From left to right: ND in DI water, ND in 10% FBS, ND in pure FBS, ND in DMEM (without FBS), ND in DMEM with 10% FBS.*

For the complete DMEM medium including 10% FBS huge results in considerable aggregates. Even though the number mean of  $188.7 \pm 19.5$  nm (washed:  $101.8 \pm 81.8$  nm) does not seem to be dramatic change (obtained using disposable sizing cuvettes), indeed relevant aggregation takes places (the corresponding Z-Average underlies this fact). The increasing (relative) standard deviation is increasing reflects the formation of big non-homogenous (and polydisperse) aggregates.

This explains the partly big differences between the results in Table 14 and Table 15, however the different cuvettes do have an effect too: In disposable folded capillary cells, homogenization is much more difficult (and even a different sedimentation behavior can be assumed).

For NDs in DMEM without any FBS, even micron-sized aggregates were observed (due to the salting-out effect known also known from literature<sup>[25]</sup>) that – as expected – (nearly) dissolve in the washing water.



## Results and Discussion

Table 14 DLS measurements related to aggregation in DMEM medium (using disposable sizing cuvettes)

| Sample                                      | Z-Average ± Std. Dev [nm] | Rel. Std-Dev [%] | PdI ± Std. Dev. | Rel. Std-Dev. [%] | Number Mean ± Std. Dev. [nm] | Rel. Std-Dev. [%] |
|---|---------------------------|------------------|-----------------|-------------------|------------------------------|-------------------|
| <b>10% FBS (Control)</b>                    | 34.9 ± 18.0               | 51.6             | 0.6 ± 0.2       | 35.62             | 5.6 ± 0.6                    | 9.8               |
| <b>10% FBS + Diamonds</b>                   | 84.6 ± 0.6                | 0.7              | 0.2 ± 0.2       | 6.0               | 51.9 ± 4.5                   | 8.6               |
| <b>10% FBS + Diamonds washed</b>            | 115.4 ± 2.9               | 2.5              | 0.4 ± 0.2       | 3.1               | 41.8 ± 6.2                   | 14.8              |
| <b>DMEM + 10% FBS + Diamonds</b>            | 713.1 ± 44.7              | 6.3              | 0.4 ± 0.1       | 22.4              | 188.7 ± 19.4                 | 10.3              |
| <b>DMEM + 10% FBS + Diamonds washed</b>     | 516.8 ± 75.5              | 14.6             | 0.5 ± 0.2       | 14.5              | 101.8 ± 81.8                 | 80.4              |
| <b>DMEM (without FBS) + Diamonds</b>        | 1904.7 ± 164.5            | 8.6              | 0.2 ± 0.2       | 14.4              | 1977.7 ± 130.2               | 6.6               |
| <b>DMEM (without FBS) + Diamonds washed</b> | 92.7 ± 2.6                | 2.8              | 0.1 ± 0.2       | 25.6              | 56.9 ± 2.2                   | 3.9               |

Table 15 DLS measurements related to aggregation in DMEM medium (disposable folded capillary cells)

| Sample                                      | Z-Average ± Std. Dev [nm] | Rel. Std-Dev [%] | PdI ± Std. Dev. | Rel. Std-Dev. [%] | Number Mean ± Std. Dev. [nm] | Rel. Std-Dev. [%] |
|---|---------------------------|------------------|-----------------|-------------------|------------------------------|-------------------|
| <b>10% FBS (Control)</b>                    | 18.5 ± 0.8                | 4.4              | 0.5 ± 0.1       | 12.0              | 5.3 ± 0.3                    | 6.0               |
| <b>10% FBS + Diamonds</b>                   | 91.6 ± 2.6                | 2.8              | 0.2 ± 0.0       | 0.6               | 54.1 ± 3.4                   | 6.2               |
| <b>10% FBS + Diamonds washed</b>            | 102.9 ± 2.1               | 2.1              | 0.3 ± 0.0       | 5.0               | 54.6 ± 2.3                   | 4.2               |
| <b>DMEM + 10% FBS + Diamonds</b>            | 797.5 ± 36.8              | 4.6              | 0.5 ± 0.1       | 12.1              | 302.7 ± 302.0                | 99.7              |
| <b>DMEM + 10% FBS + Diamonds washed</b>     | 504.8 ± 5.2               | 1.0              | 0.5 ± 0.1       | 10.7              | 156.8 ± 14.6                 | 9.3               |
| <b>DMEM (without FBS) + Diamonds</b>        | 4107.3 ± 999.2            | 24.3             | 0.3 ± 0.1       | 26.5              | 3712.7 ± 14.6                | 0.4               |
| <b>DMEM (without FBS) + Diamonds washed</b> | 94.4 ± 2.1                | 2.2              | 0.1 ± 0.0       | 3.3               | 59.5 ± 3.7                   | 6.2               |

Figure 11 visualizes the number means printed in Table 14 and Table 10:

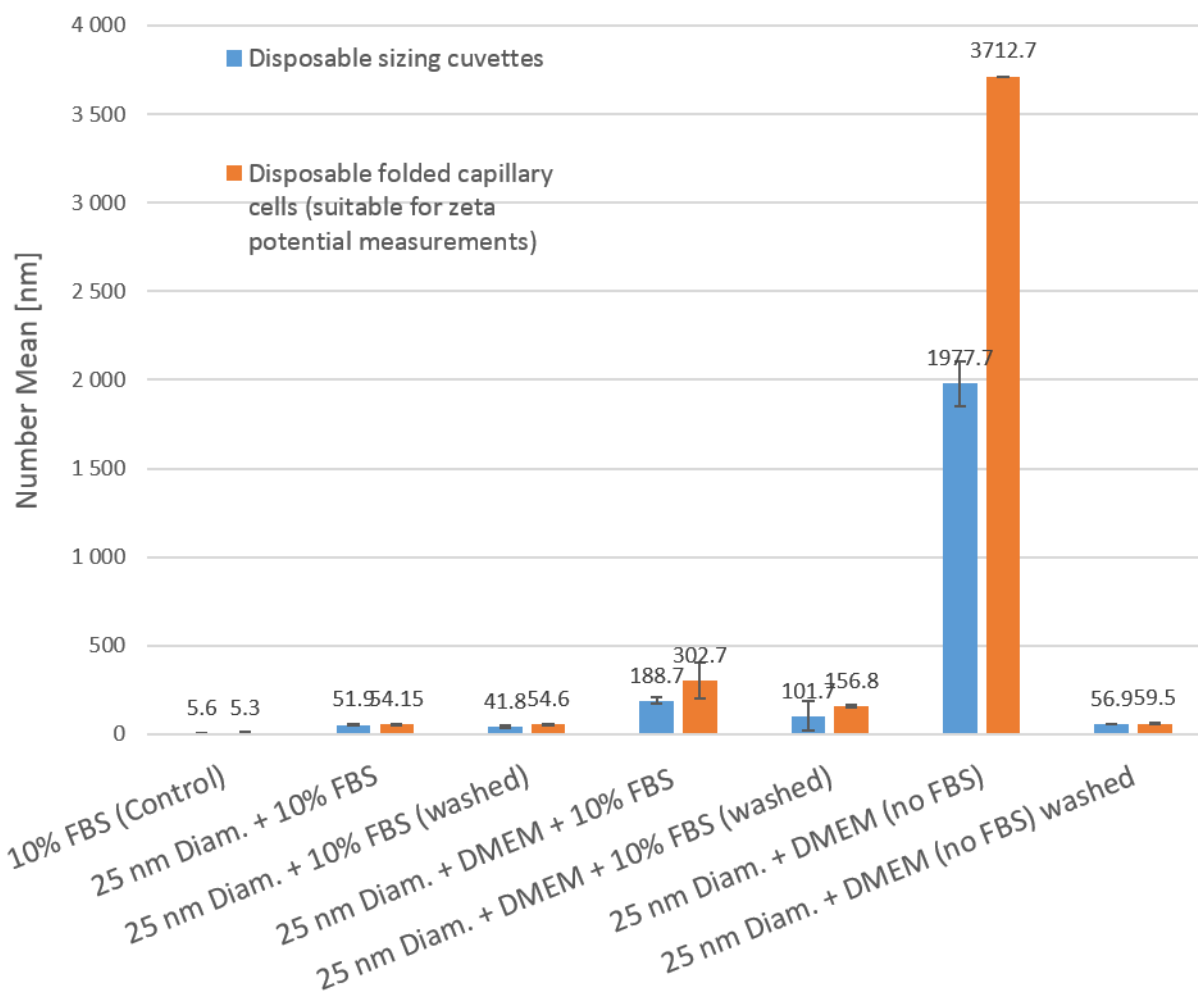


Figure 11 Blue: Measurements with disposable sizing cuvettes. Orange: Measurements with disposable folded capillary cells. The error bar corresponds to the standard deviation.

The corresponding zeta potentials measured are listed in Table 16:

Table 16 Zeta potential measurements related to aggregation in DMEM medium

| Sample                                   | Zeta potential ± Std. Dev [mV] | Rel. Std. Dev [%] |
|--|--------------------------------|-------------------|
| 10% FBS (Control)                        | -15.80 ± 0.52                  | 3.29              |
| 25 nm Diamonds + 10% FBS                 | -18.13 ± 0.21                  | 1.15              |
| 25 nm Diamonds + 10% FBS (washed)        | -27.90 ± 1.15                  | 4.13              |
| 25 nm Diamonds + DMEM + 10% FBS          | -9.85 ± 0.88                   | 8.95              |
| 25 nm Diamonds + DMEM + 10% FBS (washed) | -28.37 ± 0.12                  | 0.41              |
| 25 nm Diamonds + DMEM (no FBS)           | -19.83 ± 1.19                  | 6.02              |
| 25 nm Diamonds + DMEM (no FBS) washed    | -37.43 ± 0.31                  | 0.82              |

Clearly, FBS leads only to a small increase of the hydrodynamic diameter while the salting-out effect leads to huge inhomogeneous polydisperse aggregates. In fact, proteins mitigate the aggregation tendency significantly, however still not enough to prevent relevant size increase. The changes in the

zeta potential as illustrated in Table 16 highlight this by the increase towards 0 mV (The rapid sedimentation for the diamonds in DMEM without FBS must be taken into account when interpreting the zeta potential of  $-19.83 \pm 1.19$  mV: Precipitated particles will not participate in the electrophoresis used to measure the zeta potential!). As a possible countermeasure for aggregation, diamonds have been measured in 100% FBS and then, added to DMEM. As shown in Table 17, while the aggregation phenomenon is still present (both in 100% FBS and the sample with diamonds added to 100% FBS before uniting it with DMEM to yield the final complete cellular medium), there is a significantly lower hydrodynamic size in contrast to the sample “DMEM + FBS + Diamonds” (for these samples, not zeta potential has been measured):

Table 17 DLS measurements aiming at mitigating the aggregation behavior for practical use.

| Sample                                  | Z-Average $\pm$ Std. Dev [nm] | Rel. Std-Dev [%] | PdI $\pm$ Std. Dev. | Rel. Std-Dev. [%] | Number Mean $\pm$ Std. Dev. [nm] | Rel. Std-Dev. [%] |
|---|-------------------------------|------------------|---------------------|-------------------|----------------------------------|-------------------|
| <b>100% FBS (Control)</b>               | 17.1 $\pm$ 0.3                | 1.7              | 0.5 $\pm$ 0.0       | 0.5               | 5.3 $\pm$ 0.1                    | 2.4               |
| <b>100% FBS + Diamonds</b>              | 554.3 $\pm$ 8.9               | 1.6              | 0.5 $\pm$ 0.0       | 8.1               | 510.3 $\pm$ 71.3                 | 14.0              |
| <b>DMEM + FBS + Diamonds</b>            | 1042.0 $\pm$ 32.5             | 3.1              | 0.5 $\pm$ 0.0       | 3.9               | 515.6 $\pm$ 382.8                | 74.3              |
| <b>Diamonds added to FBS, then DMEM</b> | 561.0 $\pm$ 129.5             | 23.1             | 0.7 $\pm$ 0.0       | 4.0               | 102.5 $\pm$ 52.5                 | 51.2              |

Thus, conjugating diamonds with FBS before adding them to DMEM medium is a viable option for biological application.

For NDs in YMB each sample was measured three times: Results are shown in Table 18. A zeta potential of  $-22.97$  mV (standard deviation: 1.43 mV; relative standard deviation: 6.22 %) was measured. Measurements for ND in YMB were performed in cooperation with Sona Guluzade.

Table 18 DLS measurements of ND aggregation in YMB

| Sample                | Z-Average $\pm$ Std. Dev [nm] | Rel. Std-Dev [%] | PdI $\pm$ Std. Dev. | Rel. Std-Dev. [%] | Number Mean $\pm$ Std. Dev. [nm] | Rel. Std-Dev. [%] |
|-----------------------|-------------------------------|------------------|---------------------|-------------------|----------------------------------|-------------------|
| <b>YMB + Diamonds</b> | 3112.0 $\pm$ 335.4            | 10.8             | 0.4 $\pm$ 0.1       | 24.3              | 1701.7 $\pm$ 289.4               | 17.0              |

The phenomenon of aggregation of NDs in YMB can be attributed to the salting out effect, analogously to the situation in DMEM without FBS.

### 3.2.2 X-ray photoelectron spectroscopy (XPS)

The element ratios for the most abundant atoms, calculated based on the known medium compositions (see in the annex), are listed in Table 19.

For various reasons, carbon was not taken into account: Differentiation between  $sp^3$  carbon from diamond and  $sp^3$  carbon from cell medium sources is virtually not possible. Moreover, having an oxygen-terminated diamond surface (which is not clearly defined) means the presence of groups such as the carboxyl- or alcohol group. This is why also oxygen has been excluded from the consideration.

Table 19 Element ratios for DMEM and YMB

|             | N [%] | Mg [%] | Na [%] | P [%] | S [%] | Cl [%] | K [%] | Ca [%] |
|-------------|-------|--------|--------|-------|-------|--------|-------|--------|
| <b>DMEM</b> | 13.0  | 0.2    | 41.4   | 0.3   | 4.7   | 38.9   | 1.3   | 0.3    |
| <b>YMB</b>  | 54.2  | 4.1    | 1.7    | 11.3  | 13.2  | 7.3    | 7.2   | 0.9    |

The summary of the XPS results for the NDs of 25 nm of median size (Microdiamant AG) in DMEM with 10% FBS are listed in Table 20 and Table 21 (atomic ratios without carbon and oxygen) and the spectrum is displayed in Figure 12. The detailed results including the peak fitting for this as well as the following samples can be found in the annex in section 5.3.

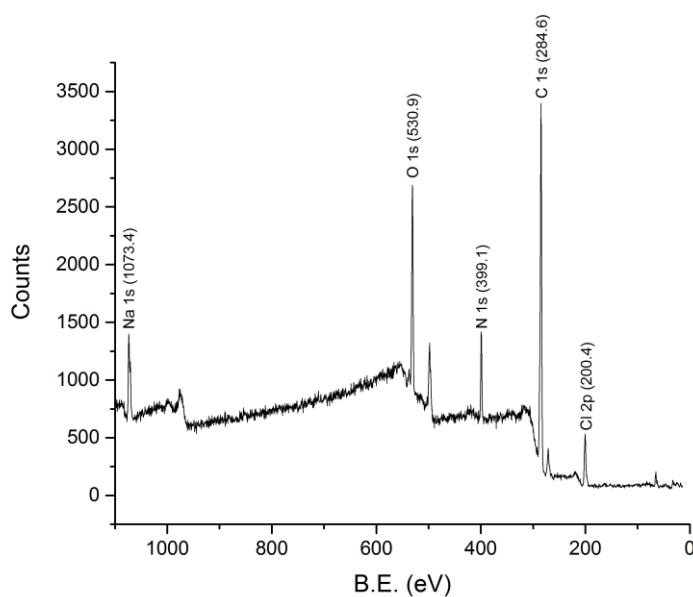


Figure 12 XPS spectrum for the NDs of 25 nm of median size (Microdiamant AG) in DMEM with 10% FBS

Table 20 XPS results for NDs of 25 nm of median size (Microdiamant AG) in DMEM with 10% FBS

| XPS Line     | B.E. [eV] | Atom [%] |
|--------------|-----------|----------|
| <b>Cl 2p</b> | 200.4     | 4.61     |
| <b>C 1s</b>  | 284.6     | 65.73    |
| <b>N 1s</b>  | 399.1     | 8.39     |
| <b>O 1s</b>  | 530.9     | 16.45    |
| <b>Na 1s</b> | 1073.4    | 4.82     |

## Results and Discussion

Table 21 Atomic ratios for NDs of 25 nm of median size (Microdiamant AG) in DMEM with 10% FBS without carbon and oxygen taken into account.

| XPS Line | Norm Area | Atom% [%] |
|----------|-----------|-----------|
| Cl       | 68.10     | 25.89     |
| N        | 123.80    | 47.07     |
| Na       | 71.10     | 27.03     |

In a complex mixture such as DMEM, yet alone with 10% FBS, the peak fit of carbon does not provide much additional information: An increase of alkyl-groups (“Pk01”) could be observed, while the relative amount of alcohol (and amine/amide) decreased. In exchange an increase of amide/carboxylate groups (as well as aldehyde, (hemi)acetal) as well as carboxylic groups (marked as “Pk04” in the analysis report in the annex) was found: This is clearly due to the absorption of proteins, however a more detailed assignment to medium components is not possible. Likewise, the complexity of the sample does not allow a more detailed interpretation of the oxygen peak fitting.

The same is qualitatively true for all the other samples discussed in the following (with the exception the carboxylic group, “Pk04”, could not be identified).

Results for NDs of 25 nm of median size (Microdiamant AG) in DMEM (without FBS) are summarized in Table 22 and Table 23 (without carbon and oxygen). As the sample was measured twice (at different spots), the first measurement is referred to as “A” and the second as “B”, respectively. The spectra are shown in Figure 13 and Figure 14.

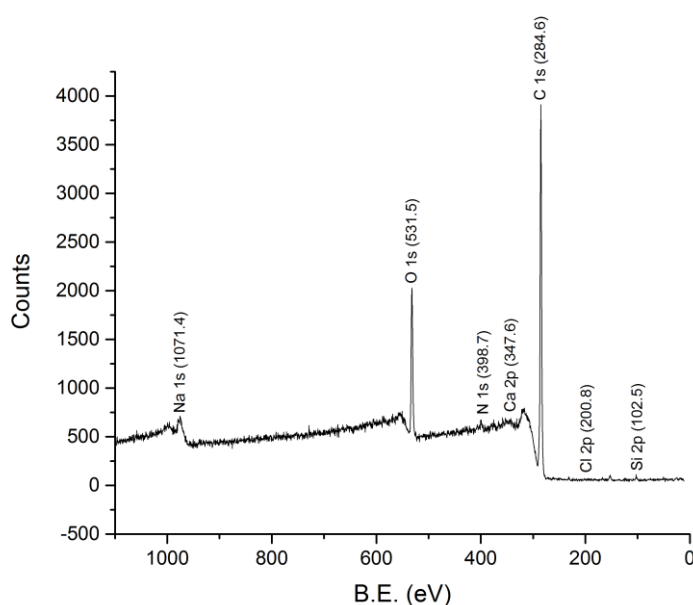


Figure 13 XPS spectrum NDs of 25 nm of median size (Microdiamant AG) in DMEM (without FBS) - Spot A

## Results and Discussion

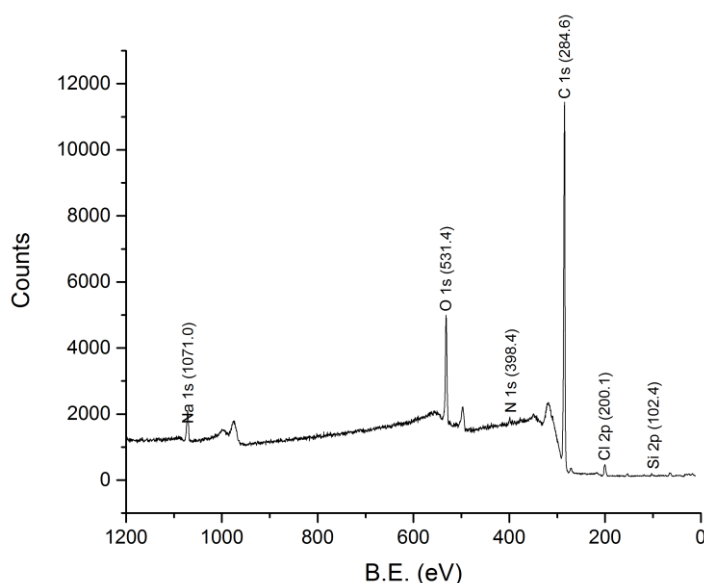


Figure 14 XPS spectrum NDs of 25 nm of median size (Microdiamant AG) in DMEM (without FBS) - Spot B

Table 22 XPS results for NDs of 25 nm of median size (Microdiamant AG) in DMEM without FBS

| XPS Line | B.E. Spot A [eV] | Atom% Spot A [%] | B.E. Spot B [eV] | Atom% Spot B [%] |
|----------|------------------|------------------|------------------|------------------|
| Si 2p    | 102.5            | 0.83             | 102.4            | 0.61             |
| Cl 2p    | 200.8            | 1.31             | 200.1            | 1.57             |
| C 1s     | 284.6            | 80.39            | 284.6            | 81.76            |
| Ca 2p    | 347.6            | 0.64             | -                | -                |
| N 1s     | 398.7            | 1.93             | 398.4            | 1.51             |
| O 1s     | 531.5            | 12.59            | 531.4            | 12.09            |
| Na 1s    | 1071.4           | 2.31             | 1071.0           | 2.46             |

Table 23 Atomic ratios for NDs of 25 nm of median size (Microdiamant AG) in DMEM without FBS without carbon and oxygen taken into account.

| Element | Norm Area Sample A | Atom% Spot A [%] | Norm Area Sample B | Atom% Spot B [%] |
|---------|--------------------|------------------|--------------------|------------------|
| Si      | 37.10              | 11.86            | 33.2               | 9.98             |
| Cl      | 58.40              | 18.66            | 84.7               | 25.45            |
| Ca      | 28.50              | 9.11             |                    |                  |
| N       | 86.00              | 27.48            | 81.8               | 24.58            |
| Na      | 102.90             | 32.89            | 133.1              | 39.99            |

The conclusions that can be drawn of the measurements with NDs of 25 nm of median size (Microdiamant AG) in DMEM with and without FBS are:

- A considerably higher ratio of nitrogen mirrors the adsorbed proteins (in the sample containing FBS compared to the one without).

- Sodium chloride is the main driving force for aggregation of NDs. While the presence of sodium chloride is known to hamper the detection of other compounds (in any case, compounds with an atom ratio of approx. 0.5% should be detectable with the instrument used), other inorganic salts are indeed of minor relevance.
- The silicon originates from contaminations, either in the medium or in the diamond material itself, which was also shown by XRD analysis (see section 3.1).
- The fact that Ca could not be measured in every sample, and in the sample without FBS in spot B only, can be seen as evidence for quite inhomogeneous aggregation. As in DMEM Ca makes up only about 0.3% of the atoms, there might be a role for the calcium (as the most abundant double charged ion) in the aggregation process (e.g. interaction with carboxyl groups on the diamond surface).
- Potassium and phosphorus, even though present at relatively high concentrations, does not play a role in the aggregates.

NDs of 25 nm of median size (Microdiamant AG) in YMB where measured at three different spots. The spectrum of Spot A is exemplarily shown in Figure 15 (see the annex for the full analysis report of all spots measured).

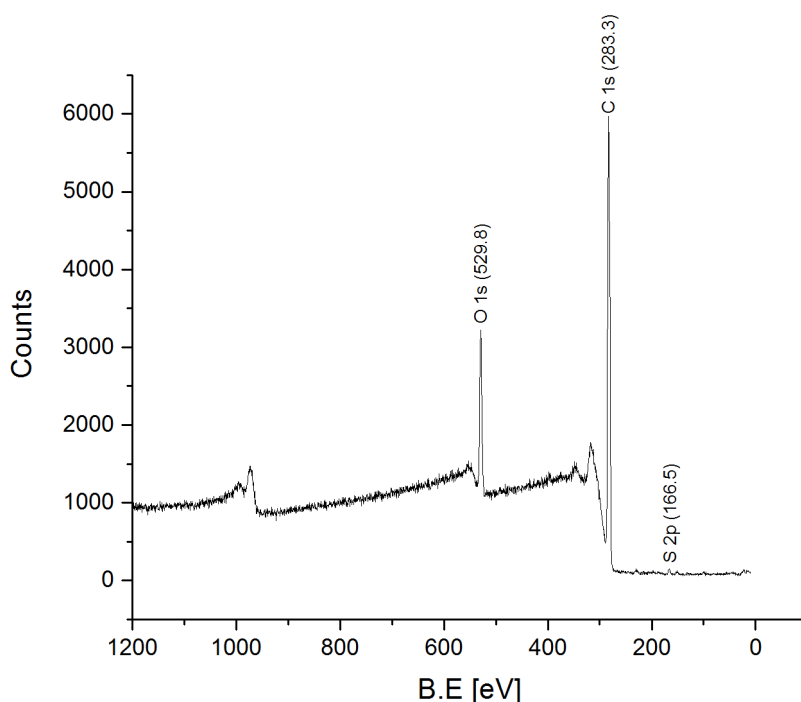


Figure 15 XPS spectrum of NDs of 25 nm of median size (Microdiamant AG) in YMB (Spot A)

In Table 24 till Table 26 the element ratios (in percent) are listed:

Table 24 XPS results for NDs of 25 nm of median size (Microdiamant AG) in YMB – Spot A

| XPS Line | B.E. [eV] | Atom% [%] |
|----------|-----------|-----------|
| P 2p     | 131.4     | 0.18      |
| N 1s     | 398.7     | 0.39      |
| S 2p     | 166.5     | 0.61      |
| C 1s     | 287.0     | 85.96     |
| O 1s     | 533.5     | 12.86     |

Table 25 XPS results for NDs of 25 nm of median size (Microdiamant AG) in YMB – Spot B

| XPS Line | B.E. [eV] | Atom% [%] |
|----------|-----------|-----------|
| S 2p     | 170.8     | 0.57      |
| C 1s     | 286.8     | 87.09     |
| O 1s     | 533.8     | 12.35     |

Table 26 XPS results for NDs of 25 nm of median size (Microdiamant AG) in YMB – Spot C

| XPS Line | B.E. [eV] | Atom% [%] |
|----------|-----------|-----------|
| P 2p     | 135.2     | 0.17      |
| N 1s     | 401.3     | 0.63      |
| Si 2s    | 151.7     | 0.93      |
| S 2p     | 170.5     | 0.83      |
| C 1s     | 287.0     | 84.55     |
| O 1s     | 533.6     | 12.88     |

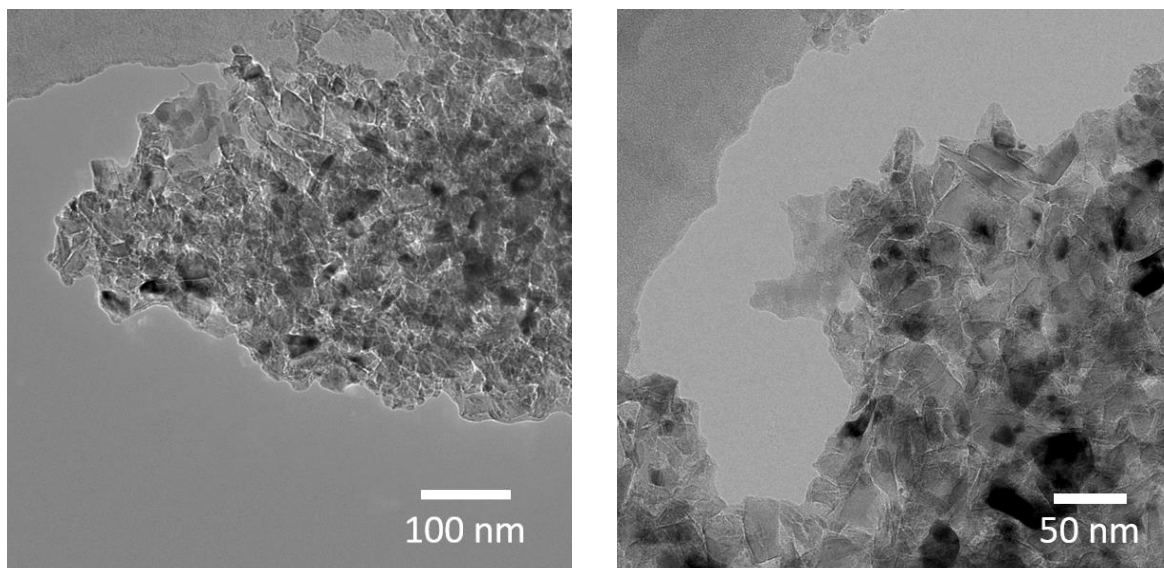
Interestingly, despite relatively big aggregates, in contrast to the samples with NDs in DMEM, sodium chloride is entirely absent. At this point, the exact mechanism for the aggregation process for both the DMEM medium and the YMB remains an educated guess only, however it does seem to be connected with the change of the zeta potential. In DMEM, this seems to be mainly driven by the sodium chloride, while in YMB nitrogen salts alongside smaller amounts of phosphorus and sulfur.

### 3.2.3 Transmission Electron Microscopy (TEM) Measurements

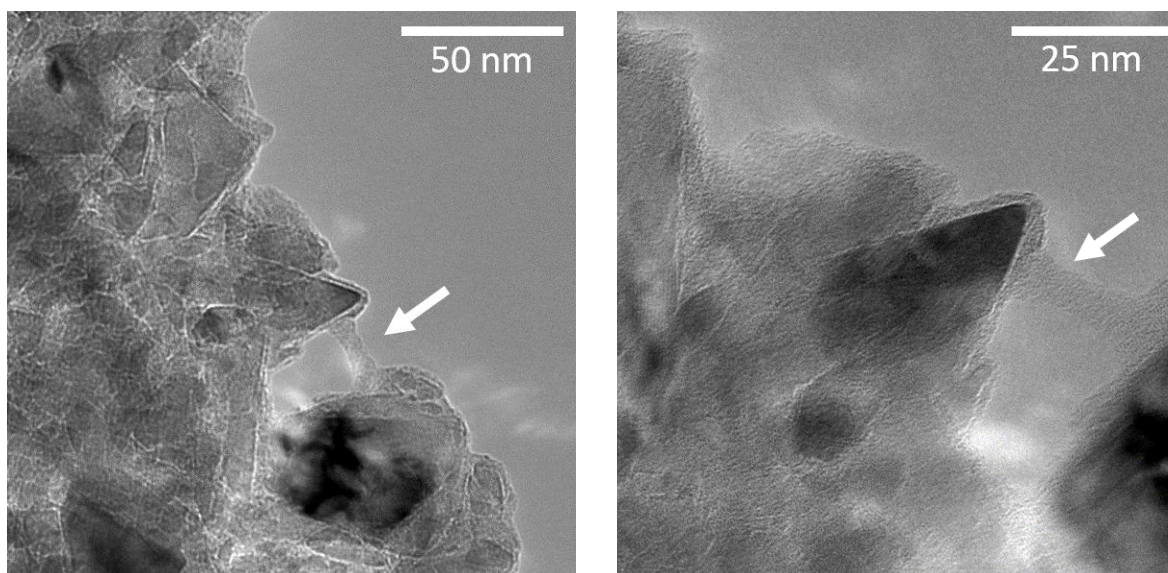
TEM images of 25 nm Diamonds (Microdiamant AG) + 10% FBS revealed huge aggregations. Figure 16 gives an overview and offers a possibility to estimate the size of the aggregations. However, drying of the sample on the TEM grids does not represent the situation in solution at physiological conditions. The diamonds are clearly recognizable by the phase contrast due to their higher density as well their sharp edges. Moreover, selected area diffraction (SAED) – data shown in section 3.1.2 – confirmed their identity.



Figure 17 shows the protein corona at a higher magnification. Clearly, proteins assemble around the crystalline diamonds (they appear brighter in the image due to lower electron density): The white arrow points at the proteins that forms a layer of approximately 2-3 nm thickness around the aggregates. These images are in line with the results of the DLS measurements: “Clusters” of NDs are formed proteins (acting as “glue”) around.



*Figure 16 Aggregates with 25 nm NDs (Microdiamant AG) in DMEM with 10% FBS (The same sample is shown at different spots.). In the upper left part (in both images), the edges of the hole on the grid are visible.*



*Figure 17 Aggregates with 25 nm NDs (Microdiamant AG) in DMEM with 10% FBS. The image on the right shows the same spot with a higher magnification. The arrow points at the proteins that forms a layer of approximately 2-3 nm thickness. “Clusters” of NDs are formed with proteins (acting as a “glue”) around.*

For the aggregation formed with 25 nm diamonds (Microdiamant AG) with YMB, a fundamentally different situation presents itself as a result of the missing proteins. Figure 18 shows how the NDs aggregate at the edges of the hole on the grid due to the salting-out effect. Again, this finding is consistent with the results from the corresponding DLS measurements.

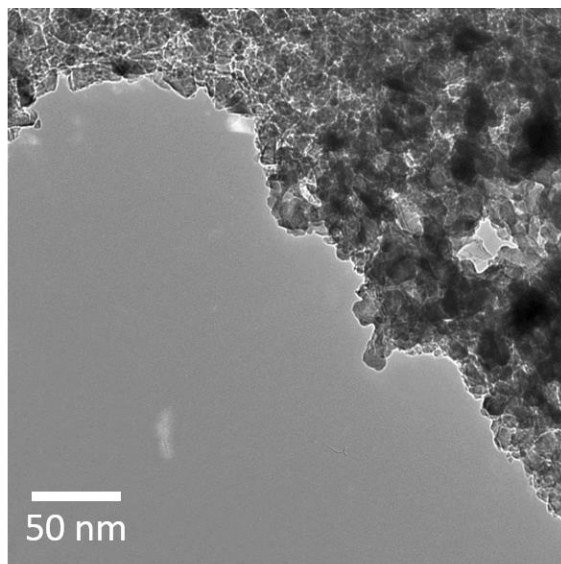


*Figure 18 25 nm ND (Microdiamant AG) aggregation with “yeast medium base without amino acids”*

#### 3.2.4 Analysis of the Protein Corona (MALDI-TOF-MS and nanoLC-MS/MS)

An excerpt of the MALDI-TOF-MS spectrum (2000 – 16000 Da) featuring the area with the most peaks is shown in Figure 19 (the full spectrum is shown in the annex). Mainly compounds of lower molecular masses (in relation to proteins) between approximately 2700 Da and 15000 Da can be found, which reflects the complexity of the sample. However, identification of the peaks based on literature<sup>[26,39]</sup> failed (neither peaks in reported in literature<sup>[39]</sup> nor the most abundant proteins of FBS<sup>[26]</sup> could be associated with peaks present in the spectrum).

Instead of a – possibly time consuming – optimization of the MALDI-TOF-MS method for higher protein masses (that may not even successful as inorganic salts present in DMEM might be responsible for ion suppression), a standard proteomics method involving a trypsin digest followed by a nanoLC-MS/MS analysis (as discussed in section 2.2.5) was undertaken. The results shall be discussed in the following pages.

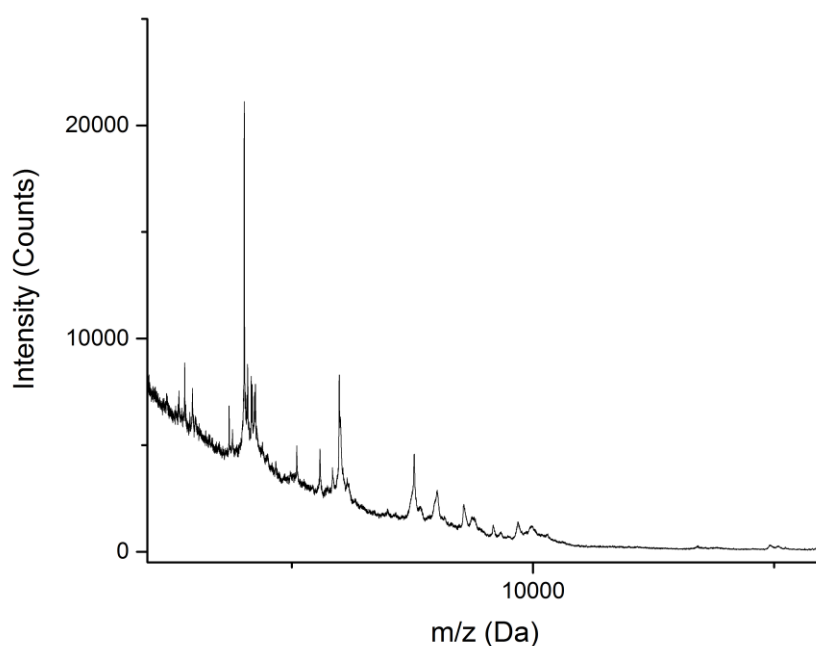


Figure 19 MALDI-TOF-MS Fingerprint of the protein corona

Table 27 shows the number of proteins that have been identified in the samples after a UniProtKB/Trembl search. The same data (using the same colors) is represented in Figure 20.

Table 27 Overview of the number of proteins found

|  | Sample 1 | Sample 2 | Sample 3 | Sample 4 | Unique #proteins | Total #Proteins |
|--|----------|----------|----------|----------|------------------|-----------------|
| Sample 1<br>FBS                                      | 23       | 0        | 0        | 0        | 2                | 25              |
| Sample 2<br>25 nm Diam. + 10% FBS                    | 10       | 3        | 0        | 0        | 0                | 13              |
| Sample 3<br>25 nm Diam. + 10% FBS<br>(washed)        | 19       | 2        | 26       | 0        | 6                | 53              |
| Sample 4<br>25 nm Diam. + DMEM + 10%<br>FBS          | 17       | 3        | 19       | 24       | 2                | 65              |
| Sample 5<br>25 nm Diam. + DMEM + 10%<br>FBS (washed) | 20       | 3        | 24       | 24       | 152              | 223             |

The FBS control sample results in a number of 25 proteins identified. In sample 2 (25 nm Diam. + 10% FBS) only a small amount of precipitation could be observed after centrifugation, and in sample 3 (which is the same as sample 2 but with a washing step added) virtually no precipitation was visible.

Therefore, proteins identified in sample 3 cannot be considered to originate from the diamond surface with full certainty (they could e.g. originate from the walls of the flask used).

Sample 4 (25 nm Diam. + DMEM + 10% FBS) results in 65 proteins identified, 24 of which are present only in sample 4 and sample 5, 2 of them unique to that sample. This reflects the complexity of the components (including inorganic salts) involved in the aggregation process. Washing of samples with DI water (done with sample 2 and sample 4) always yields a higher number of proteins, possibly washing away the “soft” corona so that proteins with higher affinity remain on the diamond surface. Due to easiness of the analysis this could be a very interesting and straightforward way to analyze trace components (e.g. very low abundant biomarkers) in complex solutions such as serum (without the otherwise overwhelming signal of the most abundant proteins such as serum albumin). It must be emphasized that proteins identified in samples 2-5 are also present in sample 1, however impossible to be detected under the measurement conditions as a result of the high abundance proteins in serum (especially Serum albumin and Alpha-2-HS-glycoprotein).

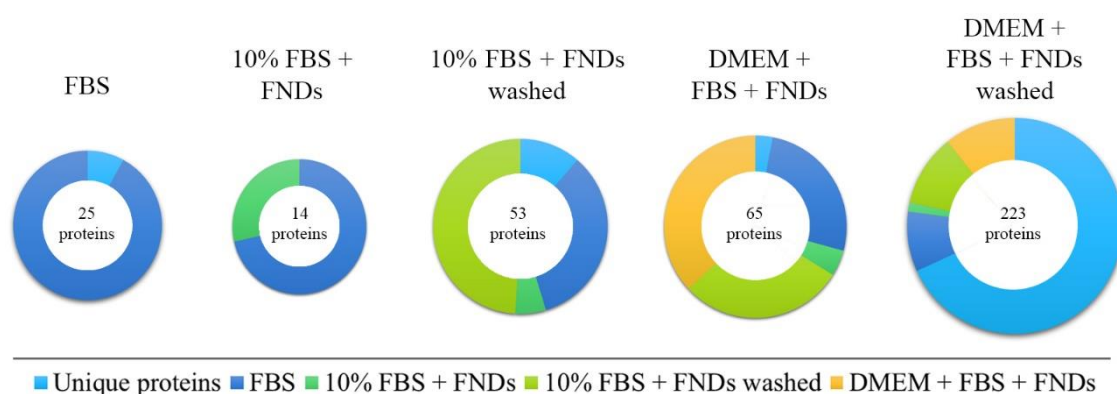


Figure 20 Overview of the number of proteins found

In Table 28 an overview over the proteins identified is given, ordered by the 30 most abundant proteins of sample 4 (25 nm Diam. + DMEM + 10% FBS), which is the most important sample as it reflects the situation present in the cell culture medium. The full list of proteins identified in samples 1-5 can be found in the annex: Table 17 till Table 26 list the identified proteins. The number of spectra assigned to a protein is given (“#Spectra” column) as well as the PEAKS Peptide Score (“-10lgP” column). It is calculated as the weighted sum of the -10lgP scores of the protein's supporting peptides, that are derived from the p-value that indicate the statistical significance of the peptide-spectrum match by an algorithm described by Zhang et al<sup>[40]</sup>. The proteins numbers provided above take redundant proteins into account: This is because some proteins are both in the Swiss-Prot database (manually annotated and reviewed) and the TrEMBL database (automatically annotated and not reviewed and therefore highly redundant). Duplicate proteins are listed in separate tables in the annex.

A semi-quantitative assessment of (relative) protein amounts was conducted using normalized spectral counts given by the following equation<sup>[18,21,41]</sup>:

$$NpSpC_k = \left( \frac{(SpC/M_w)_k}{\sum_{i=1}^n (SpC/M_w)_i} \right) * 100$$

where  $NpSpC_k$  is the normalized percentage of spectral count (which is the number of spectra associated to a protein) for protein  $k$ ,  $SpC$  is the spectral count identified, and  $M_w$  is the molecular weight (in Da) of the protein  $k$ . The protein corona does not reflect the relative abundance of proteins of sample 1, which is the pure FBS, suggesting some specificity of the adsorption process.

Sample 1 revealed the most abundant proteins (also known from literature<sup>[21,26]</sup>): Serum albumin and Alpha-2-HS-glycoprotein make up 66% of the normalized spectral counts. Sample 2 and Sample 3 reflect that with pure FBS, hardly any aggregation is happening. The protein pattern closely resembles the one from sample 1.

For the most important sample 4 (as well as any other sample), no clear correlation between the adsorption to diamond and theoretic isoelectric point IEP (from [http://web.expasy.org/compute\\_pi/](http://web.expasy.org/compute_pi/)) or the average molecular mass could be found. Also, no significant difference between the (theoretical) IEP of the 25 most abundant proteins of sample 1 and sample 4 could be found. This is in alignment with other similar studies on other nanoparticles<sup>[20,21,38]</sup>. It can be explained with the fact, that proteins have an inhomogeneous distribution of charges at their surfaces<sup>[21]</sup>. Even with an overall negative net charge of the protein, positive charge domains may allow an electrostatic interaction with the particle surface<sup>[21]</sup>. For multiple layers protein-protein interactions also have to be taken into account, thus possibly reducing the importance of the charge and polarity of the nanodiamonds.

However, proteins present in sample 4 which are marked with green in Table 28 show a molecular function (based on information from <http://www.uniprot.org/>) related to binding to negative compounds (e.g. heparin or ATP). This is a possible explanation for the favored adsorption on the oxygen-terminated FNDs with a negative zeta potential.

Of notable interest is the relatively high abundance of apolipoproteins that have been connected to cellular uptake in several ways: Nanoparticles with adsorbed lipoproteins were reported to easily cross the blood—brain barrier and taken up by brain capillary endothelial cells<sup>[20]</sup>. The enrichment of apolipoproteins could indicate a binding of complete HDL complexes, suggesting that they may physiologically interact with receptors for the VLDL/LDL/HDL pathway<sup>[16]</sup>. Beta-2-glycoprotein 1 (Apolipoprotein H) promotes the internalization of nanoparticles into human mesenchymal stem cells<sup>[16]</sup>. It is known to bind to negatively charged phospholipids, which could explain the interaction

with cell membranes (and diamond surfaces), however it is still unclear if this is unspecific interaction or if it is receptor-mediated<sup>[16]</sup>.

Amongst the proteins of sample 4, Prothrombin, Gelsolin, Platelet factor 4, Fibulin-1 and Tetranectin (marked with a star in Table 28) are known to be binding to calcium, which is present in DMEM medium and was proven to play a role in the agglomeration process by XPS analysis.

To fully understand the fate of the FNDs in biological systems, the dynamical formation and change of the protein corona needs to be better understood. Conformal changes of proteins might change the biological functions, leading to changed biocompatibility, uptake or unexpected biological reactions. It has to be kept in mind, that the protein corona investigated is involved in the aggregation process. Nanoparticles that are (more) stable in a suspension (e.g. in sample 3, where there is only few aggregation and precipitation) there could be another protein corona with different proteins involved.

Table 28 Most abundant proteins (\*Ca-binding)

| Protein                                      | Accession              | Avg. Mass [Da] | IEP  | Sample 4<br>NpSpC <sub>i</sub> [%] | Sample 5<br>NpSpC <sub>i</sub> [%] | Sample 1<br>NpSpC <sub>i</sub> [%] | Sample 2<br>NpSpC <sub>i</sub> [%] | Sample 3<br>NpSpC <sub>i</sub> [%] | Molecular function   |
|--|------------------------|----------------|------|------------------------------------|------------------------------------|------------------------------------|------------------------------------|------------------------------------|--|
| Hemoglobin fetal subunit beta                | P02081 HBBF_BOVIN      | 15859          | 6.51 | 10.97                              | 6.20                               | 2.87                               |                                    | 8.68                               | Heme binding, iron binding, oxygen binding, oxygen transporter activity  |
| Hemoglobin subunit alpha                     | P01966 HBA_BOVIN       | 15184          | 8.19 | 10.74                              | 4.71                               | 5.24                               | 4.79                               | 5.67                               | Heme binding, iron binding, oxygen binding, oxygen transporter activity  |
| Serum albumin                                | P02769 ALBU_BOVIN      | 69294          | 5.60 | 9.34                               | 2.10                               | 32.32                              | 22.56                              | 16.64                              | DNA binding, drug binding, fatty acid binding, metal ion binding, oxygen binding, pyridoxal phosphate binding, toxic substance binding   |
| Alpha-2-HS-glycoprotein                      | P12763 FETUA_BOVIN     | 38419          | 5.10 | 8.92                               | 1.34                               | 34.02                              | 38.32                              | 15.46                              | Cysteine-type endopeptidase inhibitor activity   |
| Apolipoprotein A-II                          | P81644 APOA2_BOVIN     | 11202          | 7.80 | 4.85                               | 1.90                               | 2.03                               |                                    | 1.54                               | Cholesterol binding, cholesterol transporter activity, high-density lipoprotein particle binding, lipase inhibitor activity, phosphatidylcholine binding, phosphatidylcholine-sterol O-acyltransferase activator activity, protein heterodimerization, triglyceride binding  |
| Fibrinogen alpha chain                       | P02672 FIBA_BOVIN      | 67012          | 6.73 | 3.57                               |                                    |                                    |                                    | 0.90                               | N/A  |
| Actin cytoplasmic 1                          | P60712 ACTB_BOVIN      | 41737          | 5.29 | 3.13                               | 1.77                               | 0.54                               |                                    | 0.62                               | ATP binding  |
| Actin cytoplasmic 2                          | P63258 ACTG_BOVIN      | 41793          | 5.31 | 3.12                               | 1.76                               | 0.54                               |                                    | 0.62                               | ATP binding, structural constituent of cytoskeleton  |
| Apolipoprotein A-I                           | P15497 APOA1_BOVIN     | 30276          | 5.71 | 3.05                               | 5.02                               |                                    |                                    | 1.14                               | Beta-amyloid binding, chemorepellent activity, cholesterol binding, cholesterol transporter activity, high-density lipoprotein particle binding, high-density lipoprotein particle receptor binding, phosphatidylcholine binding, phosphatidylcholine-sterol O-acyltransferase activator activity  |
| Apolipoprotein E                             | Q03247 APOE_BOVIN      | 35980          | 5.55 | 2.42                               | 2.58                               |                                    |                                    | 0.72                               | Antioxidant activity, beta-amyloid binding, cholesterol binding, cholesterol transporter activity, heparin binding, lipoprotein particle binding, low-density lipoprotein particle receptor binding, metal chelating activity, phosphatidylcholine-sterol O-acyltransferase activator activity, phospholipid binding, very-low-density lipoprotein particle receptor binding |
| Cytochrome c                                 | P62894 CYC_BOVIN       | 11704          | 9.52 | 2.32                               | 0.29                               | 3.88                               | 10.87                              | 4.41                               | Electron carrier activity Source, heme binding, iron ion binding   |
| Vitamin D-binding protein                    | Q3MHN5 VTDB_BOVIN      | 53342          | 5.36 | 2.14                               |                                    |                                    |                                    | 2.10                               | Vitamin D binding, vitamin transporter activity  |
| Regucalcin-1                                 | P82943 REG1_BOVIN      | 10281          | 8.80 | 2.12                               | 0.43                               |                                    | 5.30                               |                                    | Heparin binding  |
| Insulin-like growth factor-binding protein 2 | P13384 IBP2_BOVIN      | 34015          | 7.13 | 2.08                               | 1.51                               |                                    |                                    |                                    |  |
| Uncharacterized protein                      | tr F1N4M7 F1N4M7_BOVIN | 68905          | 8.07 | 2.05                               | 1.35                               | 0.48                               |                                    | 0.62                               | Insulin-like growth factor binding, insulin-like growth factor II binding  |
| Prothrombin*                                 | P00735 THRB_BOVIN      | 70506          | 5.97 | 2.00                               | 1.47                               |                                    |                                    |                                    | Scavenger receptor activity, serine-type endopeptidase activity  |
| Gelsolin*                                    | tr F1N1I6 F1N1I6_BOVIN | 85687          | 5.86 | 1.59                               | 2.33                               |                                    |                                    | 0.70                               | Calcium ion binding  |
| Beta-2-glycoprotein 1 / Apolipoprotein H     | P17690 APOH_BOVIN      | 38252          | 8.53 | 1.56                               | 0.88                               |                                    | 1.90                               | 2.25                               | Heparin binding Source, lipoprotein lipase activator activity, phospholipid binding  |
| Inter-alpha-trypsin inhibitor heavy chain    | Q87052 ITH4_BOVIN      | 101513         | 6.22 | 1.55                               | 1.68                               | 0.22                               |                                    | 0.59                               | Serine-type endopeptidase inhibitor activity   |
| Platelet factor 4*                           | tr F1MD83 F1MD83_BOVIN | 12567          | 9.30 | 1.30                               | 1.42                               | 3.62                               | 5.78                               |                                    | CXCR3 chemokine receptor binding, heparin binding  |
| Complement factor H                          | Q28085 CFAH_BOVIN      | 140374         | 6.43 | 1.24                               | 1.15                               |                                    |                                    | 0.43                               | N/A  |
| Fibulin-1 *                                  | tr F1MYN5 F1MYN5_BOVIN | 77486          | 4.94 | 1.19                               | 0.37                               | 1.47                               | 0.70                               |                                    | Calcium ion binding, peptidase activator activity  |
| Alpha-2-macroglobulin                        | Q75IH1 A2MG_BOVIN      | 167575         | 5.71 | 1.14                               | 1.01                               |                                    |                                    | 1.95                               | Serine-type endopeptidase inhibitor activity   |
| Insulin-like growth factor-binding protein 6 | Q05718 IBP6_BOVIN      | 24967          | 8.73 | 1.09                               | 0.63                               |                                    |                                    |                                    | N/A  |
| Fetuin-B                                     | Q58D62 FETUB_BOVIN     | 42663          | 5.59 | 1.02                               | 0.76                               | 0.80                               |                                    | 3.63                               | Cysteine-type endopeptidase inhibitor activity, metalloendopeptidase inhibitor activity  |
| Apolipoprotein C-III                         | P19035 APOC3_BOVIN     | 10692          | 5.02 | 1.02                               | 0.84                               |                                    |                                    |                                    | Lipase inhibitor activity, phospholipid binding  |
| Uncharacterized protein                      | tr Q3ZBS7 Q3ZBS7_BOVIN | 53575          | 5.92 | 0.91                               | 1.06                               |                                    |                                    |                                    |  |
| Protein AMBP                                 | P00978 AMBP_BOVIN      | 39235          | 7.81 | 0.83                               |                                    | 2.03                               | 2.78                               |                                    | Extracellular matrix binding, polysaccharide binding, scavenger receptor activity  |
| Alpha-fetoprotein                            | Q8S257 FETA_BOVIN      | 68588          | 5.92 | 0.79                               | 0.28                               |                                    |                                    | 2.01                               | Heme binding, IGA binding, protein homodimerization activity, serine-type endopeptidase inhibitor activity, small molecule binding   |
| Tetranectin*                                 | Q2KIS7 TETN_BOVIN      | 22144          | 5.47 | 0.74                               | 1.06                               |                                    |                                    |                                    | Metal ion binding  |

### 3.2.5 Conclusion

Aggregation of NDs in biological media is a complex phenomenon depending on inorganic salts and proteins. Dynamic light scattering revealed a drastic increase in the hydrodynamic parameter in DMEM without FBS and YMB that can be clearly attributed to the salting out effect. With FBS involved, indeed a mitigation of the aggregation can be observed. Even then however, relevant aggregation can be observed, which could be visualized with TEM measurements: While the salting out effect leads to precipitation of NDs (seen on the edge of holey carbon grids) in media without proteins, in DMEM medium with 10% FBS “clusters” of NDs with a proteins around (acting as “glue”) could be identified.

Interestingly, while sodium chloride is the main driving force for aggregation of NDs, other abundant inorganic elements such as calcium, potassium and phosphorus could not be identified. It seems, the concentration of sodium chloride is the main parameter leading to aggregation, which then involves also proteins when present. After the trypsin digest, using nLC-MS/MS, a high number of proteins could be identified. It turned out that in fact not the most abundant proteins present in the FBS are adsorbed to the NDs. Correlating the relative protein concentrations of the adsorbed proteins with the (theoretic) isoelectric point or the molecular mass failed. However, numerous proteins identified could be related to binding to negative compounds. This is a possible explanation for the favored adsorption on the oxygen-terminated FNDs with a negative zeta potential. One protein class identified of special interest is the high abundance of apolipoproteins, which are known to play a vital role in cellular uptake.

Based on the findings of this work, conjugation of NDs with FBS (based on the protocol used for the conjugation with antibodies in section 3.3) was used by David Roig in the group to circumvent the aggregation for the uptake of NDs in yeast cells: With untreated NDs, aggregations were formed whereas with FBS conjugation the diamonds were not aggregated but attached to the cell membrane. Thus, in the future, targeted protein adsorption could be used to not only prevent the NDs from aggregation, but also facilitate the uptake.

### 3.3 Nanodiamond Modification

To evaluate the binding of antibodies to diamonds and to test the stability of diamond/AB conjugates the particles were adhered to a glass plate and dried. Even though, initial images from the Leica SP2 confocal microscope suggested promising co-localization (data not shown), measurements using the Zeiss LSM 780 confocal microscope revealed that in fact huge aggregates formed during the drying of the suspensions were imaged (exemplarily shown in Figure 21). And when spin-coating was not



performed thoroughly enough, crystals remained on glass slides prepared from samples in PBS and DMEM with 10% FBS (exemplarily shown in Figure 21).

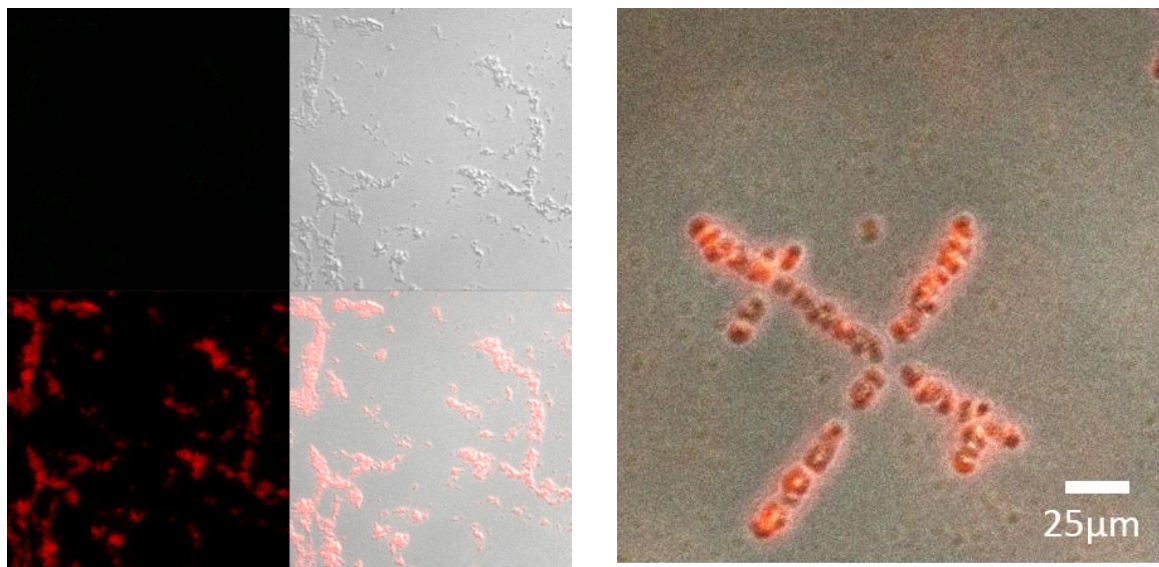


Figure 21 Left: Confocal microscopy images of 70 nm FNDs conjugated with FITC-labelled antibodies. Huge aggregations formed in the drying process are visible. The picture is split into 4, showing the FITC-signal in green in the top left, the differential interference contrast (DIC) in the top right and the FND signal in the bottom left. The sizes are 224.7  $\mu\text{m}$  x 224.7  $\mu\text{m}$ . Right: Salt crystals with NDs that are formed in DMEM if not sufficiently spin coated (similar results are obtained for NDs in PBS). As a result, the droplet was spin-coated 2x for 30 seconds for the samples in PBS and DMEM, which solved the issue.

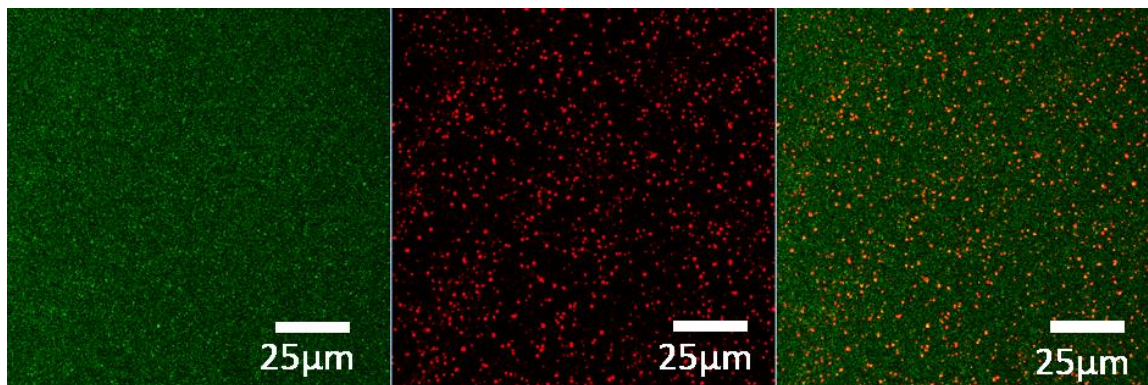
Therefore, a spin-coating step (as described in section 2.3) was added before imaging, resulting in the images shown in Figure 22 till Figure 27. The degree of co-localization was determined using a software program in the research group (by Johnny Saulnier). Although the obtained values vary greatly with the settings used (removal of noise and recognition of dots), they provide a good indication of magnitude the co-localization giving the number of pixels associated with FNDs/antibodies (see Table 29).

Table 29 Overview of the magnitude of co-localization

| Sample                                       | FNDs<br>[#Pixels] | Antibodies<br>[#Pixels] | FNDs + Antibodies<br>[#Pixels] | Antibodies with<br>FNDs [%] |
|--|-------------------|-------------------------|--------------------------------|-----------------------------|
| NDs/ABs in DI water                          | 128030            | 32806                   | 24174                          | 73                          |
| NDs/ABs in PBS                               | 205497            | 817833                  | 166863                         | 20                          |
| NDs/ABs in FBS                               | 1024416           | 821333                  | 806065                         | 98                          |
| NDs/ABs in 10% FBS                           | 768088            | 965853                  | 734469                         | 76                          |
| NDs/ABs in DMEM with 10% FBS                 | 1036785           | 658974                  | 651766                         | 98                          |
| NDs/ABs in DMEM with 10% FBS (indicatorless) | 424584            | 19996                   | 16695                          | 83                          |

In Figure 22, the co-localization between NDs (red) and antibodies (green) is shown. As shown by Huang and Chang<sup>[22]</sup> for Cytochrome C, washing NDs with DI water leaves the proteins attached to the

diamond surface. Likewise, also for NDs with antibodies co-localization (and therefore adsorption) is visible in DI water:



*Figure 22 NDs of 70 nm (Adámas) with antibodies (in DI water). Contrast and brightness were increased by to improve visibility.*

In PBS (see Figure 23), however the proteins do not remain adsorbed: Apparently, as a rather good solvent for proteins (due to the pH of 7.4 and isotonicity), working in PBS is not recommended for NDs with physically adsorbed proteins.

However, in pure FBS (see Figure 24) and 10% FBS Figure 25 a high degree of co-localization can be observed. In the latter sample, only few NDs and antibodies (as well as some aggregation) can be observed. As the experiment was successful for DI water and pure FBS, a failure in the sample preparation for the 10% FBS sample can be assumed. Particularly interesting in this sample is the fact, that the antibodies are not displaced by proteins with higher affinity to the NDs. The formation of the protein corona that is happening upon addition of the FBS to the NDs, leaves the antibodies intact. For the use in biological systems, this is indeed crucial.

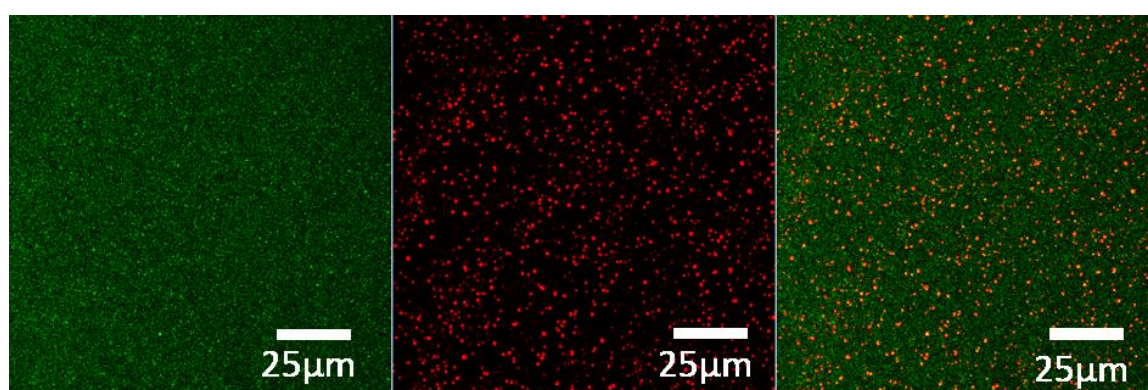


*Figure 23 NDs of 70 nm (Adámas) with antibodies in PBS. Contrast and brightness were increased to improve visibility.*

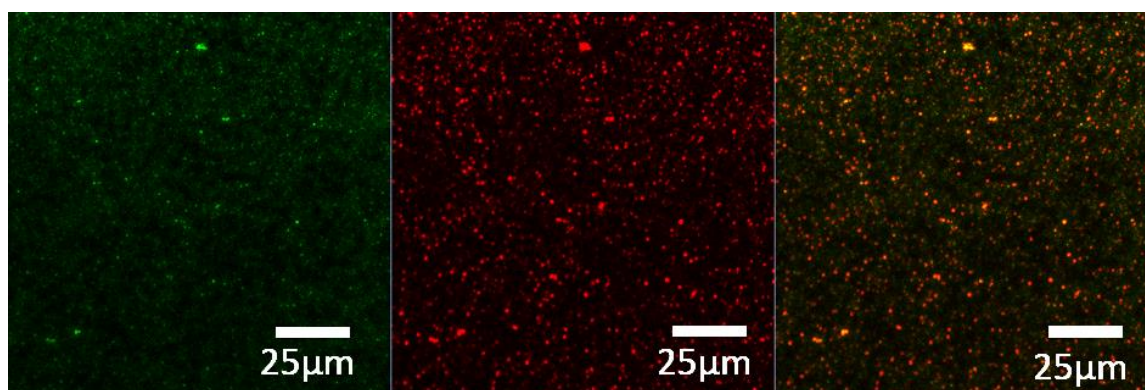


Figure 24 NDs of 70 nm (Adámas) with antibodies in FBS. Contrast and brightness were increased to improve visibility.

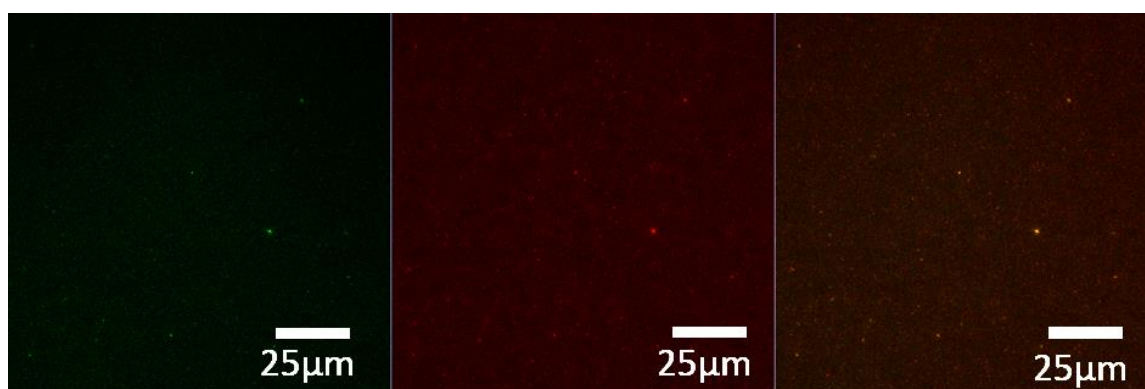


Figure 25 NDs of 70 nm (Adámas) with antibodies in 10% FBS. Contrast and brightness were increased to improve visibility.

In Figure 26 the behavior of NDs with adsorbed proteins in DMEM with 10% FBS (which is the medium as it is used in cell culture) is displayed. Phenol red serves as an indicator in DMEM, which leads to a high background (and therefore relatively bad visibility of NDs and ABs in the picture). This is why an identically prepared sample in DMEM with 10% FBS without phenol red was measured (see Figure 27). A very high degree of co-localization can be observed.

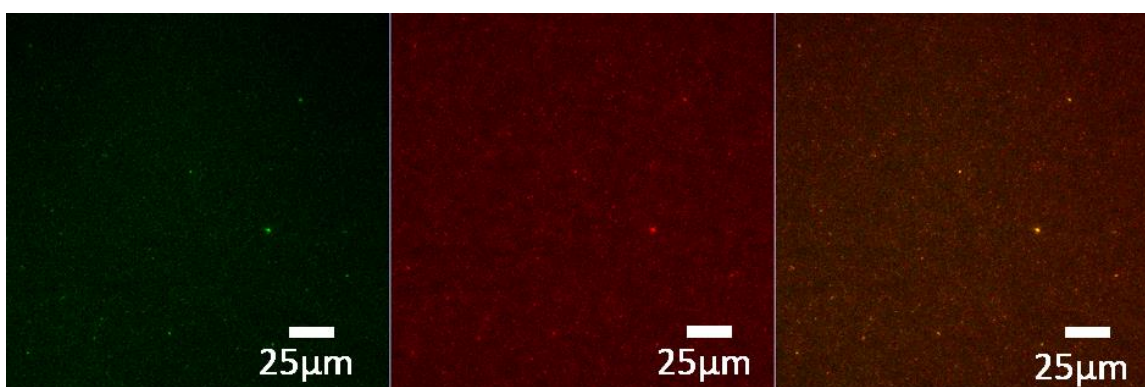


Figure 26 NDs of 70 nm (Adámas) with antibodies in DMEM with 10% FBS. Contrast and brightness were increased to improve visibility.

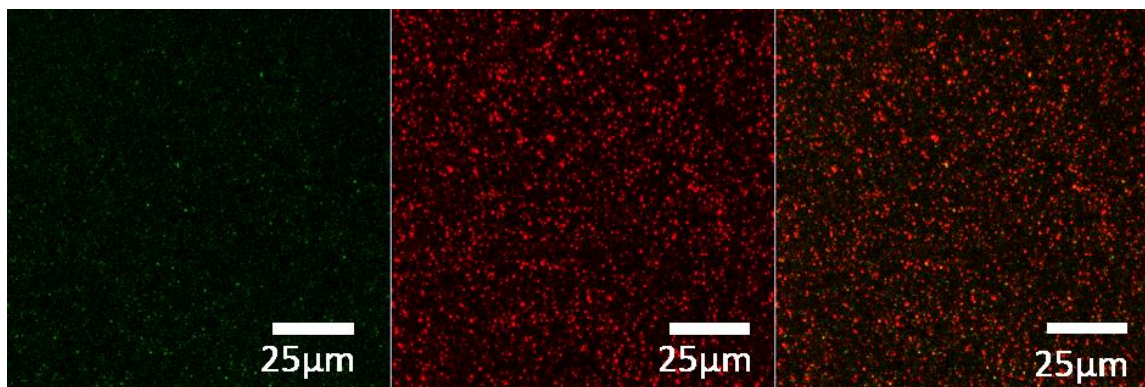


Figure 27 NDs of 70 nm (Adámas) with antibodies in indicatorless DMEM with 10% FBS. Contrast and brightness were increased to improve visibility.

Concluding, it can be assumed that NDs with adsorbed antibodies are sufficiently stable to be used in biological environments. Therefore, in the future work has to focus on testing the antibodies adsorbed on the NDs for their biofunctionality.

Another open question is the necessity of the overnight incubation during the preparation of the conjugated NDs. In literature, various incubation times are reported ranging from 20 minutes<sup>[25]</sup> till overnight (20h)<sup>[29]</sup>. Different temperatures are varying greatly too from 4°C<sup>[29]</sup> till 37°C<sup>[38]</sup>, where in the latter Shannahan et al. simulate cell culture conditions. As the conjugated antibodies in this work are intended to be used in cell culture too, 37°C overnight incubation was chosen. This however, is not necessarily the ideal condition for protein adsorption. Future studies will have to address this question.

### 3.4 Quantification of ND Uptake in Cells

In the quantification of the ND uptake in cells, three major challenges presented themselves: (1) The Raman band of water between 625 – 670 nm interfering with the NV-center's fluorescence between 550 – 850 nm. (2) The grating in use had the consequence of measuring also the second order of diffraction of the laser and thus limiting the exposure time at the CCD camera. (3) As a non-permanent measurement setup, despite the high stability of the signal for the same measurement day, the excellent primary results could not be reproduced later (the alignment and focusing of the laser beam was slightly different for each measurement day). Therefore, the initial plan to adjust a given calibration by a standard with a known ND concentration to the new alignment, could not be realized. Even the maximum exposure time varied between 0.2 s and 0.8 s between individual alignments (always the highest exposure time not leading to saturation – at position of the second order diffraction of the laser – of the detector was used).

In a first attempt, each standard was measured once with 500 spectra accumulated (each spectrum with 0.8 seconds exposure time resulting in an accumulate cycle time of 0.83374 seconds). Figure 28 illustrates the issue (1) and (2) (for an extract of the spectrum above between 550 – 900 nm see Figure 29):

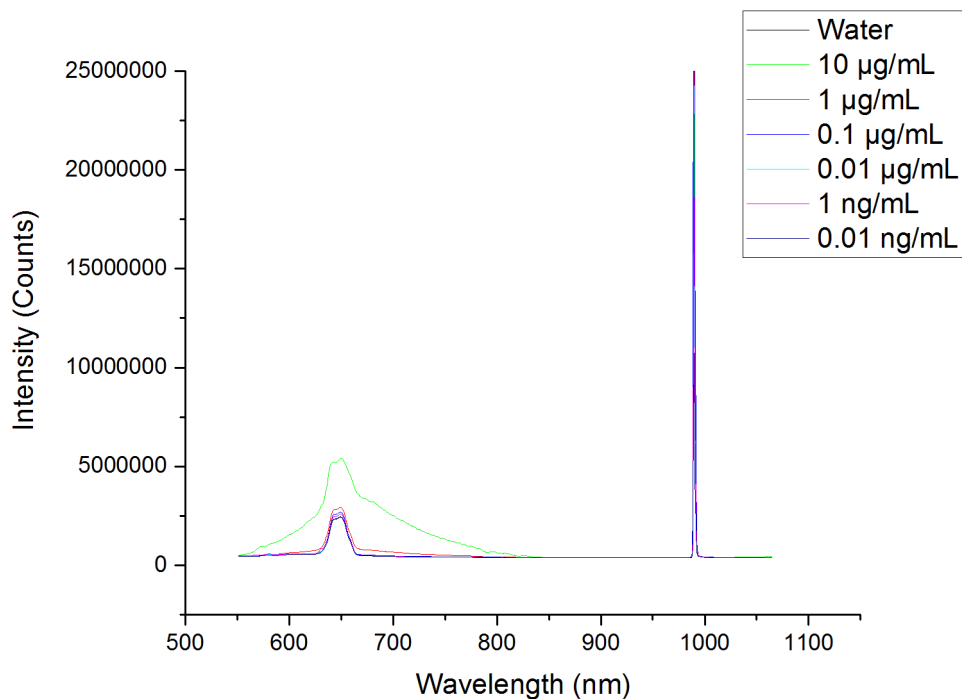


Figure 28 Fluorescence spectrum obtained for standard solutions with NDs in DI water. Between 550 – 850 nm, the fluorescence of the NV-center as well as the Raman peak of water can be seen. The right shows the second order diffraction of the 532 nm laser limiting the acquisition time.

## Results and Discussion

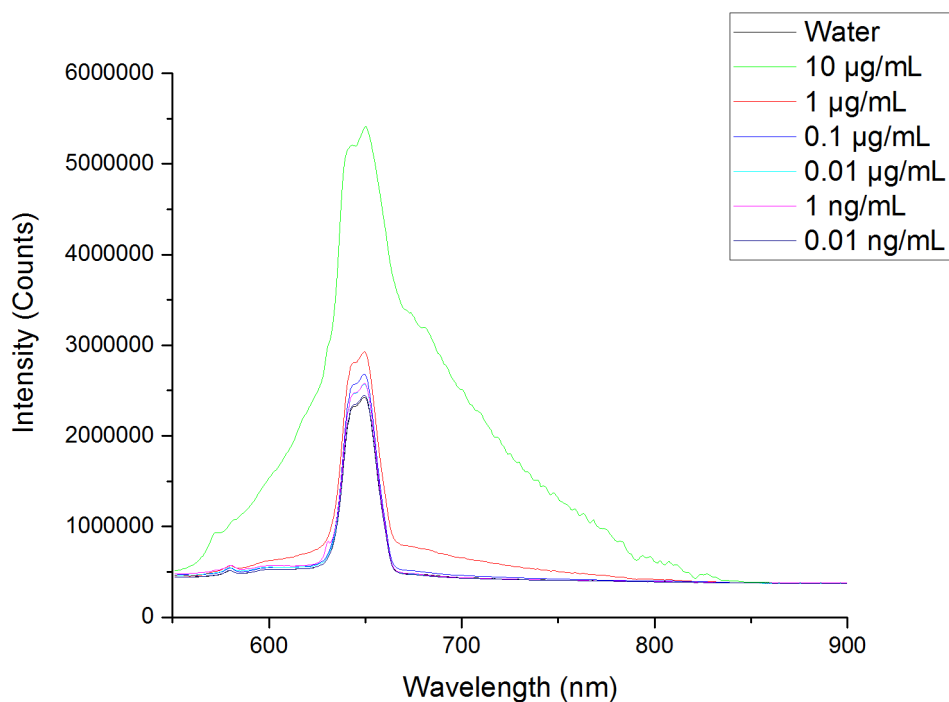


Figure 29 Extract of the spectrum from Figure 28 showing the area between 550 – 900 nm.

Subtraction of the water spectrum resulted in the following spectrum displayed in Figure 30:

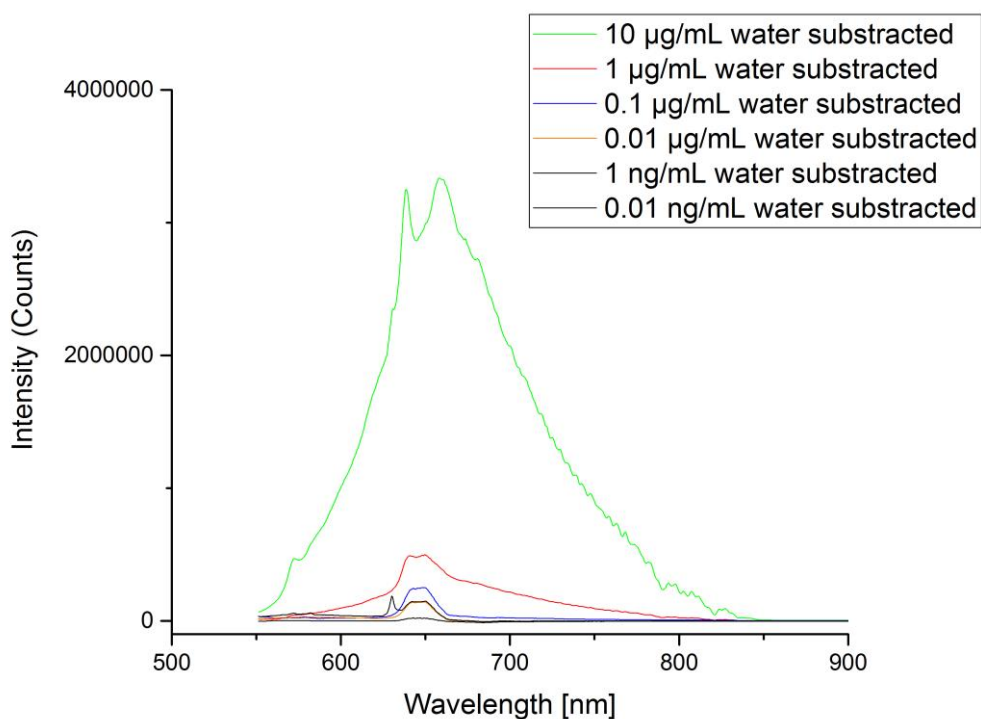


Figure 30 Fluorescence spectrum of the NV- center obtained after subtracting the water spectrum.

After peak integration (integration range: 560.75354 – 859.80408 nm) a calibration curve resulting in an empiric correlation coefficient of 0.9994 could be obtained. With an assumed LOD of 1 ng/mL and

approximately  $8 \times 10^6$  cells/mL, this corresponds to an LOD of about 0.2 ND particles per cell (for ND particles of 70 nm size), an excellent value that exceeded expectations. Here, the ND suspensions as well as the water blank were only measured once: Therefore, after this initial experiments, a complete method validation (with both water and cell lysate as matrices) was pursued.

In Table 30 measurements are summarized with 200 spectra accumulated, each of them with a 0.2 seconds exposure time resulting in an accumulate cycle time of 0.23374 seconds. Water blanks measured 10 times (before measuring the ND standard samples, after measuring Sample 3 and after measuring all the ND standard samples) used to test the stability of the system (the integrated peak area is the area of the water Raman band). Sample 1 (10  $\mu\text{g/mL}$ ) and Sample 6 were also measured 10 times, whereas the other samples were measured 3 times. Integration was performed between 550.96423 – 850.22998 nm.

Table 30 Water blanks and ND standards (in DI water) measured with 0.2 s exposure time and 200 accumulations.

| Sample                            | Avg. Peak Area [a.u.] | Std. Dev. [a.u.] | Rel. Std. Dev. [%] |
|-----------------------------------|-----------------------|------------------|--------------------|
| Water Blank Before                | 5.19E+07              | 4.44E+05         | 0.85               |
| Sample 1 (10 $\mu\text{g/mL}$ )   | 8.46E+07              | 1.53E+05         | 0.18               |
| Sample 2 (1 $\mu\text{g/mL}$ )    | 5.48E+07              | 2.79E+04         | 0.05               |
| Sample 3 (0.1 $\mu\text{g/mL}$ )  | 5.16E+07              | 4.96E+04         | 0.10               |
| Blank After Sample 3              | 5.20E+07              | 6.09E+05         | 1.17               |
| Sample 4 (0.01 $\mu\text{g/mL}$ ) | 5.12E+07              | 2.17E+04         | 0.04               |
| Sample 5 (1 ng/mL)                | 5.14E+07              | 3.17E+04         | 0.06               |
| Sample 6 (0.1 ng/mL)              | 5.13E+07              | 3.24E+04         | 0.06               |
| Blank After Sample 6              | 5.22E+07              | 6.16E+05         | 1.18               |

Clearly, the system is very stable with low relative standard deviations below 1.5%. A significant difference of the variance and mean of the peak area of the water blank measurements (compared to the water blank before measuring the ND standard samples) was excluded by performing an F-Test and a T-Test (both at a significance level of 0.5), respectively.

However, the calibration failed as the subtraction of the peak area of the water blank (directly subtracting the water spectrum from the standard spectra resulted in the same outcome) lead to negative peak areas for the standard with a ND concentration of 0.1  $\mu\text{g/mL}$  and below. A lower signal than in the water blank can be attributed to scattering of the nanoparticles (which is, after all, the prerequisite for the successful application of DLS methods in this work).

This is why the experiments have been repeated with 750 accumulated scans (all other parameters unchanged). Here an additional sample with a ND concentration of 5  $\mu\text{g/mL}$  was measured. Table 31 summarizes the outcomes of the experiment. Again, very low standard deviations of the integrated peak areas (integration between 555.77271 – 850.34467 nm) were found, with the exception of the

water blank measured at the end (3.04% rel. standard deviation). In this case, the F-Test as well as the T-Test revealed significant differences between the two water blanks.

Table 31 Water blanks and ND standards (in DI water) measured with 0.2 s exposure time and 500 accumulations.

|                              | Avg. Peak Area [a.u.] | Std. Dev. [a.u.] | Rel. Std. Dev. [%] |
|------------------------------|-----------------------|------------------|--------------------|
| <b>Water Blank Before</b>    | 1.95E+08              | 2,67E+05         | 0.14               |
| <b>Sample 1 (10 µg/mL)</b>   | 3.45E+08              | 1,93E+05         | 0.06               |
| <b>Sample 2 (5 µg/mL)</b>    | 2.00E+08              | 8,13E+05         | 0.41               |
| <b>Sample 3 (1 µg/mL)</b>    | 2.07E+08              | 6,77E+05         | 0.33               |
| <b>Sample 4 (0.1 µg/mL)</b>  | 1.92E+08              | 5,95E+05         | 0.31               |
| <b>Sample 5 (0.01 µg/mL)</b> | 1.92E+08              | 1,33E+06         | 0.69               |
| <b>Sample 6 (1 ng/mL)</b>    | 1.93E+08              | 5,04E+05         | 0.26               |
| <b>Sample 7 (0.1 ng/mL)</b>  | 1.93E+08              | 1,19E+06         | 0.62               |
| <b>Water Blank After</b>     | 1.89E+08              | 5,73E+06         | 3.04               |

The calibration, however, failed also in this case giving negative peak areas for all standards with an ND concentration with 0.1 µg/mL and below.

Measurements with (spiked) cell lysate led to the same outcome as shown in Table 32 (200 spectra accumulated, 0.2 seconds exposure time and an accumulate cycle time of 0.23374 s) and Table 33 (750 spectra accumulated, 0.2 seconds exposure time and an accumulate cycle time of 0.23374). Boundaries for the peak integration were 550.96423 – 850.22998 nm for the measurements with 200 accumulations whereas, for 750 accumulations the range was 555.77271 – 850.34467 nm.

Table 32 Stability of the signal of cell lysate (spiked with ND). Parameters: 200 spectra accumulated, 0.2 seconds exposure time and an accumulate cycle time of 0.23374 s.

|                             | Avg. Peak Area [a.u.] | Std. Dev. [a.u.] | Re. Std. Dev. [%] |
|-----------------------------|-----------------------|------------------|-------------------|
| <b>Cell Lysate Blank</b>    | 6.58E+07              | 2.05E+06         | 3.11              |
| <b>Lysate 1 (10 µg/mL)</b>  | 8.57E+07              | 1.57E+06         | 1.83              |
| <b>Lysate 2 (1 µg/mL)</b>   | 6.58E+07              | 1.03E+06         | 1.57              |
| <b>Lysate 3 (0,1 µg/mL)</b> | 6.35E+07              | 1.31E+06         | 2.06              |

Table 33 Stability of the signal of cell lysate (spiked with ND). Measurements were performed 5 times. Parameters: 750 spectra accumulated, 0.2 seconds exposure time and an accumulate cycle time of 0.23374 s.

|                           | Avg. Peak Area [a.u.] | Std. Dev. [a.u.] | Rel. Std. Dev. [%] |
|---------------------------|-----------------------|------------------|--------------------|
| <b>Lysate Blank</b>       | 1.95E+08              | 4.49E+06         | 2.30               |
| <b>Lysate 10 µg/mL ND</b> | 2.37E+08              | 8.05E+06         | 3.40               |

For cell lysates, the relative standard deviation is considerably higher. Calibration was not successful sample with a concentration of 1 µg/mL and below. With 750 accumulations, no negative peak areas were obtained, however the calibration failed too. Figure 31 illustrates the situation: The peak heights



(and areas) are not in alignment with the concentrations, e.g. the standard with 0.01  $\mu\text{g}/\text{mL}$  is higher than the standard with 1  $\mu\text{g}/\text{mL}$ .

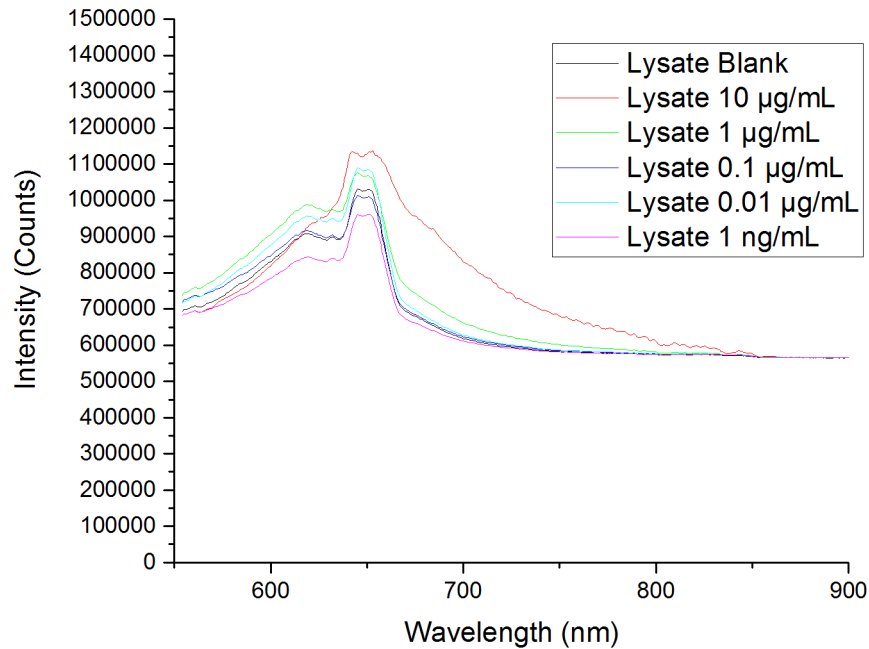


Figure 31 Fluorescence of the cell lysates between 500 – 900 nm.

To conclude, we can say:

- Principally a detection of fluorescent NDs of 70 nm size with around 300 NV per particle should be possible down to a concentration of approximately 1 ng. However, with the instrument used, despite the high stability of the signal, the calibration and method validation failed. As the main limit, the saturation of the second order diffraction band of the 532 nm laser (not allowing an increase of the exposure time at the detector) was identified.
- Therefore, these results can be seen as proof of concept: Quantification of NDs by fluorescence is in reach using a 532 nm laser. As a consequence, a permanent experimental setup using a more sensitive APD (avalanche photodiode) detector shall be realized in the future. Utilizing optical filters, photons of the appropriate energy between 550 and 850 nm shall be selected (this is equivalent to the integration of the peak between the same wavelength range).

#### 4. Conclusion and Outlook

In this work, NDs were characterized for the designated use in biological cells to perform diamond magnetometry. The shape of those nanoparticles was investigated to allow better understanding of its

impact on magnetometry, biocompatibility and uptake. A rather blocky shape with sharp edges as opposed to the spherical shape could be found, and evidence suggests that indeed the particles have a flat, flake-like shape.

Furthermore, the main goal of this thesis was to deal with all the issues on the way from the ND slurry to ready-to-use ND in biological systems in and outside of cells. Taking surface chemistry of the diamonds into account, the phenomenon of ND aggregation in cellular medium was – for the first time ever – investigated in detail. Sodium chloride was identified to be the main inorganic compound driving the aggregation process in DMEM medium, while in YMB nitrogen salts alongside smaller amounts of phosphorus and sulfur seem to be responsible. With proteomic techniques, the protein corona of the diamonds in these aggregates was evaluated. Indeed, a great number of proteins were identified to take part in the aggregation. No correlation between protein adsorption and the (theoretical) isoelectric point or the molecular mass of the proteins could be found. However several proteins which bind to the ND surface are known to bind to negatively charged compounds.

As a matter of fact, the ability of NDs to have a certain specificity to adsorb proteins that are not the most abundant proteins in fetal bovine serum poses a chance for serum analysis: Human serum is a complex mixture with about 3700 proteins with concentrations up to  $70 \text{ mg ml}^{-1}$ , in which the most abundant proteins (such as albumin, immuno-globulin G (IgG) and  $\alpha$ 2-macroglobulin) represent 97% of the total protein content<sup>[21]</sup>. This is why, in serum analysis, enormous efforts have to be made to deplete those high abundance proteins to allow the detection of potentially relevant biomarkers. Consequently, this finding spawned a side-project in the research group to systematically evaluate the adsorption of proteins to NDs for (human) serum analysis (as sodium chloride is the main driving force for agglomeration, instead of the complex DMEM an aqueous solution of sodium chloride is used to adsorb proteins).

The identification of the proteins adsorbed to proteins will help to “design” a protein corona that promotes the uptake of cells. The effect of methods aiming at the endosomal escape as review by Varkouhi<sup>[42]</sup> (or as the introduction of 1,2-diaminoethane side chains<sup>[43]</sup> or the acidification of the endocytic and exocytic pathways<sup>[44]</sup>) has to be systematically explored for their effect on the protein corona.

As a result of the importance of proteins for the fate of NDs in biological systems, it was decided to use the adsorption of proteins, antibodies, to direct NDs to targets in- and outside of cells. Antibody-conjugated NDs have proven to be stable in DMEM medium with 10% FBS as used in cell culture and are therefore ready to use in biological systems. First labelling experiments undertaken in the group by Simon R. Hemelaar with antibodies against Fibronectin, a membrane protein, suggest an intact

biological function of the antibodies, even though this experiment has yet to be proven to be reproducible. Therefore, in the future work has to focus on testing the antibodies adsorbed on the NDs for their functionality (not only for membrane proteins, but also within cells). Circular dichroism can be used to detect conformational changes of the proteins adsorbed (advantageously with using NDs from Microdiamant AG that have shown to be a usable model system for the fluorescent diamonds from Adámas Technologies as circular dichroism requires larger sample amounts).

However, as the adsorption is not stable in PBS, for certain applications a covalent bonding might be considered in the future: Suzuki et al.<sup>[45]</sup> attached antibodies covalently to DLC plates while Dahoumane et al.<sup>[46]</sup> show a way to covalently functionalize NDs with antibodies.

As the last part of this thesis, a proof-of-principle for the detection of NDs (relying on the fluorescence of the NV<sup>-</sup>centers) in water and cell lysate with ND concentrations of around 1 ng/mL was shown. Transferring this method to the setup of the research group with more sensitive avalanche photodiode detectors is necessary in the future in order to take advantage of the finding. Fast screening of diamond uptake in various cell types would be made possible then.

To summarize, in this work new findings about the shape of diamonds that are relevant for magnetometry applications and use in biological cells were made. Fundamental understanding of the physicochemical behavior of NDs in cellular medium was obtained by investigating the phenomenon of ND aggregation. Antibody-conjugated NDs were prepared by physical adsorption of antibodies and are now ready to use in the biological environment. The cellular uptake of diamonds can be screened efficiently after implementing the method based on the proof-of-principle of fluorescence measurements in this work.

## 5. References

- [1] C. Nathan, A. Cunningham-Bussel, *Nat. Rev. Immunol.* **2013**, *13*, 349.
- [2] C. L. Degen, *Appl. Phys. Lett.* **2008**, *92*, 22.
- [3] J. M. Taylor, P. Cappellaro, L. Childress, L. Jiang, D. Budker, P. R. Hemmer, a. Yacoby, R. Walsworth, M. D. Lukin, **2008**, *4*, 29.
- [4] G. Balasubramanian, I. Y. Chan, R. Kolesov, M. Al-Hmoud, J. Tisler, C. Shin, C. Kim, A. Wojcik, P. R. Hemmer, A. Krueger, T. Hanke, A. Leitenstorfer, R. Bratschitsch, F. Jelezko, J. Wrachtrup, *Nature* **2008**, *455*, 648.
- [5] R. Schirhagl, K. Chang, M. Loretz, C. L. Degen, *Annu. Rev. Phys. Chem.* **2014**, *65*, 83.
- [6] L. Rondin, J.-P. Tetienne, T. Hingant, J.-F. Roch, P. Maletinsky, V. Jacques, *Rep. Prog. Phys.* **2014**, *77*, 056503.
- [7] J. P. Tetienne, T. Hingant, L. Rondin, a. Cavallès, L. Mayer, G. Dantelle, T. Gacoin, J. Wrachtrup, J. F. Roch, V. Jacques, *Phys. Rev. B - Condens. Matter Mater. Phys.* **2013**, *87*, 1.
- [8] T. Roskopf, a. Dussaux, K. Ohashi, M. Loretz, R. Schirhagl, H. Watanabe, S. Shikata, K. M. Itoh, C. L. Degen, *Phys. Rev. Lett.* **2014**, *112*, 1.
- [9] A. O. Sushkov, N. Chisholm, I. Lovchinsky, M. Kubo, P. K. Lo, S. D. Bennett, D. Hunger, A. Akimov, R. L. Walsworth, H. Park, M. D. Lukin, *Nano Lett.* **2014**, DOI 10.1021/nl502988n.
- [10] A. Nagl, S. R. Hemelaar, R. Schirhagl, *Anal. Bioanal. Chem.* **2015**, DOI 10.1007/s00216-015-8849-1.
- [11] M. V. Hauf, B. Grotz, B. Naydenov, M. Dankerl, S. Pezzagna, J. Meijer, F. Jelezko, J. Wrachtrup, M. Stutzmann, F. Reinhard, J. a. Garrido, *Phys. Rev. B - Condens. Matter Mater. Phys.* **2011**, *83*, 1.
- [12] H. J. Mamin, M. H. Sherwood, D. Rugar, *Phys. Rev. B - Condens. Matter Mater. Phys.* **2012**, *86*, 1.
- [13] E. Hahn, *Phys. Rev.* **1950**, *80*, 580.
- [14] A. L. Capriotti, G. Caracciolo, C. Cavaliere, V. Colapicchioni, S. Piovesana, D. Pozzi, A. Laganà, *Chromatographia* **2014**, *77*, 755.
- [15] M. P. Monopoli, C. Aberg, A. Salvati, K. a Dawson, *Nat. Nanotechnol.* **2012**, *7*, 779.
- [16] S. Ritz, S. Schöttler, N. Kotman, G. Baier, A. Musyanovych, J. Kuharev, K. Landfester, H. Schild, O. Jahn, S. Tenzer, V. Mailänder, *Biomacromolecules* **2015**, 150320125141006.
- [17] S. Zhang, S. Zhang, L. Ju, L. Ju, G. Lykotrafitis, G. Lykotrafitis, G. Bao, G. Bao, S. Suresh, S. Suresh, *Adv. Mater.* **2009**, *21*, 419.

## References

- [18] U. Sakulku, L. Maurizi, M. Mahmoudi, M. M. Motazacker, M. Vries, A. Gramoun, M.-G. Beuzelin Ollivier, J.-P. Vallee, F. Rezaee, H. Hofmann, *Nanoscale* **2014**, 11439.
- [19] M. Schäffler, M. Semmler-Behnke, H. Sarioglu, S. Takenaka, A. Wenk, C. Schleh, S. M. Hauck, B. D. Johnston, W. G. Kreyling, *Nanotechnology* **2013**, 24, 265103.
- [20] C. Ge, J. Tian, Y. Zhao, C. Chen, R. Zhou, Z. Chai, *Arch. Toxicol.* **2015**, 519.
- [21] S. Usawadee, M. Morteza, MauriziLionel, C. Geraldine, H.-A. Margarethe, V. Marcel, M. Mahdi, R. Farhad, H. Heinrich, *Biomater. Sci.* **2015**, 3, 265.
- [22] L. C. L. Huang, H. C. Chang, *Langmuir* **2004**, 20, 5879.
- [23] A. Krüger, F. Kataoka, M. Ozawa, T. Fujino, Y. Suzuki, a. E. Aleksenskii, a. Y. Vul', E. Osawa, *Carbon N. Y.* **2005**, 43, 1722.
- [24] M. V Korobov, D. S. Volkov, N. V Avramenko, L. A. Belyaeva, P. I. Semenyuk, M. A. Proskurnin, *Nanoscale* **2013**, 5, 1529.
- [25] J. W. Lee, S. Lee, S. Jang, K. Y. Han, Y. Kim, J. Hyun, S. K. Kim, Y. Lee, *Mol. Biosyst.* **2013**, 9, 1004.
- [26] X. Zheng, H. Baker, W. S. Hancock, F. Fawaz, M. McCaman, E. Pungor, *Biotechnol. Prog.* **2006**, 22, 1294.
- [27] X. L. Kong, L. C. L. Huang, C. M. Hsu, W. H. Chen, C. C. Han, H. C. Chang, *Anal. Chem.* **2005**, 77, 259.
- [28] V. Vermeeren, L. Grieten, N. Vanden Bon, N. Bijmens, S. Wenmackers, S. D. Janssens, K. Haenen, P. Wagner, L. Michiels, *Sensors Actuators, B Chem.* **2011**, 157, 130.
- [29] S. Siddiqui, Z. Dai, C. J. Stavis, H. Zeng, N. Moldovan, R. J. Hamers, J. a. Carlisle, P. U. Arumugam, *Biosens. Bioelectron.* **2012**, 35, 284.
- [30] E. Perevedentseva, **2013**, DOI 10.1007/s11051-013-1834-8.
- [31] P. W. May, J. a. Smith, K. N. Rosser, *Diam. Relat. Mater.* **2008**, 17, 199.
- [32] A. C. Ferrari, J. Robertson, *Philos. Trans. A. Math. Phys. Eng. Sci.* **2004**, 362, 2477.
- [33] V. Jacques, E. Wu, T. Toury, F. Treussart, a. Aspect, P. Grangier, J. F. Roch, *Eur. Phys. J. D* **2005**, 35, 561.
- [34] S. M. Pimenov, I. I. Vlasov, A. a. Khomich, B. Neuenschwander, M. Mural, V. Romano, *Appl. Phys. A Mater. Sci. Process.* **2011**, 105, 673.
- [35] R. Telling, C. Pickard, M. Payne, J. Field, **2000**, DOI 10.1103/PhysRevLett.84.5160.
- [36] A. Kubo, Y. Mochida, J. Tamaki, K. Harano, H. Sumiya, a. M. M. Sharif Ullah, *Adv. Mater. Res.* **2011**, 325, 153.

## References

- [37] S. George, S. Lin, Z. Ji, C. R. Thomas, L. Li, M. Mecklenburg, H. Meng, X. Wang, H. Zhang, T. Xia, J. N. Hohman, S. Lin, J. I. Zink, P. S. Weiss, A. E. Nel, *ACS Nano* **2012**, *6*, 3745.
- [38] J. H. Shannahan, X. Lai, P. C. Ke, R. Podila, J. M. Brown, F. a. Witzmann, *PLoS One* **2013**, *8*, DOI 10.1371/journal.pone.0074001.
- [39] a. R. Boyd, G. a. Burke, H. Duffy, M. Holmberg, C. O'Kane, B. J. Meenan, P. Kingshott, *J. Mater. Sci. Mater. Med.* **2011**, *22*, 74.
- [40] J. Zhang, L. Xin, B. Shan, W. Chen, M. Xie, D. Yuen, W. Zhang, Z. Zhang, G. a. Lajoie, B. Ma, *Mol. Cell. Proteomics* **2012**, *11*, M111.010587.
- [41] W. Zhu, J. W. Smith, C. M. Huang, *J. Biomed. Biotechnol.* **2010**, *2010*, DOI 10.1155/2010/840518.
- [42] A. K. Varkouhi, M. Scholte, G. Storm, H. J. Haisma, *J. Control. Release* **2011**, *151*, 220.
- [43] K. Miyata, M. Oba, M. Nakanishi, S. Fukushima, Y. Yamasaki, H. Koyama, N. Nishiyama, K. Kataoka, *J. Am. Chem. Soc.* **2008**, *130*, 16287.
- [44] I. Mellman, R. Fuchs, A. Helenius, *Annu. Rev. Biochem.* **1986**, *55*, 663.
- [45] K. Suzuki, M. Hiyoshi, H. Tada, M. Bando, T. Ichioka, N. Kamemura, H. Kido, *Anal. Chim. Acta* **2011**, *706*, 321.
- [46] S. A. Dahoumane, M. N. Nguyen, A. Thorel, J. P. Boudou, M. M. Chehimi, C. Mangeney, *Langmuir* **2009**, *25*, 9633.

## 6. Annex

### 5.1 Medium Compositions

Table 34 DMEM medium composition

DMEM complete medium (DMEM (Dulbecco's Modified Eagle Medium) + Glutamax (1%) + and penicillin/streptomycin (1%) + Fetal bovine serum (FBS) (10%), Gibco Life Technologies, Bleiswijk, The Netherlands). FBS was purchased from Sigma Aldrich, St. Louis, United States.

| <b>Components</b>                          | <b>Molecular Weight</b> | <b>Concentration (mg/L)</b> | <b>mM</b>    |
|--|-------------------------|-----------------------------|--------------|
| <b>Amino Acids</b>                         |                         |                             |              |
| Glycine                                    | 75.0                    | 18.75                       | 0.25         |
| L-Alanine                                  | 89.0                    | 4.45                        | 0.049999997  |
| L-Arginine hydrochloride                   | 211.0                   | 147.5                       | 0.69905216   |
| L-Asparagine-H <sub>2</sub> O              | 150.0                   | 7.5                         | 0.05         |
| L-Aspartic acid                            | 133.0                   | 6.65                        | 0.05         |
| L-Cysteine hydrochloride-H <sub>2</sub> O  | 176.0                   | 17.56                       | 0.09977272   |
| L-Cystine 2HCl                             | 313.0                   | 31.29                       | 0.09996805   |
| L-Glutamic Acid                            | 147.0                   | 7.35                        | 0.05         |
| L-Glutamine                                | 146.0                   | 365.0                       | 2.5          |
| L-Histidine hydrochloride-H <sub>2</sub> O | 210.0                   | 31.48                       | 0.14990476   |
| L-Isoleucine                               | 131.0                   | 54.47                       | 0.41580153   |
| L-Leucine                                  | 131.0                   | 59.05                       | 0.45076334   |
| L-Lysine hydrochloride                     | 183.0                   | 91.25                       | 0.4986339    |
| L-Methionine                               | 149.0                   | 17.24                       | 0.11570469   |
| L-Phenylalanine                            | 165.0                   | 35.48                       | 0.2150303    |
| L-Proline                                  | 115.0                   | 17.25                       | 0.15         |
| L-Serine                                   | 105.0                   | 26.25                       | 0.25         |
| L-Threonine                                | 119.0                   | 53.45                       | 0.44915968   |
| L-Tryptophan                               | 204.0                   | 9.02                        | 0.04421569   |
| L-Tyrosine disodium salt dihydrate         | 261.0                   | 55.79                       | 0.21375479   |
| L-Valine                                   | 117.0                   | 52.85                       | 0.4517094    |
| <b>Vitamins</b>                            |                         |                             |              |
| Biotin                                     | 244.0                   | 0.0035                      | 1.4344263E-5 |
| Choline chloride                           | 140.0                   | 8.98                        | 0.06414285   |
| D-Calcium pantothenate                     | 477.0                   | 2.24                        | 0.0046960167 |
| Folic Acid                                 | 441.0                   | 2.65                        | 0.0060090707 |
| Niacinamide                                | 122.0                   | 2.02                        | 0.016557377  |
| Pyridoxine hydrochloride                   | 206.0                   | 2.0                         | 0.009708738  |
| Riboflavin                                 | 376.0                   | 0.219                       | 5.824468E-4  |

## Annex

|  |        |        |              |
|--|--------|--------|--------------|
| Thiamine hydrochloride   | 337.0  | 2.17   | 0.0064391694 |
| Vitamin B12  | 1355.0 | 0.68   | 5.0184503E-4 |
| i-Inositol   | 180.0  | 12.6   | 0.07         |
| <b>Inorganic Salts</b>   |        |        |              |
| Calcium Chloride (CaCl <sub>2</sub> ) (anhyd.)                                     | 111.0  | 116.6  | 1.0504504    |
| Cupric sulfate (CuSO <sub>4</sub> ·5H <sub>2</sub> O)                              | 250.0  | 0.0013 | 5.2E-6       |
| Ferric Nitrate (Fe(NO <sub>3</sub> ) <sub>3</sub> ·9H <sub>2</sub> O)              | 404.0  | 0.05   | 1.2376238E-4 |
| Ferric sulfate (FeSO <sub>4</sub> ·7H <sub>2</sub> O)                              | 278.0  | 0.417  | 0.0015       |
| Magnesium Chloride (anhydrous)   | 95.0   | 28.64  | 0.30147368   |
| Magnesium Sulfate (MgSO <sub>4</sub> ) (anhyd.)                                    | 120.0  | 48.84  | 0.407        |
| Potassium Chloride (KCl)   | 75.0   | 311.8  | 4.1573334    |
| Sodium Bicarbonate (NaHCO <sub>3</sub> )   | 84.0   | 1200.0 | 14.285714    |
| Sodium Chloride (NaCl)   | 58.0   | 6995.5 | 120.61207    |
| Sodium Phosphate dibasic (Na <sub>2</sub> HPO <sub>4</sub> )<br>anhydrous          | 142.0  | 71.02  | 0.50014085   |
| Sodium Phosphate monobasic<br>(NaH <sub>2</sub> PO <sub>4</sub> ·H <sub>2</sub> O) | 138.0  | 62.5   | 0.45289856   |
| Zinc sulfate (ZnSO <sub>4</sub> ·7H <sub>2</sub> O)                                | 288.0  | 0.432  | 0.0015       |
| <b>Other Components</b>  |        |        |              |
| D-Glucose (Dextrose)   | 180.0  | 3151.0 | 17.505556    |
| HEPES  | 238.0  | 3574.5 | 15.018908    |
| Hypoxanthine Na  | 159.0  | 2.39   | 0.015031448  |
| Linoleic Acid  | 280.0  | 0.042  | 1.4999999E-4 |
| Lipoic Acid  | 206.0  | 0.105  | 5.097087E-4  |
| Putrescine 2HCl  | 161.0  | 0.081  | 5.031056E-4  |
| Sodium Pyruvate  | 110.0  | 55.0   | 0.5          |
| Thymidine  | 242.0  | 0.365  | 0.0015082645 |

Table 35 Yeast medium base without amino acids (Formedium), YMB

Yeast medium base without amino acids (Formedium™, King's Lynn, United Kingdom).

### Yeast Morphology Agar

#### Nitrogen Source g/l

|                          |      |
|--------------------------|------|
| Ammonium Sulphate        | -    |
| Asparagine               | -    |
| Potassium Nitrate        | 0.78 |
| Caseine Hydrolysate      | -    |
| Carbon Source g/l        |      |
| Glucose.H <sub>2</sub> O | -    |
| Galactose                | -    |



|                                 |      |
|---------------------------------|------|
| Raffinose                       | -    |
| Amino Acids mg/l                |      |
| Histidine.HCl                   | 1    |
| Methionine                      | 2    |
| Tryptophan                      | 2    |
| <b>Vitamins µg/l</b>            |      |
| Biotin                          | 2    |
| Ca-Panhotenate                  | 400  |
| Folic Acid                      | 2    |
| Inositol                        | 2000 |
| Nicotinic Acid                  | 400  |
| p-Aminobenzoic Acid             | 200  |
| Pyridoxine HCl                  | 400  |
| Riboflavin                      | 200  |
| Thiamine HCl                    | 400  |
| <b>Trace Elements µg/l</b>      |      |
| Boric Acid                      | 500  |
| Copper Sulfate                  | 40   |
| Potassium Iodide                | 100  |
| Ferric Chloride                 | 200  |
| Manganese Sulfate               | 400  |
| Sodium Molybdate                | 200  |
| Zinc Sulfate                    | 400  |
| <b>Minerals g/l</b>             |      |
| KH <sub>2</sub> PO <sub>4</sub> | 1    |
| Magnesium Sulphate.anh          | 0.5  |
| Sodium Chloride                 | 0.1  |
| Calcium Chloride.anh            | 0.1  |

## 5.2 X-ray Powder Diffraction (XRD)

The analysis report for the x-ray powder diffraction of NDs of 25 nm of median size (Microdiamant AG) is given in the following:

### Analysis Report

#### Data Files

```
Data      file      1      :      L:\_Projekte      ab
2014\_Extern\Diamant_Holland\XCEL_26min_rot_msy0_microdiamant_febr2015_5
_135.xy
Data      file      2      :      H:\_Projekte      ab
2014\_Extern\Diamant_Holland\XCEL_26min_rot_1_75nm_diamant_apr2015_5_135
.xy
Data      file      3      :      H:\_Projekte      ab
2014\_Extern\Diamant_Holland\XCEL_26min_rot_2_125nm_diamant_apr2015_5_13
5.xy
```

#### Global R-Values

```
Rexp : 3.62      Rwp : 6.68      Rp  : 5.08      GOF : 1.84
Rexp` : 2.85     Rwp` : 5.25     Rp`  : 4.17     DW  : 0.65
```

```
File      1      :      "L:\_Projekte      ab
2014\_Extern\Diamant_Holland\XCEL_26min_rot_msy0
_microdiamant_febr2015_5_135.xy"
```

Range Number : 1

#### R-Values

```
Rexp : 4.06      Rwp : 5.09      Rp  : 3.99      GOF : 1.25
Rexp` : 2.03     Rwp` : 2.55     Rp`  : 2.05     DW  : 1.31
```

#### Quantitative Analysis - Rietveld

```
Phase 1 : Diamant      100.000 %
```

#### Background

```
One on X      73395.5
Chebychev polynomial, Coefficient  0      -599.5377
                                          1      424.6273
                                          2      -83.69835
                                          3      37.80193
                                          4      -12.1669
                                          5      9.147154
                                          6      -14.03935
```

#### Instrument

```
Primary radius (mm)      200
Secondary radius (mm)    200
Linear PSD 2Th angular range (°)  2.546
  FDS angle (°)          0.5
  Beam spill, sample length (mm)  20
  Intensity corrected
Full Axial Convolution
  Filament length (mm)    15
  Sample length (mm)     15
  Receiving Slit length (mm)  15
```

Annex

Primary Sollers (°) 4.6  
 Secondary Sollers (°) 4.6  
 Tube\_Tails  
 Source Width (mm) 0.0006405515  
 Z1 (mm) -7.282288e-005  
 Z2 (mm) 1.165302  
 Fraction 2.113079e-005

**Corrections**

Zero error -0.06760718  
 LP Factor 0  
 Absorption (1/cm) 500

**Miscellaneous**

X Calculation Step 0.02  
 Start X 35  
 Finish X 130

**Structure 1**

Phase name Diamant  
 R-Bragg 0.987  
 Spacegroup Fd-3m  
 Scale 0.563560136  
 Cell Mass 96.088  
 Cell Volume (Å<sup>3</sup>) 45.31917  
 Wt% - Rietveld 100.000  
 Crystallite Size  
 Cry size Lorentzian (nm) 13.8  
 Crystal Linear Absorption Coeff. (1/cm) 15.926  
 Crystal Density (g/cm<sup>3</sup>) 3.521  
 Lattice parameters  
 a (Å) 3.5652828

| Site | Np | x       | y       | z       | Atom | Occ | Beq   |
|------|----|---------|---------|---------|------|-----|-------|
| C1   | 8  | 0.00000 | 0.00000 | 0.00000 | C    | 1   | 2.859 |

**File 2 : "H:\\_Projekte ab  
 2014\\_Extern\Diamant\_Holland\XCEL\_26min\_rot\_1\_75  
 nm\_diamant\_apr2015\_5\_135.xy"**

Range Number : 1

**R-Values**

Rexp : 4.93 Rwp : 6.58 Rp : 5.19 GOF : 1.33  
 Rexp` : 1.85 Rwp` : 2.47 Rp` : 2.05 DW : 1.19

**Quantitative Analysis - Rietveld**

Phase 1 : Diamant 95.47(16) %  
 Phase 2 : "Moissanite 6H" 4.53(16) %

**Background**

One on X 62000 (34000)  
 Chebychev polynomial, Coefficient 0 -690 (540)  
 1 550 (380)  
 2 -180 (130)  
 3 89 (47)  
 4 -37 (16)

## Annex

|   |           |
|---|-----------|
| 5 | 18.5 (54) |
| 6 | -9.0 (18) |

### Instrument

|                                  |                |
|----------------------------------|----------------|
| Primary radius (mm)              | 200            |
| Secondary radius (mm)            | 200            |
| Linear PSD 2Th angular range (°) | 2.546          |
| FDS angle (°)                    | 0.5            |
| Beam spill, sample length (mm)   | 20             |
| Intensity corrected              |                |
| Full Axial Convolution           |                |
| Filament length (mm)             | 15             |
| Sample length (mm)               | 15             |
| Receiving Slit length (mm)       | 15             |
| Primary Sollers (°)              | 4.6            |
| Secondary Sollers (°)            | 4.6            |
| Tube_Tails                       |                |
| Source Width (mm)                | 0.0006405515   |
| Z1 (mm)                          | -7.282288e-005 |
| Z2 (mm)                          | 1.165302       |
| Fraction                         | 2.113079e-005  |

### Corrections

|                   |             |
|-------------------|-------------|
| Zero error        | 0.0168 (35) |
| LP Factor         | 0           |
| Absorption (1/cm) | 500 (1200)  |

### Miscellaneous

|                    |      |
|--------------------|------|
| X Calculation Step | 0.02 |
| Start X            | 30   |
| Finish X           | 130  |

### Structure 1

|   |              |
|---|--------------|
| Phase name                              | Diamant      |
| R-Bragg                                 | 1.214        |
| Spacegroup                              | Fd-3m        |
| Scale                                   | 0.4013 (16)  |
| Cell Mass                               | 96.088       |
| Cell Volume (Å <sup>3</sup> )           | 45.3752 (57) |
| Wt% - Rietveld                          | 95.47 (16)   |
| Crystallite Size                        |              |
| Cry size Lorentzian (nm)                | 38.54 (26)   |
| Crystal Linear Absorption Coeff. (1/cm) | 15.9061 (20) |
| Crystal Density (g/cm <sup>3</sup> )    | 3.51643 (44) |
| Lattice parameters                      |              |
| a (Å)                                   | 3.56675 (15) |

| Site | Np | x       | y       | z       | Atom | Occ | Beq        |
|------|----|---------|---------|---------|------|-----|------------|
| C1   | 8  | 0.00000 | 0.00000 | 0.00000 | C    | 1   | 2.915 (21) |

### Structure 2

|                               |               |
|-------------------------------|---------------|
| Phase name                    | Moissanite 6H |
| R-Bragg                       | 1.966         |
| Spacegroup                    | P63mc         |
| Scale                         | 0.00462 (17)  |
| Cell Mass                     | 144.133       |
| Cell Volume (Å <sup>3</sup> ) | 124.64 (14)   |
| Wt% - Rietveld                | 4.53 (16)     |
| Crystallite Size              |               |
| Cry size Lorentzian (nm)      | 12.41 (50)    |

## Annex

Crystal Linear Absorption Coeff. (1/cm) 8.6862 (98)  
 Crystal Density (g/cm<sup>3</sup>) 1.9203 (22)  
 Lattice parameters  
   a (Å) 3.0827 (13)  
   c (Å) 15.144 (11)

| Site | Np | x       | y       | z       | Atom | Occ | Beq       |
|------|----|---------|---------|---------|------|-----|-----------|
| Si1  | 2  | 0.00000 | 0.00000 | 0.00000 | C    | 1   | 0.45 (18) |
| Si2  | 2  | 0.66667 | 0.33333 | 0.16678 | C    | 1   | 0.45 (18) |
| Si3  | 2  | 0.33333 | 0.66667 | 0.33323 | C    | 1   | 0.45 (18) |
| C1   | 2  | 0.00000 | 0.00000 | 0.12527 | C    | 1   | 0.45 (18) |
| C2   | 2  | 0.66667 | 0.33333 | 0.29188 | C    | 1   | 0.45 (18) |
| C3   | 2  | 0.33333 | 0.66667 | 0.45850 | C    | 1   | 0.45 (18) |

**File 3 : "H:\\_Projekte ab  
 2014\\_Extern\Diamant\_Holland\XCEL\_26min\_rot\_2\_12  
 5nm\_diamant\_apr2015\_5\_135.xy"**

Range Number : 1

### R-Values

Rexp : 3.62    Rwp : 6.68    Rp : 5.08    GOF : 1.84  
 Rexp` : 2.85    Rwp` : 5.25    Rp` : 4.17    DW : 0.65

### Quantitative Analysis - Rietveld

Phase 1 : Diamant 99.498 (43) %  
 Phase 2 : Natron 0.502 (43) %

### Background

One on X 33300 (1100)  
 Chebychev polynomial, Coefficient  
   0 -303 (28)  
   1 620 (32)  
   2 -376 (19)  
   3 298 (10)  
   4 -173.5 (59)  
   5 87.1 (29)  
   6 -34.6 (16)

### Instrument

Primary radius (mm) 200  
 Secondary radius (mm) 200  
 Linear PSD 2Th angular range (°) 2.546  
   FDS angle (°) 0.5  
   Beam spill, sample length (mm) 20  
   Intensity corrected  
 Full Axial Convolution  
   Filament length (mm) 15  
   Sample length (mm) 15  
   Receiving Slit length (mm) 15  
   Primary Sollers (°) 4.6  
   Secondary Sollers (°) 4.6  
 Tube\_Tails  
   Source Width (mm) 0.0006405515  
   Z1 (mm) -7.282288e-005  
   Z2 (mm) 1.165302  
   Fraction 2.113079e-005

### Corrections

## Annex

|                   |             |
|-------------------|-------------|
| Zero error        | 0.0071 (25) |
| LP Factor         | 0           |
| Absorption (1/cm) | 500 (850)   |

**Miscellaneous**

|                    |      |
|--------------------|------|
| X Calculation Step | 0.02 |
| Start X            | 10   |

**Structure 1**

|   |              |
|---|--------------|
| Phase name                              | Diamant      |
| R-Bragg                                 | 1.652        |
| Spacegroup                              | Fd-3m        |
| Scale                                   | 0.9678 (32)  |
| Cell Mass                               | 96.088       |
| Cell Volume (Å <sup>3</sup> )           | 45.3705 (41) |
| Wt% - Rietveld                          | 99.498 (43)  |
| Crystallite Size                        |              |
| Cry size Lorentzian (nm)                | 44.59 (23)   |
| Crystal Linear Absorption Coeff. (1/cm) | 15.9077 (14) |
| Crystal Density (g/cm <sup>3</sup> )    | 3.51680 (32) |
| Lattice parameters                      |              |
| a (Å)                                   | 3.56663 (11) |

| Site | Np | x       | y       | z       | Atom | Occ | Beq        |
|------|----|---------|---------|---------|------|-----|------------|
| C1   | 8  | 0.00000 | 0.00000 | 0.00000 | C    | 1   | 2.643 (16) |

**Structure 2**

|   |                |
|---|----------------|
| Phase name                              | Natron         |
| R-Bragg                                 | 8.775          |
| Spacegroup                              | C1c1           |
| Scale                                   | 0.0000155 (13) |
| Cell Mass                               | 1063.930       |
| Cell Volume (Å <sup>3</sup> )           | 1294.1 (12)    |
| Wt% - Rietveld                          | 0.502 (43)     |
| Crystallite Size                        |                |
| Cry size Lorentzian (nm)                | 83 (16)        |
| Crystal Linear Absorption Coeff. (1/cm) | 19.590 (18)    |
| Crystal Density (g/cm <sup>3</sup> )    | 1.3652 (13)    |
| Lattice parameters                      |                |
| a (Å)                                   | 12.6877 (62)   |
| b (Å)                                   | 8.9956 (37)    |
| c (Å)                                   | 13.4426 (72)   |
| beta (°)                                | 122.493 (39)   |

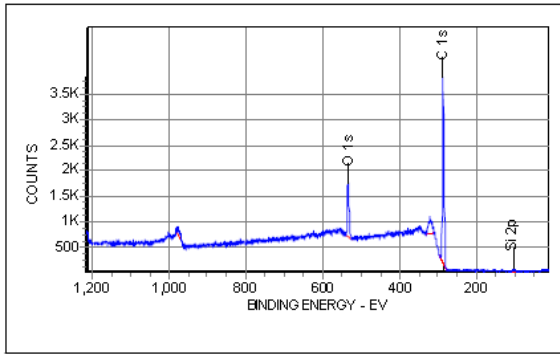
| Site | Np | x          | y          | z           | Atom | Occ | Beq        |
|------|----|------------|------------|-------------|------|-----|------------|
| Na1  | 4  | 0.231 (13) | 0.228 (15) | 0.123 (13)  | Na+1 | 1   | -1.01 (79) |
| Na2  | 4  | 0.225 (12) | 0.327 (12) | -0.107 (13) | Na+1 | 1   | -1.01 (79) |
| O1   | 4  | 0.12500    | -0.01200   | 0.09100     | O-2  | 1   | -1.01 (79) |
| O2   | 4  | 0.37600    | -0.44000   | 0.20800     | O-2  | 1   | -1.01 (79) |
| O3   | 4  | 0.09300    | 0.31200    | 0.17500     | O-2  | 1   | -1.01 (79) |
| O4   | 4  | 0.37400    | 0.12100    | 0.32200     | O-2  | 1   | -1.01 (79) |
| O5   | 4  | 0.13900    | 0.37400    | -0.05800    | O-2  | 1   | -1.01 (79) |
| O6   | 4  | 0.35500    | 0.12500    | 0.04700     | O-2  | 1   | -1.01 (79) |
| O7   | 4  | 0.12800    | 0.04900    | -0.21500    | O-2  | 1   | -1.01 (79) |
| O8   | 4  | 0.37200    | 0.50200    | -0.08000    | O-2  | 1   | -1.01 (79) |
| O9   | 4  | 0.12000    | 0.37600    | -0.33200    | O-2  | 1   | -1.01 (79) |
| O10  | 4  | 0.39900    | 0.18700    | -0.18600    | O-2  | 1   | -1.01 (79) |
| C1   | 4  | 0.25000    | 0.75400    | 0.00000     | C    | 1   | -1.01 (79) |
| O11  | 4  | 0.26600    | 0.71800    | 0.09700     | O-2  | 0.5 | -1.01 (79) |
| O12  | 4  | 0.34400    | 0.79300    | -0.00300    | O-2  | 0.5 | -1.01 (79) |

Annex

|     |   |         |         |          |     |     |            |
|-----|---|---------|---------|----------|-----|-----|------------|
| O13 | 4 | 0.13900 | 0.79400 | -0.09600 | O-2 | 0.5 | -1.01 (79) |
| O14 | 4 | 0.25300 | 0.83400 | -0.07300 | O-2 | 0.5 | -1.01 (79) |
| O15 | 4 | 0.15100 | 0.67500 | -0.00100 | O-2 | 0.5 | -1.01 (79) |
| O16 | 4 | 0.33600 | 0.80900 | 0.09300  | O-2 | 0.5 | -1.01 (79) |

### 5.3 X-ray photoelectron spectroscopy (XPS)

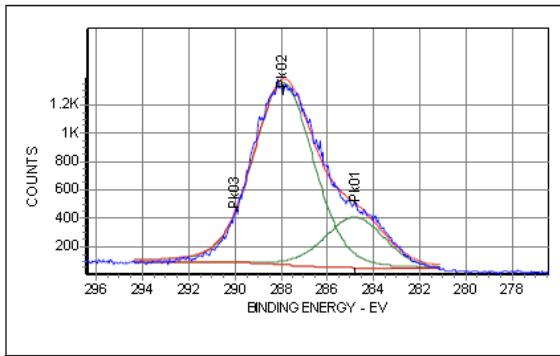
NDs of 25 nm of median size (Microdiamant AG), Spot 1 (Page 1)



| Region | Spotsize    | Resolution | nr. Scans | Date                 |
|--------|-------------|------------|-----------|----------------------|
| Survey | 250x1000 µm | 150 eV     | 5         | 7/29/2015 4:57:46 PM |

Composition Table

| XPS Line | Adj BE | Scans | Area  | Norm Area | Sigma | Atom % |
|----------|--------|-------|-------|-----------|-------|--------|
| P 2p     | 135.9  | 15    | 899   | 3.5       | 1.3   | 0.18   |
| N 1s     | 401.7  | 15    | 2948  | 8.9       | 1.7   | 0.45   |
| Si 2p    | 104.9  | 5     | 600   | 32.7      | 0.9   | 1.65   |
| C 1s     | 287.4  | 5     | 34629 | 1700.7    | 1.0   | 86.07  |
| O 1s     | 534.4  | 5     | 11683 | 230.1     | 2.5   | 11.65  |

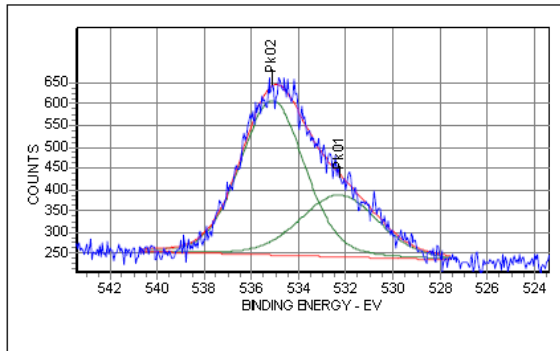


| Region | Spotsize    | Resolution | nr. Scans | Date                 |
|--------|-------------|------------|-----------|----------------------|
| C 1s   | 250x1000 µm | 50 eV      | 8         | 7/29/2015 5:05:59 PM |

Peak Fit Table

| XPS Line | Peak ID | Ch'm Shift | Adj BE | Area  | FWHM | % Assy | % Gauss | Group % |
|----------|---------|------------|--------|-------|------|--------|---------|---------|
| C 1s     | Pk03    |            | 289.94 | 0     | 3.00 | 0      | 80      | 0.00    |
| C 1s     | Pk02    |            | 287.89 | 86022 | 3.00 | 0      | 80      | 78.23   |
| C 1s     | Pk01    |            | 284.79 | 23943 | 3.00 | 0      | 80      | 21.77   |

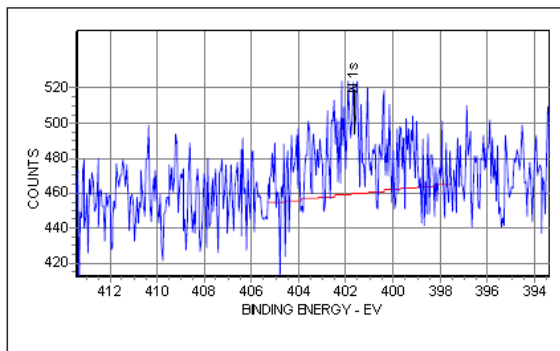
NDs of 25 nm of median size (Microdiamant AG), Spot 1 (Page 2)



| Region | Spotsize    | Resolution | nr. Scans | Date                 |
|--------|-------------|------------|-----------|----------------------|
| O 1s   | 250x1000 µm | 50 eV      | 8         | 7/29/2015 5:13:59 PM |

Peak Fit Table

| XPS Line | Peak ID | Ch'm Shift | Adj BE | Area  | FWHM | % Assy | % Gauss | Group % |
|----------|---------|------------|--------|-------|------|--------|---------|---------|
|          | Pk02    |            | 535.12 | 25677 | 3.16 | 0      | 80      | 67.41   |
|          | Pk01    |            | 532.28 | 12414 | 3.85 | 0      | 80      | 32.59   |



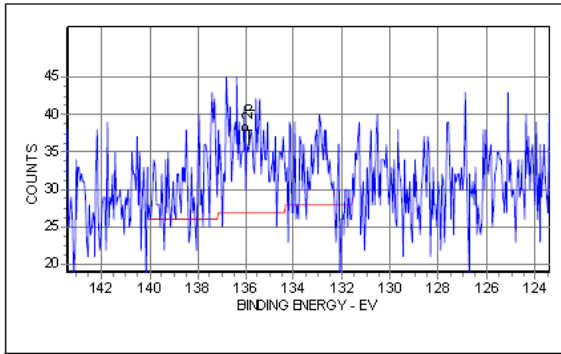
| Region | Spotsize    | Resolution | nr. Scans | Date                 |
|--------|-------------|------------|-----------|----------------------|
| N 1s   | 250x1000 µm | 50 eV      | 15        | 7/29/2015 5:28:58 PM |

Composition Table

| XPS Line | Adj BE | Scans | Area  | Norm Area | Sigma | Atom % |
|----------|--------|-------|-------|-----------|-------|--------|
| P 2p     | 135.9  | 15    | 899   | 3.5       | 1.3   | 0.18   |
| N 1s     | 401.7  | 15    | 2948  | 8.9       | 1.7   | 0.45   |
| Si 2p    | 104.9  | 5     | 600   | 32.7      | 0.9   | 1.65   |
| C 1s     | 287.4  | 5     | 34629 | 1700.7    | 1.0   | 86.07  |
| O 1s     | 534.4  | 5     | 11683 | 230.1     | 2.5   | 11.65  |



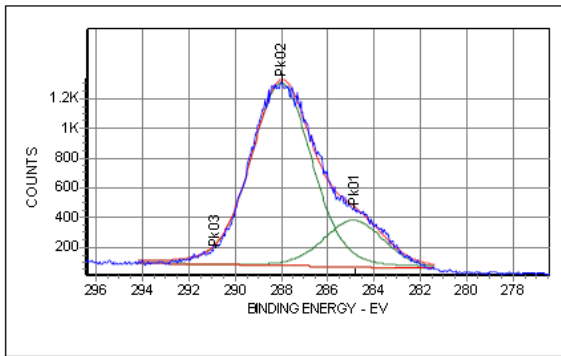
NDs of 25 nm of median size (Microdiamant AG), Spot 1 (Page 3)



| Region | Spotsize    | Resolution | nr. Scans | Date                 |
|--------|-------------|------------|-----------|----------------------|
| P 2p   | 250x1000 µm | 50 eV      | 15        | 7/29/2015 5:43:57 PM |

Composition Table

| XPS Line | Adj BE | Scans | Area  | Norm Area | Sigma | Atom % |
|----------|--------|-------|-------|-----------|-------|--------|
| P 2p     | 135.9  | 15    | 899   | 3.5       | 1.3   | 0.18   |
| N 1s     | 401.7  | 15    | 2948  | 8.9       | 1.7   | 0.45   |
| Si 2p    | 104.9  | 5     | 600   | 32.7      | 0.9   | 1.65   |
| C 1s     | 287.4  | 5     | 34629 | 1700.7    | 1.0   | 86.07  |
| O 1s     | 534.4  | 5     | 11683 | 230.1     | 2.5   | 11.65  |

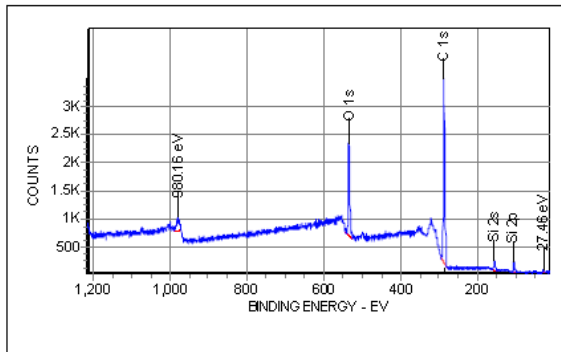


| Region | Spotsize    | Resolution | nr. Scans | Date                 |
|--------|-------------|------------|-----------|----------------------|
| C 1s   | 250x1000 µm | 50 eV      | 8         | 7/29/2015 5:51:58 PM |

Peak Fit Table

| XPS Line | Peak ID | Ch'm Shift | Adj BE | Area  | FWHM | % Assy | % Gauss | Group % |
|----------|---------|------------|--------|-------|------|--------|---------|---------|
|          | Pk03    |            | 290.82 | 0     | 3.00 | 0      | 80      | 0.00    |
|          | Pk02    |            | 287.99 | 83031 | 3.00 | 0      | 80      | 79.74   |
|          | Pk01    |            | 284.86 | 21101 | 3.00 | 0      | 80      | 20.26   |

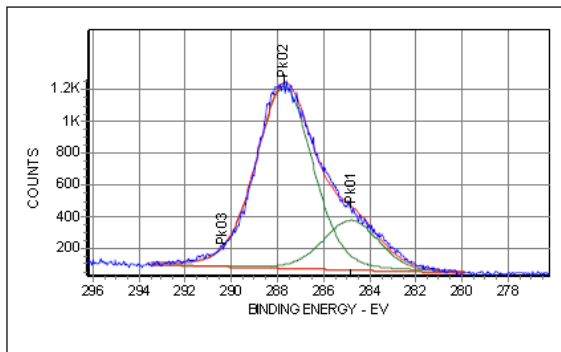
NDs of 25 nm of median size (Microdiamant AG), Spot 2 (Page 1)



| Region | Spotsize    | Resolution | nr. Scans | Date                 |
|--------|-------------|------------|-----------|----------------------|
| Survey | 250x1000 µm | 150 eV     | 5         | 7/29/2015 6:15:01 PM |

Composition Table

| XPS Line | Adj BE | Scans | Area  | Norm Area | Sigma | Atom % |
|----------|--------|-------|-------|-----------|-------|--------|
| N 1s     | 400.3  | 15    | 2562  | 7.8       | 1.7   | 0.40   |
| Si 2p    | 105.5  | 5     | 1659  | 90.3      | 0.9   | 4.69   |
| Si 2s    | 155.8  | 5     | 1852  | 88.5      | 1.0   | 4.60   |
| C 1s     | 287.4  | 5     | 29248 | 1436.3    | 1.0   | 74.62  |
| O 1s     | 534.7  | 5     | 15326 | 302.0     | 2.5   | 15.69  |

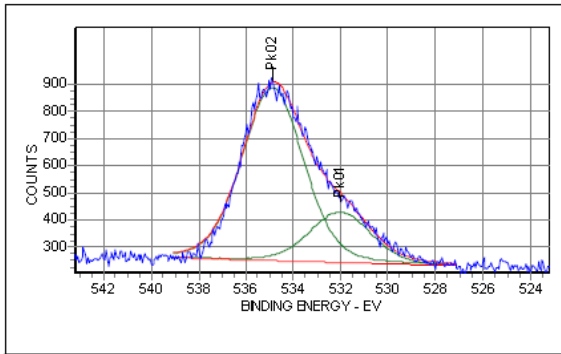


| Region | Spotsize    | Resolution | nr. Scans | Date                 |
|--------|-------------|------------|-----------|----------------------|
| C 1s   | 250x1000 µm | 50 eV      | 8         | 7/29/2015 6:23:14 PM |

Peak Fit Table

| XPS Line | Peak ID | Ch'm Shift | Adj BE | Area  | FWHM | % Assy | % Gauss | Group % |
|----------|---------|------------|--------|-------|------|--------|---------|---------|
| C 1s     | Pk03    |            | 290.33 | 0     | 2.80 | 0      | 80      | 0.00    |
| C 1s     | Pk02    |            | 287.69 | 71910 | 2.80 | 0      | 80      | 78.51   |
| C 1s     | Pk01    |            | 284.80 | 19681 | 2.80 | 0      | 80      | 21.49   |

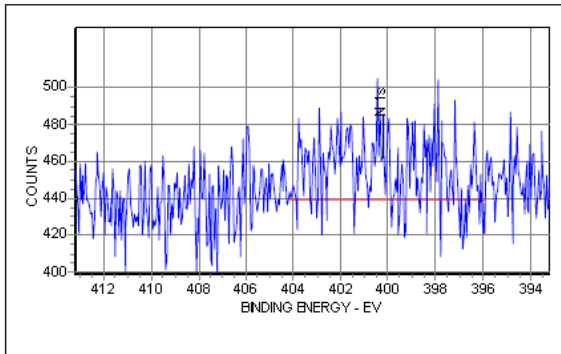
NDs of 25 nm of median size (Microdiamant AG), Spot 2 (Page 2)



| Region | Spotsize    | Resolution | nr. Scans | Date                 |
|--------|-------------|------------|-----------|----------------------|
| O 1s   | 250x1000 µm | 50 eV      | 8         | 7/29/2015 6:31:14 PM |

Peak Fit Table

| XPS Line | Peak ID | Ch'm Shift | Adj BE | Area  | FWHM | % Assy | % Gauss | Group % |
|----------|---------|------------|--------|-------|------|--------|---------|---------|
|          | Pk02    |            | 534.87 | 42701 | 3.00 | 0      | 80      | 77.28   |
|          | Pk01    |            | 532.01 | 12551 | 3.00 | 0      | 80      | 22.72   |

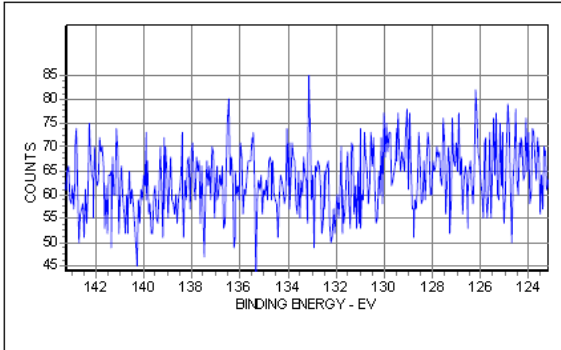


| Region | Spotsize    | Resolution | nr. Scans | Date                 |
|--------|-------------|------------|-----------|----------------------|
| N 1s   | 250x1000 µm | 50 eV      | 15        | 7/29/2015 6:46:13 PM |

Composition Table

| XPS Line | Adj BE | Scans | Area  | Norm Area | Sigma | Atom % |
|----------|--------|-------|-------|-----------|-------|--------|
| N 1s     | 400.3  | 15    | 2562  | 7.8       | 1.7   | 0.40   |
| Si 2p    | 105.5  | 5     | 1659  | 90.3      | 0.9   | 4.69   |
| Si 2s    | 155.8  | 5     | 1852  | 88.5      | 1.0   | 4.60   |
| C 1s     | 287.4  | 5     | 29248 | 1436.3    | 1.0   | 74.62  |
| O 1s     | 534.7  | 5     | 15326 | 302.0     | 2.5   | 15.69  |

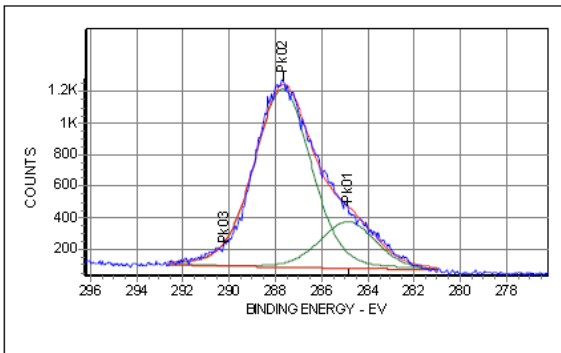
NDs of 25 nm of median size (Microdiamant AG), Spot 2 (Page 3)



| Region | Spotsize    | Resolution | nr. Scans | Date                 |
|--------|-------------|------------|-----------|----------------------|
| P 2p   | 250x1000 µm | 50 eV      | 15        | 7/29/2015 7:01:13 PM |

Composition Table

| XPS Line | Adj BE | Scans | Area  | Norm Area | Sigma | Atom % |
|----------|--------|-------|-------|-----------|-------|--------|
| N 1s     | 400.3  | 15    | 2562  | 7.8       | 1.7   | 0.40   |
| Si 2p    | 105.5  | 5     | 1659  | 90.3      | 0.9   | 4.69   |
| Si 2s    | 155.8  | 5     | 1852  | 88.5      | 1.0   | 4.60   |
| C 1s     | 287.4  | 5     | 29248 | 1436.3    | 1.0   | 74.62  |
| O 1s     | 534.7  | 5     | 15326 | 302.0     | 2.5   | 15.69  |

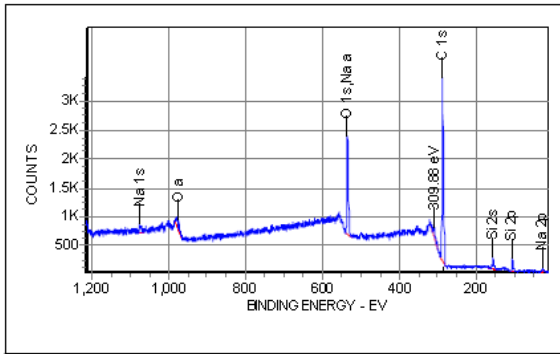


| Region | Spotsize    | Resolution | nr. Scans | Date                 |
|--------|-------------|------------|-----------|----------------------|
| C 1s   | 250x1000 µm | 50 eV      | 8         | 7/29/2015 7:09:13 PM |

Peak Fit Table

| XPS Line | Peak ID | Ch'm Shift | Adj BE | Area  | FWHM | % Assy | % Gauss | Group % |
|----------|---------|------------|--------|-------|------|--------|---------|---------|
|          | Pk03    |            | 290.16 | 0     | 2.80 | 0      | 80      | 0.00    |
|          | Pk02    |            | 287.67 | 70912 | 2.80 | 0      | 80      | 79.33   |
|          | Pk01    |            | 284.85 | 18480 | 2.80 | 0      | 80      | 20.67   |

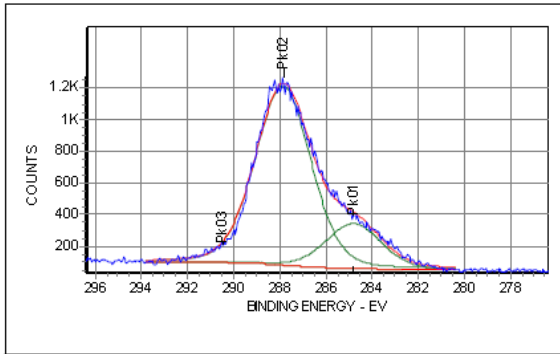
NDs of 25 nm of median size (Microdiamant AG), Spot 3 (Page 1)



| Region | Spotsize    | Resolution | nr. Scans | Date                 |
|--------|-------------|------------|-----------|----------------------|
| Survey | 250x1000 µm | 150 eV     | 5         | 7/29/2015 7:32:16 PM |

Composition Table

| XPS Line | Adj BE | Scans | Area  | Norm Area | Sigma | Atom % |
|----------|--------|-------|-------|-----------|-------|--------|
| N 1s     | 401.8  | 15    | 2029  | 6.1       | 1.7   | 0.35   |
| Si 2p    | 106.3  | 5     | 1698  | 92.5      | 0.9   | 5.21   |
| C 1s     | 287.8  | 5     | 27602 | 1355.8    | 1.0   | 76.39  |
| O 1s     | 534.9  | 5     | 15431 | 304.1     | 2.5   | 17.13  |
| Na 1s    | 1074.8 | 5     | 1335  | 16.3      | 4.0   | 0.92   |

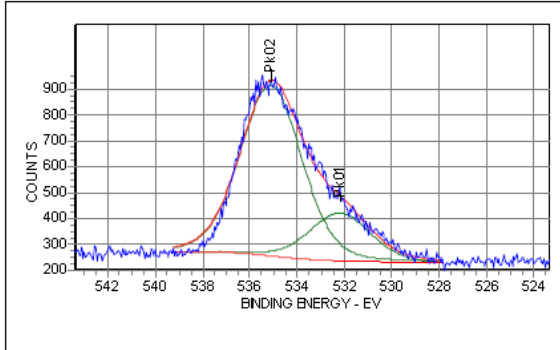


| Region | Spotsize    | Resolution | nr. Scans | Date                 |
|--------|-------------|------------|-----------|----------------------|
| C 1s   | 250x1000 µm | 50 eV      | 8         | 7/29/2015 7:40:33 PM |

Peak Fit Table

| XPS Line | Peak ID | Ch'm Shift | Adj BE | Area  | FWHM | % Assy | % Gauss | Group % |
|----------|---------|------------|--------|-------|------|--------|---------|---------|
| C 1s     | Pk03    |            | 290.44 | 0     | 2.80 | 0      | 80      | 0.00    |
| C 1s     | Pk02    |            | 287.84 | 71296 | 2.80 | 0      | 80      | 79.95   |
| C 1s     | Pk01    |            | 284.79 | 17881 | 2.80 | 0      | 80      | 20.05   |

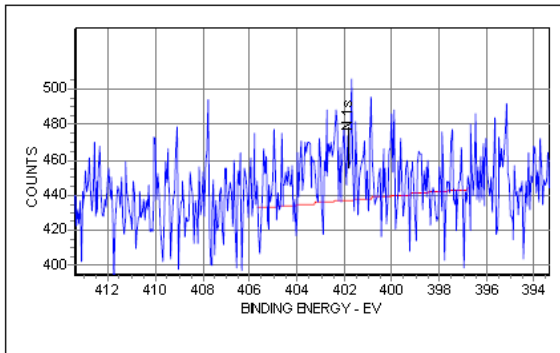
NDs of 25 nm of median size (Microdiamant AG), Spot 3 (Page 2)



| Region | Spotsize    | Resolution | nr. Scans | Date                 |
|--------|-------------|------------|-----------|----------------------|
| O 1s   | 250x1000 µm | 50 eV      | 8         | 7/29/2015 7:48:34 PM |

Peak Fit Table

| XPS Line | Peak ID | Ch'm Shift | Adj BE | Area  | FWHM | % Assy | % Gauss | Group % |
|----------|---------|------------|--------|-------|------|--------|---------|---------|
|          | Pk02    |            | 535.10 | 44141 | 3.00 | 0      | 80      | 78.11   |
|          | Pk01    |            | 532.19 | 12368 | 3.00 | 0      | 80      | 21.89   |

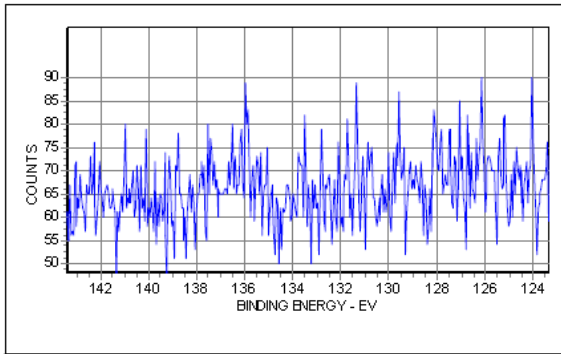


| Region | Spotsize    | Resolution | nr. Scans | Date                 |
|--------|-------------|------------|-----------|----------------------|
| N 1s   | 250x1000 µm | 50 eV      | 15        | 7/29/2015 8:03:33 PM |

Composition Table

| XPS Line | Adj BE | Scans | Area  | Norm Area | Sigma | Atom % |
|----------|--------|-------|-------|-----------|-------|--------|
| N 1s     | 401.8  | 15    | 2029  | 6.1       | 1.7   | 0.35   |
| Si 2p    | 106.3  | 5     | 1698  | 92.5      | 0.9   | 5.21   |
| C 1s     | 287.8  | 5     | 27602 | 1355.8    | 1.0   | 76.39  |
| O 1s     | 534.9  | 5     | 15431 | 304.1     | 2.5   | 17.13  |
| Na 1s    | 1074.8 | 5     | 1335  | 16.3      | 4.0   | 0.92   |

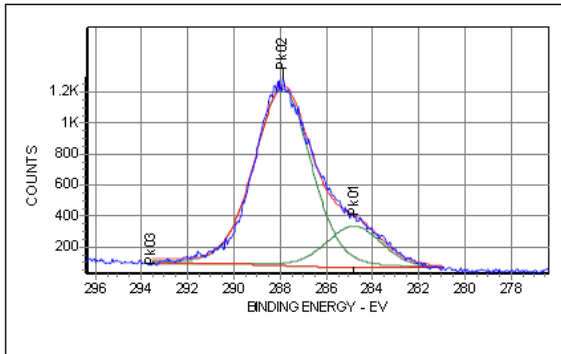
NDs of 25 nm of median size (Microdiamant AG), Spot 3 (Page 3)



| Region | Spotsize    | Resolution | nr. Scans | Date                 |
|--------|-------------|------------|-----------|----------------------|
| P 2p   | 250x1000 µm | 50 eV      | 15        | 7/29/2015 8:18:32 PM |

Composition Table

| XPS Line | Adj BE | Scans | Area  | Norm Area | Sigma | Atom % |
|----------|--------|-------|-------|-----------|-------|--------|
| N 1s     | 401.8  | 15    | 2029  | 6.1       | 1.7   | 0.35   |
| Si 2p    | 106.3  | 5     | 1698  | 92.5      | 0.9   | 5.21   |
| C 1s     | 287.8  | 5     | 27602 | 1355.8    | 1.0   | 76.39  |
| O 1s     | 534.9  | 5     | 15431 | 304.1     | 2.5   | 17.13  |
| Na 1s    | 1074.8 | 5     | 1335  | 16.3      | 4.0   | 0.92   |

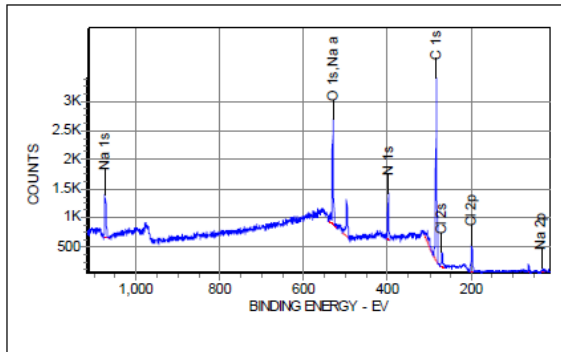


| Region | Spotsize    | Resolution | nr. Scans | Date                 |
|--------|-------------|------------|-----------|----------------------|
| C 1s   | 250x1000 µm | 50 eV      | 8         | 7/29/2015 8:26:33 PM |

Peak Fit Table

| XPS Line | Peak ID | Ch'm Shift | Adj BE | Area  | FWHM | % Assy | % Gauss | Group % |
|----------|---------|------------|--------|-------|------|--------|---------|---------|
|          | Pk03    |            | 293.51 | 487   | 1.43 | 0      | 80      | 0.55    |
|          | Pk02    |            | 287.87 | 71773 | 2.80 | 0      | 80      | 80.57   |
|          | Pk01    |            | 284.78 | 16825 | 2.80 | 0      | 80      | 18.89   |

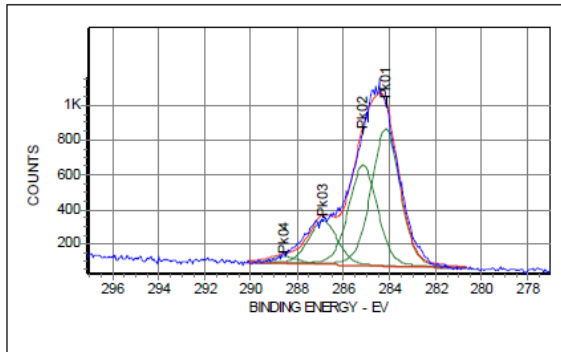
NDs of 25 nm of median size (Microdiamant AG) in DMEM with 10% FBS (Page 1)



| Region   | Spotsize    | Resolution | nr. Scans | Date                 |
|----------|-------------|------------|-----------|----------------------|
| Widescan | 250x1000 µm | 150 eV     | 5         | 7/16/2014 2:27:14 PM |

Composition Table

| XPS Line | Adj BE | Scans | Area  | Norm Area | Sigma | Atom % |
|----------|--------|-------|-------|-----------|-------|--------|
| Cl 2p    | 200.4  | 5     | 3418  | 68.1      | 2.4   | 4.61   |
| C 1s     | 284.6  | 5     | 20324 | 970.3     | 1.0   | 65.73  |
| N 1s     | 399.1  | 5     | 4353  | 123.8     | 1.7   | 8.39   |
| O 1s     | 530.9  | 5     | 12691 | 242.8     | 2.5   | 16.45  |
| Na 1s    | 1073.4 | 5     | 6011  | 71.1      | 4.0   | 4.82   |

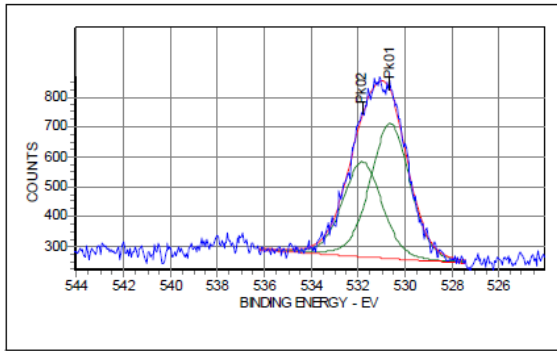


| Region | Spotsize    | Resolution | nr. Scans | Date                 |
|--------|-------------|------------|-----------|----------------------|
| C 1s   | 250x1000 µm | 50 eV      | 8         | 7/16/2014 2:35:37 PM |

Peak Fit Table

| XPS Line | Peak ID | Ch'm Shift | Adj BE | Area  | FWHM | % Assy | % Gauss | Group % |
|----------|---------|------------|--------|-------|------|--------|---------|---------|
|          | Pk04    |            | 288.53 | 1230  | 1.41 | 0      | 80      | 2.31    |
|          | Pk03    |            | 286.88 | 8124  | 1.40 | 0      | 80      | 15.29   |
|          | Pk02    |            | 285.14 | 18514 | 1.40 | 0      | 80      | 34.84   |
|          | Pk01    |            | 284.17 | 25266 | 1.40 | 0      | 80      | 47.55   |

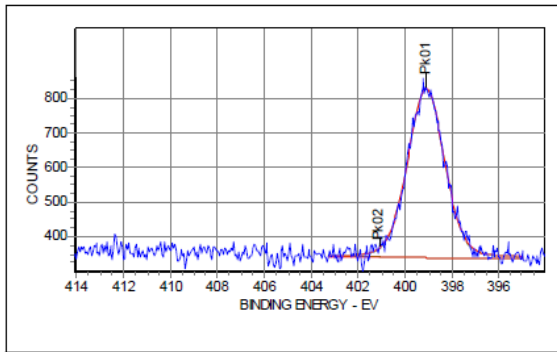
NDs of 25 nm of median size (Microdiamant AG) in DMEM with 10% FBS (Page 2)



| Region | Spotsize    | Resolution | nr. Scans | Date                 |
|--------|-------------|------------|-----------|----------------------|
| O 1s   | 250x1000 µm | 50 eV      | 8         | 7/16/2014 2:43:49 PM |

Peak Fit Table

| XPS Line | Peak ID | Ch'm Shift | Adj BE | Area  | FWHM | % Assy | % Gauss | Group % |
|----------|---------|------------|--------|-------|------|--------|---------|---------|
|          | Pk02    |            | 531.81 | 13612 | 1.90 | 0      | 80      | 41.35   |
|          | Pk01    |            | 530.62 | 19304 | 1.90 | 0      | 80      | 58.65   |

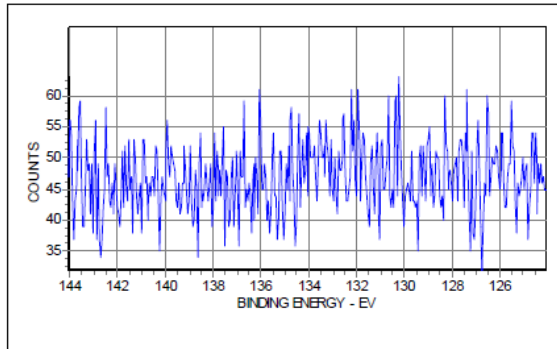


| Region | Spotsize    | Resolution | nr. Scans | Date                 |
|--------|-------------|------------|-----------|----------------------|
| N 1s   | 250x1000 µm | 50 eV      | 15        | 7/16/2014 2:59:08 PM |

Peak Fit Table

| XPS Line | Peak ID | Ch'm Shift | Adj BE | Area  | FWHM | % Assy | % Gauss | Group % |
|----------|---------|------------|--------|-------|------|--------|---------|---------|
|          | Pk02    |            | 401.10 | 0     | 1.80 | 0      | 80      | 0.00    |
|          | Pk01    |            | 399.10 | 19455 | 1.77 | 0      | 80      | 100.00  |

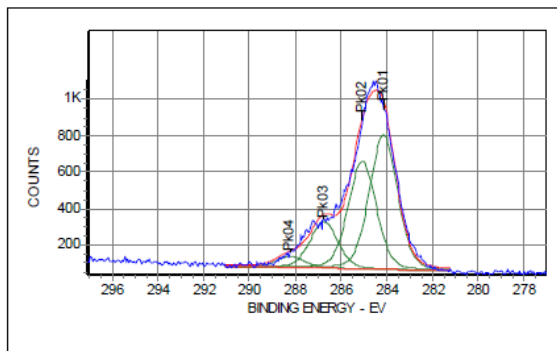
NDs of 25 nm of median size (Microdiamant AG) in DMEM with 10% FBS (Page 3)



| Region | Spotsize    | Resolution | nr. Scans | Date                 |
|--------|-------------|------------|-----------|----------------------|
| P 2p   | 250x1000 µm | 50 eV      | 15        | 7/16/2014 3:14:36 PM |

Composition Table

| XPS Line | Adj BE | Scans | Area  | Norm Area | Sigma | Atom % |
|----------|--------|-------|-------|-----------|-------|--------|
| Cl 2p    | 200.4  | 5     | 3418  | 68.1      | 2.4   | 4.61   |
| C 1s     | 284.6  | 5     | 20324 | 970.3     | 1.0   | 65.73  |
| N 1s     | 399.1  | 5     | 4353  | 123.8     | 1.7   | 8.39   |
| O 1s     | 530.9  | 5     | 12691 | 242.8     | 2.5   | 16.45  |
| Na 1s    | 1073.4 | 5     | 6011  | 71.1      | 4.0   | 4.82   |

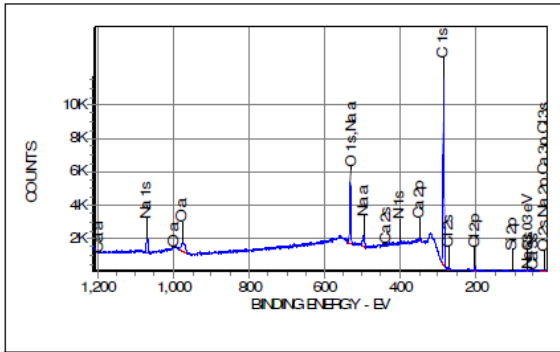


| Region | Spotsize    | Resolution | nr. Scans | Date                 |
|--------|-------------|------------|-----------|----------------------|
| C 1s   | 250x1000 µm | 50 eV      | 8         | 7/16/2014 3:22:47 PM |

Peak Fit Table

| XPS Line | Peak ID | Ch'm Shift | Adj BE | Area  | FWHM | % Assy | % Gauss | Group % |
|----------|---------|------------|--------|-------|------|--------|---------|---------|
|          | Pk04    |            | 288.20 | 1971  | 1.40 | 0      | 80      | 3.78    |
|          | Pk03    |            | 286.75 | 8090  | 1.40 | 0      | 80      | 15.50   |
|          | Pk02    |            | 285.07 | 18782 | 1.40 | 0      | 80      | 35.99   |
|          | Pk01    |            | 284.15 | 23343 | 1.40 | 0      | 80      | 44.73   |

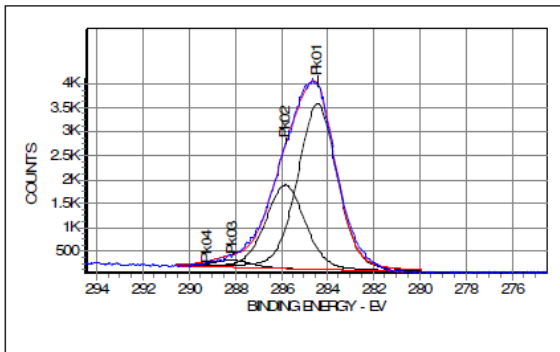
NDs of 25 nm of median size (Microdiamant AG) in DMEM (without FBS) – A (Page 1)



| Region | Spotsize    | Resolution | nr. Scans | Date                  |
|--------|-------------|------------|-----------|-----------------------|
| Survey | 250x1000 µm | 150 eV     | 5         | 4/23/2015 12:40:06 PM |

Composition Table

| XPS Line | Adj BE | Scans | Area  | Norm Area | Sigma | Atom % |
|----------|--------|-------|-------|-----------|-------|--------|
| Si 2p    | 102.5  | 5     | 683   | 37.1      | 0.9   | 0.83   |
| Cl 2p    | 200.8  | 5     | 2854  | 58.4      | 2.4   | 1.31   |
| C 1s     | 284.6  | 5     | 72993 | 3578.9    | 1.0   | 80.39  |
| Ca 2p    | 347.6  | 5     | 2835  | 28.5      | 4.9   | 0.64   |
| N 1s     | 398.7  | 5     | 2944  | 86.0      | 1.7   | 1.93   |
| O 1s     | 531.5  | 5     | 28506 | 560.3     | 2.5   | 12.59  |
| Na 1s    | 1071.4 | 5     | 8496  | 102.9     | 4.0   | 2.31   |

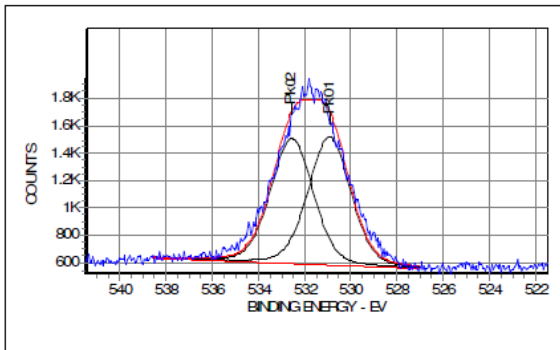


| Region | Spotsize    | Resolution | nr. Scans | Date               |
|--------|-------------|------------|-----------|--------------------|
| C 1s   | 250x1000 µm | 50 eV      | 8         | 4/23/2015 12:48:19 |

Peak Fit Table

| XPS Line | Peak ID | Ch'm Shift | Adj BE | Area   | FWHM | % Assy | % Gauss | Group % |
|----------|---------|------------|--------|--------|------|--------|---------|---------|
|          | Pk04    | 0.00       | 289.19 | 0      | 1.90 | 0      | 80      | 0.00    |
|          | Pk03    | 0.00       | 288.11 | 6085   | 1.90 | 0      | 80      | 2.66    |
|          | Pk02    | 0.00       | 285.82 | 75058  | 1.90 | 0      | 80      | 32.78   |
|          | Pk01    | 0.00       | 284.42 | 147831 | 1.90 | 0      | 80      | 64.56   |

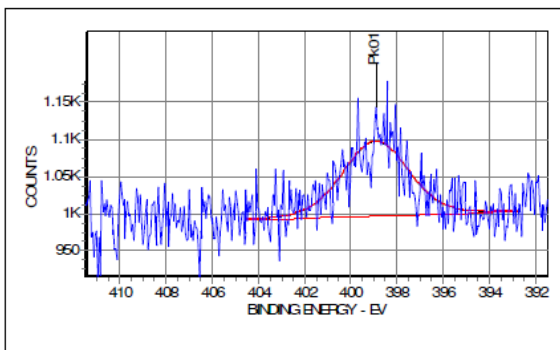
NDs of 25 nm of median size (Microdiamant AG) in DMEM (without FBS) – A (Page 2)



| Region | Spotsize    | Resolution | nr. Scans | Date               |
|--------|-------------|------------|-----------|--------------------|
| O 1s   | 250x1000 µm | 50 eV      | 8         | 4/23/2015 12:56:19 |

Peak Fit Table

| XPS Line | Peak ID | Ch'm Shift | Adj BE | Area  | FWHM | % Assy | % Gauss | Group % |
|----------|---------|------------|--------|-------|------|--------|---------|---------|
|          | Pk02    | 0.00       | 532.54 | 43443 | 2.10 | 0      | 80      | 49.52   |
|          | Pk01    | 0.00       | 530.91 | 44285 | 2.10 | 0      | 80      | 50.48   |

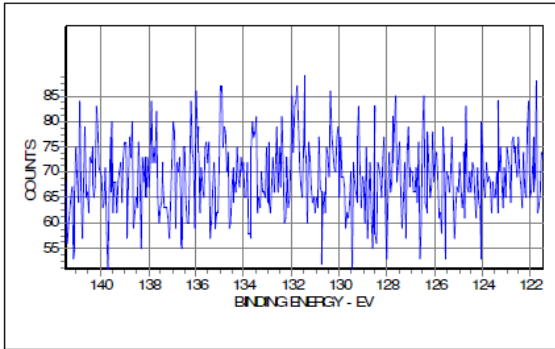


| Region | Spotsize    | Resolution | nr. Scans | Date                 |
|--------|-------------|------------|-----------|----------------------|
| N 1s   | 250x1000 µm | 50 eV      | 15        | 4/23/2015 1:11:18 PM |

Peak Fit Table

| XPS Line | Peak ID | Ch'm Shift | Adj BE | Area | FWHM | % Assy | % Gauss | Group % |
|----------|---------|------------|--------|------|------|--------|---------|---------|
|          | Pk01    | 0.00       | 398.91 | 7492 | 3.31 | 0      | 80      | 100.00  |

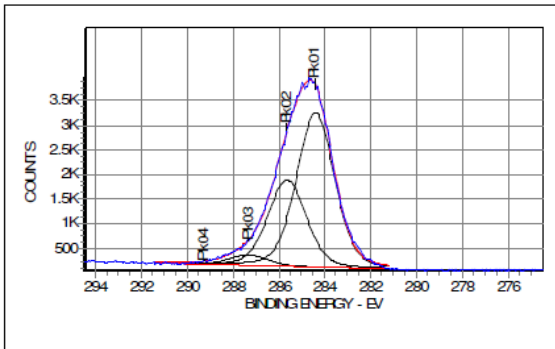
NDs of 25 nm of median size (Microdiamant AG) in DMEM (without FBS) – A (Page 3)



| Region | Spotsize    | Resolution | nr. Scans | Date                 |
|--------|-------------|------------|-----------|----------------------|
| P 2p   | 250x1000 µm | 50 eV      | 15        | 4/23/2015 1:26:17 PM |

Composition Table

| XPS Line | Adj BE | Scans | Area  | Norm Area | Sigma | Atom % |
|----------|--------|-------|-------|-----------|-------|--------|
| Si 2p    | 102.5  | 5     | 683   | 37.1      | 0.9   | 0.83   |
| Cl 2p    | 200.8  | 5     | 2854  | 58.4      | 2.4   | 1.31   |
| C 1s     | 284.6  | 5     | 72993 | 3578.9    | 1.0   | 80.39  |
| Ca 2p    | 347.6  | 5     | 2835  | 28.5      | 4.9   | 0.64   |
| N 1s     | 398.7  | 5     | 2944  | 86.0      | 1.7   | 1.93   |
| O 1s     | 531.5  | 5     | 28506 | 560.3     | 2.5   | 12.59  |
| Na 1s    | 1071.4 | 5     | 8496  | 102.9     | 4.0   | 2.31   |

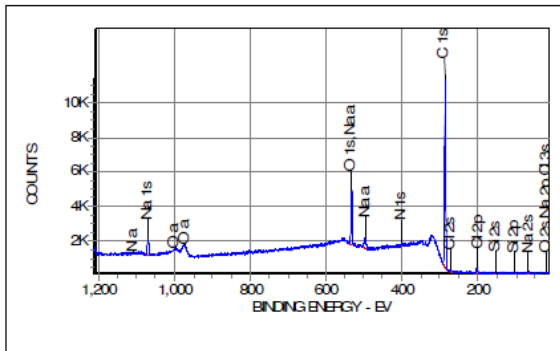


| Region | Spotsize    | Resolution | nr. Scans | Date                 |
|--------|-------------|------------|-----------|----------------------|
| C 1s   | 250x1000 µm | 50 eV      | 8         | 4/23/2015 1:34:17 PM |

Peak Fit Table

| XPS Line | Peak ID | Ch'm Shift | Adj BE | Area   | FWHM | % Assy | % Gauss | Group % |
|----------|---------|------------|--------|--------|------|--------|---------|---------|
|          | Pk04    | 0.00       | 289.21 | 0      | 1.90 | 0      | 80      | 0.00    |
|          | Pk03    | 0.00       | 287.32 | 9055   | 1.90 | 0      | 80      | 4.15    |
|          | Pk02    | 0.00       | 285.63 | 75518  | 1.90 | 0      | 80      | 34.58   |
|          | Pk01    | 0.00       | 284.38 | 133788 | 1.90 | 0      | 80      | 61.27   |

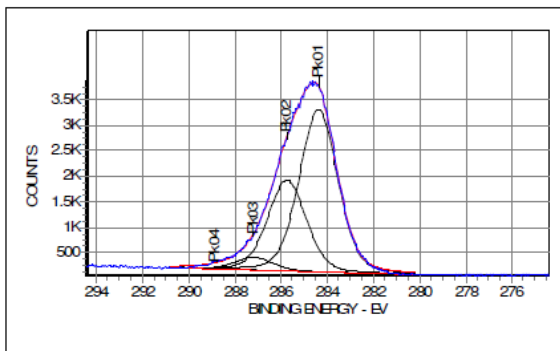
NDs of 25 nm of median size (Microdiamant AG) in DMEM (without FBS) – B (Page 1)



| Region | Spotsize    | Resolution | nr. Scans | Date                 |
|--------|-------------|------------|-----------|----------------------|
| Survey | 250x1000 µm | 150 eV     | 4         | 4/23/2015 3:15:32 PM |

Composition Table

| XPS Line | Adj BE | Scans | Area  | Norm Area | Sigma | Atom % |
|----------|--------|-------|-------|-----------|-------|--------|
| Si 2p    | 102.4  | 4     | 489   | 33.2      | 0.9   | 0.61   |
| Cl 2p    | 200.1  | 4     | 3312  | 84.7      | 2.4   | 1.57   |
| C 1s     | 284.6  | 4     | 72140 | 4421.3    | 1.0   | 81.76  |
| N 1s     | 398.4  | 4     | 2242  | 81.8      | 1.7   | 1.51   |
| O 1s     | 531.4  | 4     | 26609 | 653.7     | 2.5   | 12.09  |
| Na 1s    | 1071.0 | 4     | 8802  | 133.1     | 4.1   | 2.46   |

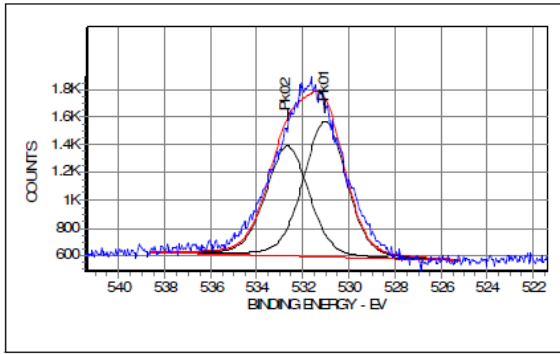


| Region | Spotsize    | Resolution | nr. Scans | Date                 |
|--------|-------------|------------|-----------|----------------------|
| C 1s   | 250x1000 µm | 50 eV      | 8         | 4/23/2015 3:23:44 PM |

Peak Fit Table

| XPS Line | Peak ID | Ch'm Shift | Adj BE | Area   | FWHM | % Assy | % Gauss | Group % |
|----------|---------|------------|--------|--------|------|--------|---------|---------|
|          | Pk04    | 0.00       | 288.77 | 1192   | 1.90 | 0      | 80      | 0.53    |
|          | Pk03    | 0.00       | 287.17 | 10430  | 1.90 | 0      | 80      | 4.65    |
|          | Pk02    | 0.00       | 285.73 | 76484  | 1.90 | 0      | 80      | 34.09   |
|          | Pk01    | 0.00       | 284.36 | 136220 | 1.90 | 0      | 80      | 60.72   |

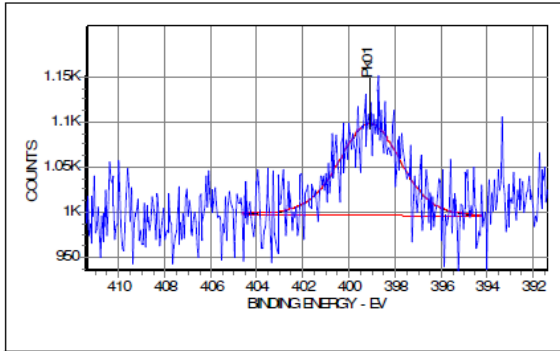
NDs of 25 nm of median size (Microdiamant AG) in DMEM (without FBS) – B (Page 2)



| Region | Spotsize    | Resolution | nr. Scans | Date                 |
|--------|-------------|------------|-----------|----------------------|
| O 1s   | 250x1000 µm | 50 eV      | 8         | 4/23/2015 3:31:44 PM |

Peak Fit Table

| XPS Line | Peak ID | Ch'm Shift | Adj BE | Area  | FWHM | % Assy | % Gauss | Group % |
|----------|---------|------------|--------|-------|------|--------|---------|---------|
|          | Pk02    | 0.00       | 532.67 | 37910 | 2.11 | 0      | 80      | 44.86   |
|          | Pk01    | 0.00       | 531.04 | 46594 | 2.10 | 0      | 80      | 55.14   |

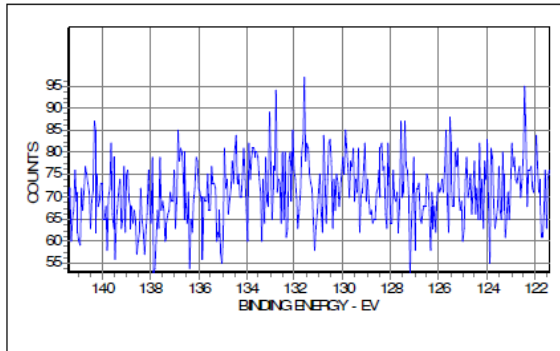


| Region | Spotsize    | Resolution | nr. Scans | Date                 |
|--------|-------------|------------|-----------|----------------------|
| N 1s   | 250x1000 µm | 50 eV      | 14        | 4/23/2015 3:46:43 PM |

Peak Fit Table

| XPS Line | Peak ID | Ch'm Shift | Adj BE | Area | FWHM | % Assy | % Gauss | Group % |
|----------|---------|------------|--------|------|------|--------|---------|---------|
|          | Pk01    | 0.00       | 399.09 | 7018 | 3.10 | 0      | 80      | 100.00  |

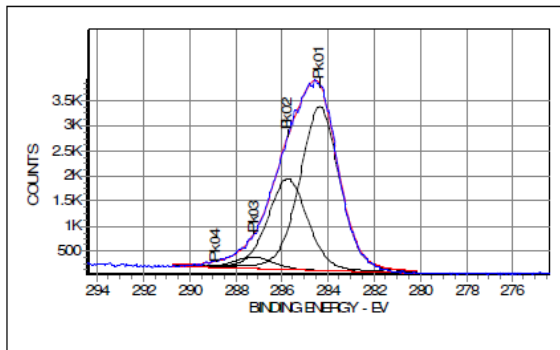
NDs of 25 nm of median size (Microdiamant AG) in DMEM (without FBS) – B (Page 3)



| Region | Spotsize    | Resolution | nr. Scans | Date                 |
|--------|-------------|------------|-----------|----------------------|
| P 2p   | 250x1000 µm | 50 eV      | 15        | 4/23/2015 4:01:42 PM |

Composition Table

| XPS Line | Adj BE | Scans | Area  | Norm Area | Sigma | Atom % |
|----------|--------|-------|-------|-----------|-------|--------|
| Si 2p    | 102.4  | 4     | 489   | 33.2      | 0.9   | 0.61   |
| Cl 2p    | 200.1  | 4     | 3312  | 84.7      | 2.4   | 1.57   |
| C 1s     | 284.6  | 4     | 72140 | 4421.3    | 1.0   | 81.76  |
| N 1s     | 398.4  | 4     | 2242  | 81.8      | 1.7   | 1.51   |
| O 1s     | 531.4  | 4     | 26609 | 653.7     | 2.5   | 12.09  |
| Na 1s    | 1071.0 | 4     | 8802  | 133.1     | 4.1   | 2.46   |



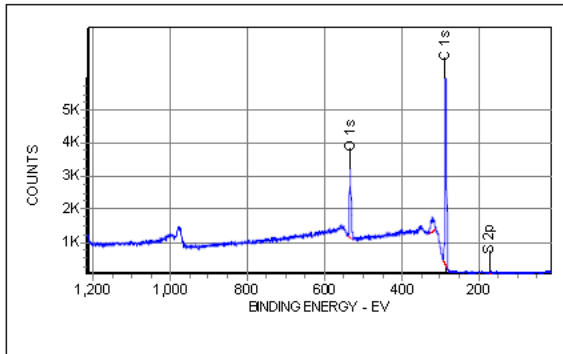
| Region | Spotsize    | Resolution | nr. Scans | Date                 |
|--------|-------------|------------|-----------|----------------------|
| C 1s   | 250x1000 µm | 50 eV      | 8         | 4/23/2015 4:09:43 PM |

Peak Fit Table

| XPS Line | Peak ID | Ch'm Shift | Adj BE | Area   | FWHM | % Assy | % Gauss | Group % |
|----------|---------|------------|--------|--------|------|--------|---------|---------|
|          | Pk04    | 0.00       | 288.79 | 1092   | 1.90 | 0      | 80      | 0.48    |
|          | Pk03    | 0.00       | 287.21 | 9780   | 1.90 | 0      | 80      | 4.30    |
|          | Pk02    | 0.00       | 285.73 | 77513  | 1.90 | 0      | 80      | 34.04   |
|          | Pk01    | 0.00       | 284.34 | 139304 | 1.90 | 0      | 80      | 61.18   |



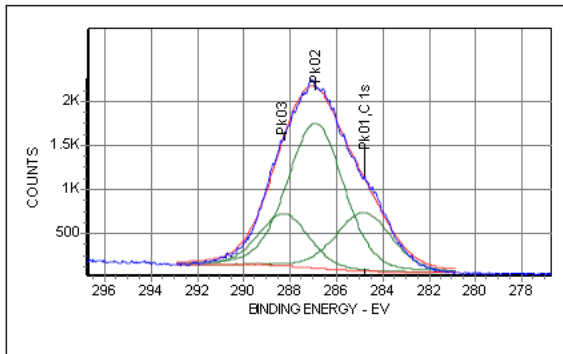
NDs of 25 nm of median size (Microdiamant AG) in YMB – A (Page 1)



| Region | Spotsize    | Resolution | nr. Scans | Date                 |
|--------|-------------|------------|-----------|----------------------|
| Survey | 250x1000 µm | 150 eV     | 5         | 7/29/2015 8:49:45 PM |

Composition Table

| XPS Line | Adj BE | Scans | Area  | Norm Area | Sigma | Atom % |
|----------|--------|-------|-------|-----------|-------|--------|
| P 2p     | 135.2  | 15    | 1474  | 5.8       | 1.3   | 0.18   |
| N 1s     | 402.4  | 15    | 4057  | 12.3      | 1.7   | 0.39   |
| S 2p     | 170.2  | 5     | 704   | 19.3      | 1.8   | 0.61   |
| C 1s     | 287.0  | 5     | 55721 | 2735.8    | 1.0   | 85.96  |
| O 1s     | 533.5  | 5     | 20799 | 409.4     | 2.5   | 12.86  |

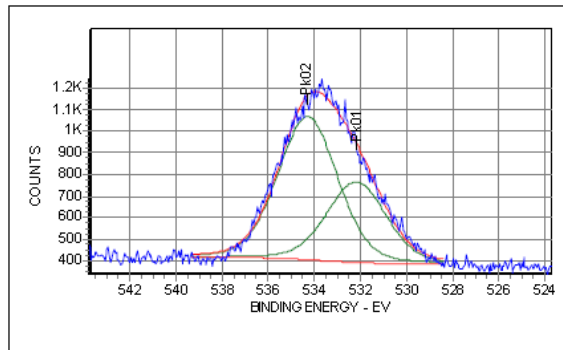


| Region | Spotsize    | Resolution | nr. Scans | Date                 |
|--------|-------------|------------|-----------|----------------------|
| C 1s   | 250x1000 µm | 50 eV      | 8         | 7/29/2015 8:57:57 PM |

Peak Fit Table

| XPS Line | Peak ID | Ch'm Shift | Adj BE | Area   | FWHM | % Assy | % Gauss | Group % |
|----------|---------|------------|--------|--------|------|--------|---------|---------|
| C 1s     | Pk03    |            | 288.26 | 33371  | 2.50 | 0      | 80      | 18.72   |
| C 1s     | Pk02    |            | 286.89 | 103320 | 2.80 | 0      | 80      | 57.96   |
| C 1s     | Pk01    |            | 284.80 | 41576  | 2.80 | 0      | 80      | 23.32   |

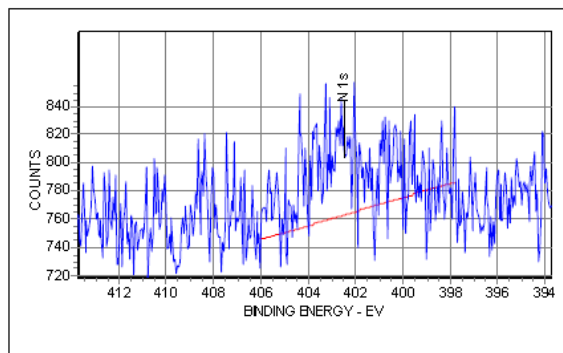
NDs of 25 nm of median size (Microdiamant AG) in YMB – A (Page 2)



| Region | Spotsize    | Resolution | nr. Scans | Date                 |
|--------|-------------|------------|-----------|----------------------|
| O 1s   | 250x1000 µm | 50 eV      | 8         | 7/29/2015 9:05:57 PM |

Peak Fit Table

| XPS Line | Peak ID | Ch'm Shift | Adj BE | Area  | FWHM | % Assy | % Gauss | Group % |
|----------|---------|------------|--------|-------|------|--------|---------|---------|
|          | Pk02    |            | 534.28 | 44203 | 3.00 | 0      | 80      | 64.11   |
|          | Pk01    |            | 532.17 | 24745 | 3.00 | 0      | 80      | 35.89   |

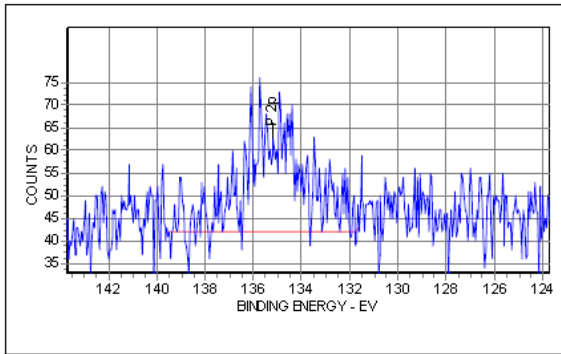


| Region | Spotsize    | Resolution | nr. Scans | Date                 |
|--------|-------------|------------|-----------|----------------------|
| N 1s   | 250x1000 µm | 50 eV      | 15        | 7/29/2015 9:20:57 PM |

Composition Table

| XPS Line | Adj BE | Scans | Area  | Norm Area | Sigma | Atom % |
|----------|--------|-------|-------|-----------|-------|--------|
| P 2p     | 135.2  | 15    | 1474  | 5.8       | 1.3   | 0.18   |
| N 1s     | 402.4  | 15    | 4057  | 12.3      | 1.7   | 0.39   |
| S 2p     | 170.2  | 5     | 704   | 19.3      | 1.8   | 0.61   |
| C 1s     | 287.0  | 5     | 55721 | 2735.8    | 1.0   | 85.96  |
| O 1s     | 533.5  | 5     | 20799 | 409.4     | 2.5   | 12.86  |

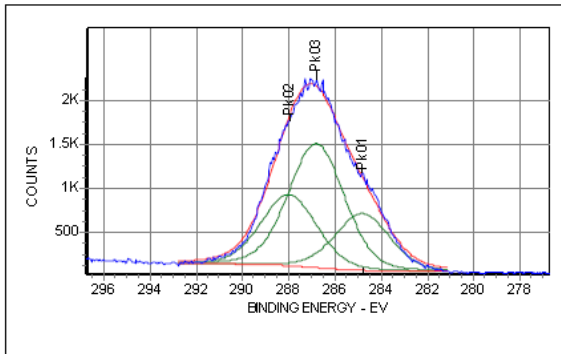
NDs of 25 nm of median size (Microdiamant AG) in YMB – A (Page 3)



| Region | Spotsize    | Resolution | nr. Scans | Date                 |
|--------|-------------|------------|-----------|----------------------|
| P 2p   | 250x1000 µm | 50 eV      | 15        | 7/29/2015 9:35:56 PM |

Composition Table

| XPS Line | Adj BE | Scans | Area  | Norm Area | Sigma | Atom % |
|----------|--------|-------|-------|-----------|-------|--------|
| P 2p     | 135.2  | 15    | 1474  | 5.8       | 1.3   | 0.18   |
| N 1s     | 402.4  | 15    | 4057  | 12.3      | 1.7   | 0.39   |
| S 2p     | 170.2  | 5     | 704   | 19.3      | 1.8   | 0.61   |
| C 1s     | 287.0  | 5     | 55721 | 2735.8    | 1.0   | 85.96  |
| O 1s     | 533.5  | 5     | 20799 | 408.4     | 2.5   | 12.86  |

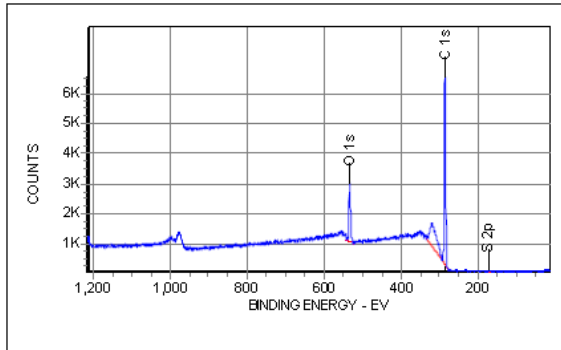


| Region | Spotsize    | Resolution | nr. Scans | Date                 |
|--------|-------------|------------|-----------|----------------------|
| C 1s   | 250x1000 µm | 50 eV      | 8         | 7/29/2015 9:43:56 PM |

Peak Fit Table

| XPS Line | Peak ID | Ch'm Shift | Adj BE | Area  | FWHM | % Assy | % Gauss | Group % |
|----------|---------|------------|--------|-------|------|--------|---------|---------|
|          | Pk03    |            | 286.79 | 88503 | 2.80 | 0      | 80      | 49.32   |
|          | Pk02    |            | 287.98 | 50596 | 2.80 | 0      | 80      | 28.20   |
|          | Pk01    |            | 284.80 | 40350 | 2.80 | 0      | 80      | 22.49   |

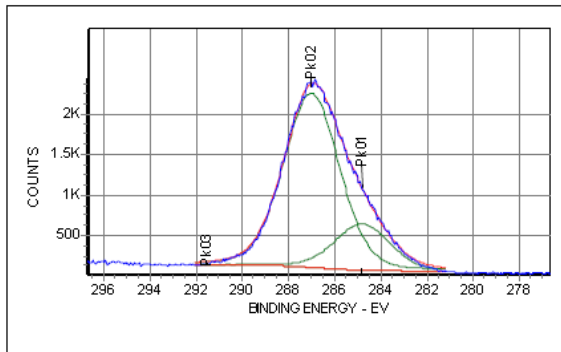
NDs of 25 nm of median size (Microdiamant AG) in YMB – B (Page 1)



| Region | Spotsize    | Resolution | nr. Scans | Date                  |
|--------|-------------|------------|-----------|-----------------------|
| Survey | 250x1000 µm | 150 eV     | 5         | 7/29/2015 10:07:00 PM |

Composition Table

| XPS Line | Adj BE | Scans | Area  | Norm Area | Sigma | Atom % |
|----------|--------|-------|-------|-----------|-------|--------|
| S 2p     | 171.0  | 5     | 623   | 17.1      | 1.8   | 0.57   |
| C 1s     | 286.8  | 5     | 53458 | 2624.4    | 1.0   | 87.09  |
| O 1s     | 533.8  | 5     | 18895 | 372.0     | 2.5   | 12.35  |

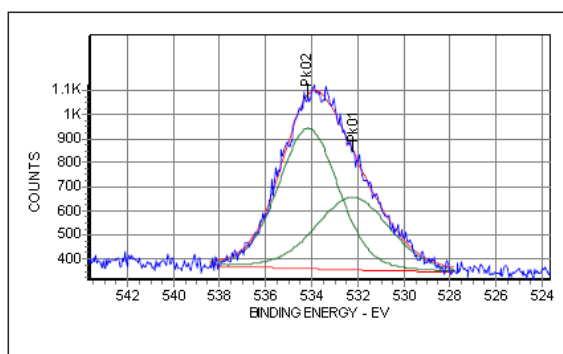


| Region | Spotsize    | Resolution | nr. Scans | Date               |
|--------|-------------|------------|-----------|--------------------|
| C 1s   | 250x1000 µm | 50 eV      | 8         | 7/29/2015 10:15:13 |

Peak Fit Table

| XPS Line | Peak ID | Ch'm Shift | Adj BE | Area   | FWHM | % Assy | % Gauss | Group % |
|----------|---------|------------|--------|--------|------|--------|---------|---------|
| C 1s     | Pk03    |            | 291.49 | 0      | 1.95 | 0      | 80      | 0.00    |
| C 1s     | Pk02    |            | 286.99 | 134102 | 2.80 | 0      | 80      | 79.07   |
| C 1s     | Pk01    |            | 284.79 | 35495  | 2.80 | 0      | 80      | 20.93   |

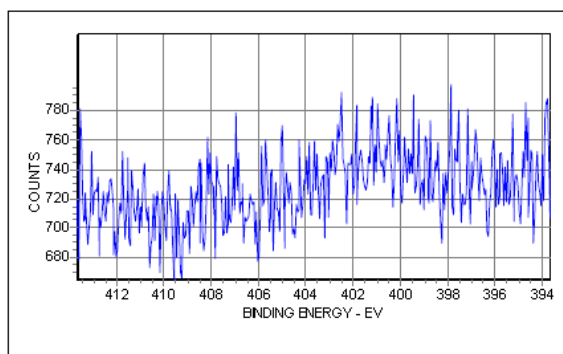
NDs of 25 nm of median size (Microdiamant AG) in YMB – B (Page 2)



| Region | Spotsize    | Resolution | nr. Scans | Date               |
|--------|-------------|------------|-----------|--------------------|
| O 1s   | 250x1000 µm | 50 eV      | 8         | 7/29/2015 10:23:13 |

Peak Fit Table

| XPS Line | Peak ID | Ch'm Shift | Adj BE | Area  | FWHM | % Assy | % Gauss | Group % |
|----------|---------|------------|--------|-------|------|--------|---------|---------|
|          | Pk02    |            | 534.15 | 38805 | 3.00 | 0      | 80      | 61.39   |
|          | Pk01    |            | 532.22 | 24401 | 3.69 | 0      | 80      | 38.61   |

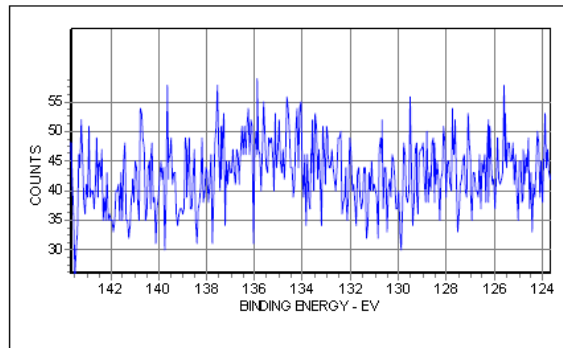


| Region | Spotsize    | Resolution | nr. Scans | Date                  |
|--------|-------------|------------|-----------|-----------------------|
| N 1s   | 250x1000 µm | 50 eV      | 15        | 7/29/2015 10:38:12 PM |

Composition Table

| XPS Line | Adj BE | Scans | Area  | Norm Area | Sigma | Atom % |
|----------|--------|-------|-------|-----------|-------|--------|
| S 2p     | 171.0  | 5     | 623   | 17.1      | 1.8   | 0.57   |
| C 1s     | 286.8  | 5     | 53458 | 2624.4    | 1.0   | 87.09  |
| O 1s     | 533.8  | 5     | 18895 | 372.0     | 2.5   | 12.35  |

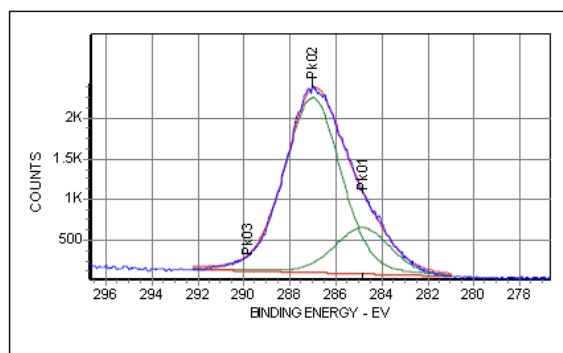
NDs of 25 nm of median size (Microdiamant AG) in YMB – B (Page 3)



| Region | Spotsize    | Resolution | nr. Scans | Date                  |
|--------|-------------|------------|-----------|-----------------------|
| P 2p   | 250x1000 µm | 50 eV      | 15        | 7/29/2015 10:53:12 PM |

Composition Table

| XPS Line | Adj BE | Scans | Area  | Norm Area | Sigma | Atom % |
|----------|--------|-------|-------|-----------|-------|--------|
| S 2p     | 171.0  | 5     | 623   | 17.1      | 1.8   | 0.57   |
| C 1s     | 286.8  | 5     | 53458 | 2624.4    | 1.0   | 87.09  |
| O 1s     | 533.8  | 5     | 18895 | 372.0     | 2.5   | 12.35  |

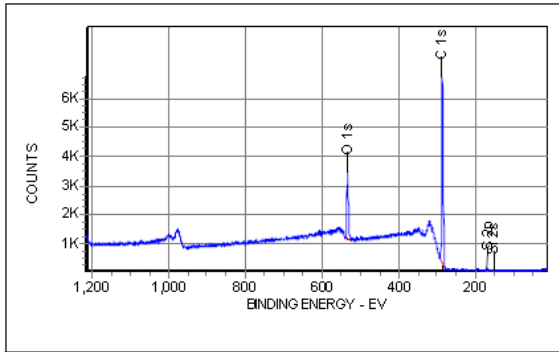


| Region | Spotsize    | Resolution | nr. Scans | Date               |
|--------|-------------|------------|-----------|--------------------|
| C 1s   | 250x1000 µm | 50 eV      | 8         | 7/29/2015 11:01:12 |

Peak Fit Table

| XPS Line | Peak ID | Ch'm Shift | Adj BE | Area   | FWHM | % Assy | % Gauss | Group % |
|----------|---------|------------|--------|--------|------|--------|---------|---------|
|          | Pk03    |            | 289.71 | 0      | 2.79 | 0      | 80      | 0.00    |
|          | Pk02    |            | 286.99 | 134948 | 2.80 | 0      | 80      | 79.08   |
|          | Pk01    |            | 284.82 | 35709  | 2.80 | 0      | 80      | 20.92   |

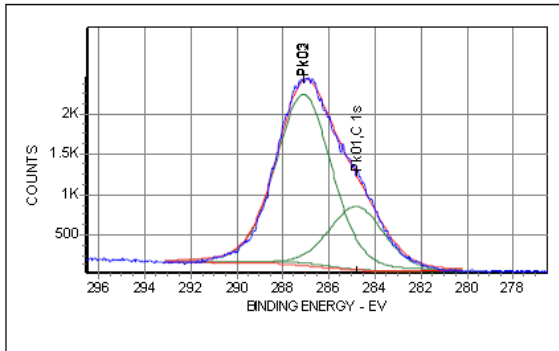
NDs of 25 nm of median size (Microdiamant AG) in YMB – C (Page 1)



| Region | Spotsize    | Resolution | nr. Scans | Date                  |
|--------|-------------|------------|-----------|-----------------------|
| Survey | 250x1000 µm | 150 eV     | 5         | 7/29/2015 11:24:16 PM |

Composition Table

| XPS Line | Adj BE | Scans | Area  | Norm Area | Sigma | Atom % |
|----------|--------|-------|-------|-----------|-------|--------|
| P 2p     | 135.2  | 15    | 1438  | 5.6       | 1.3   | 0.17   |
| N 1s     | 401.3  | 15    | 6823  | 20.7      | 1.7   | 0.63   |
| Si 2s    | 151.7  | 5     | 637   | 30.4      | 1.0   | 0.93   |
| S 2p     | 170.5  | 5     | 999   | 27.4      | 1.8   | 0.83   |
| C 1s     | 287.0  | 5     | 56568 | 2777.4    | 1.0   | 84.55  |
| O 1s     | 533.6  | 5     | 21499 | 423.2     | 2.5   | 12.88  |

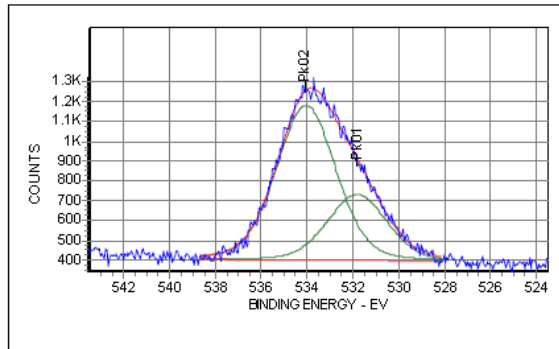


| Region | Spotsize    | Resolution | nr. Scans | Date               |
|--------|-------------|------------|-----------|--------------------|
| C 1s   | 250x1000 µm | 50 eV      | 8         | 7/29/2015 11:32:28 |

Peak Fit Table

| XPS Line | Peak ID | Ch'm Shift | Adj BE | Area   | FWHM | % Assy | % Gauss | Group % |
|----------|---------|------------|--------|--------|------|--------|---------|---------|
| C 1s     | Pk03    |            | 287.06 | 2293   | 2.80 | 0      | 80      | 1.23    |
| C 1s     | Pk02    |            | 287.07 | 134773 | 2.80 | 0      | 80      | 72.12   |
| C 1s     | Pk01    |            | 284.79 | 49808  | 2.80 | 0      | 80      | 26.65   |

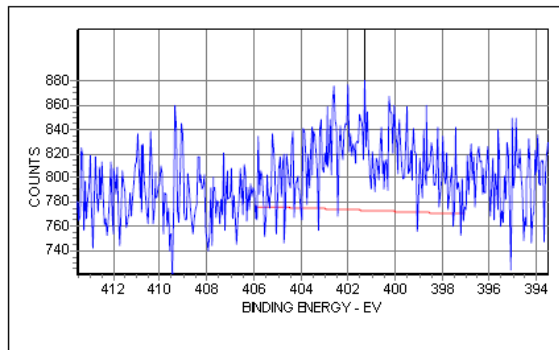
NDs of 25 nm of median size (Microdiamant AG) in YMB – C (Page 2)



| Region | Spotsize    | Resolution | nr. Scans | Date               |
|--------|-------------|------------|-----------|--------------------|
| O 1s   | 250x1000 µm | 50 eV      | 8         | 7/29/2015 11:40:28 |

Peak Fit Table

| XPS Line | Peak ID | Ch'm Shift | Adj BE | Area  | FWHM | % Assy | % Gauss | Group % |
|----------|---------|------------|--------|-------|------|--------|---------|---------|
|          | Pk02    |            | 534.05 | 51942 | 3.00 | 0      | 80      | 70.18   |
|          | Pk01    |            | 531.82 | 22066 | 3.00 | 0      | 80      | 29.82   |

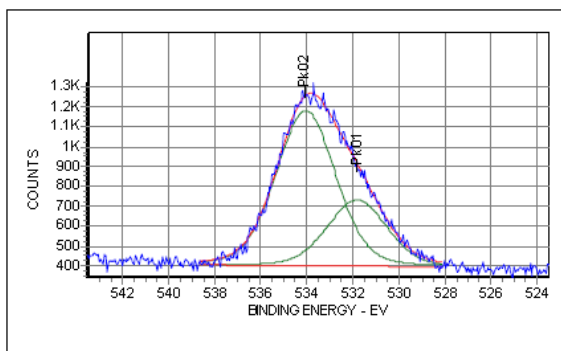


| Region | Spotsize    | Resolution | nr. Scans | Date                  |
|--------|-------------|------------|-----------|-----------------------|
| N 1s   | 250x1000 µm | 50 eV      | 15        | 7/29/2015 11:55:28 PM |

Composition Table

| XPS Line | Adj BE | Scans | Area  | Norm Area | Sigma | Atom % |
|----------|--------|-------|-------|-----------|-------|--------|
| P 2p     | 135.2  | 15    | 1438  | 5.6       | 1.3   | 0.17   |
| N 1s     | 401.3  | 15    | 6823  | 20.7      | 1.7   | 0.63   |
| Si 2s    | 151.7  | 5     | 637   | 30.4      | 1.0   | 0.93   |
| S 2p     | 170.5  | 5     | 999   | 27.4      | 1.8   | 0.83   |
| C 1s     | 287.0  | 5     | 56568 | 2777.4    | 1.0   | 84.55  |
| O 1s     | 533.6  | 5     | 21499 | 423.2     | 2.5   | 12.88  |

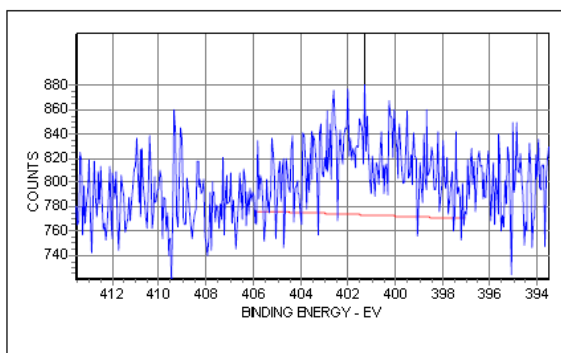
NDs of 25 nm of median size (Microdiamant AG) in YMB – C (Page 3)



| Region | Spotsize    | Resolution | nr. Scans | Date               |
|--------|-------------|------------|-----------|--------------------|
| O 1s   | 250x1000 µm | 50 eV      | 8         | 7/29/2015 11:40:28 |

Peak Fit Table

| XPS Line | Peak ID | Ch' m Shift | Adj BE | Area  | FWHM | % Assy | % Gauss | Group % |
|----------|---------|-------------|--------|-------|------|--------|---------|---------|
|          | Pk02    |             | 534.05 | 51942 | 3.00 | 0      | 80      | 70.18   |
|          | Pk01    |             | 531.82 | 22066 | 3.00 | 0      | 80      | 29.82   |

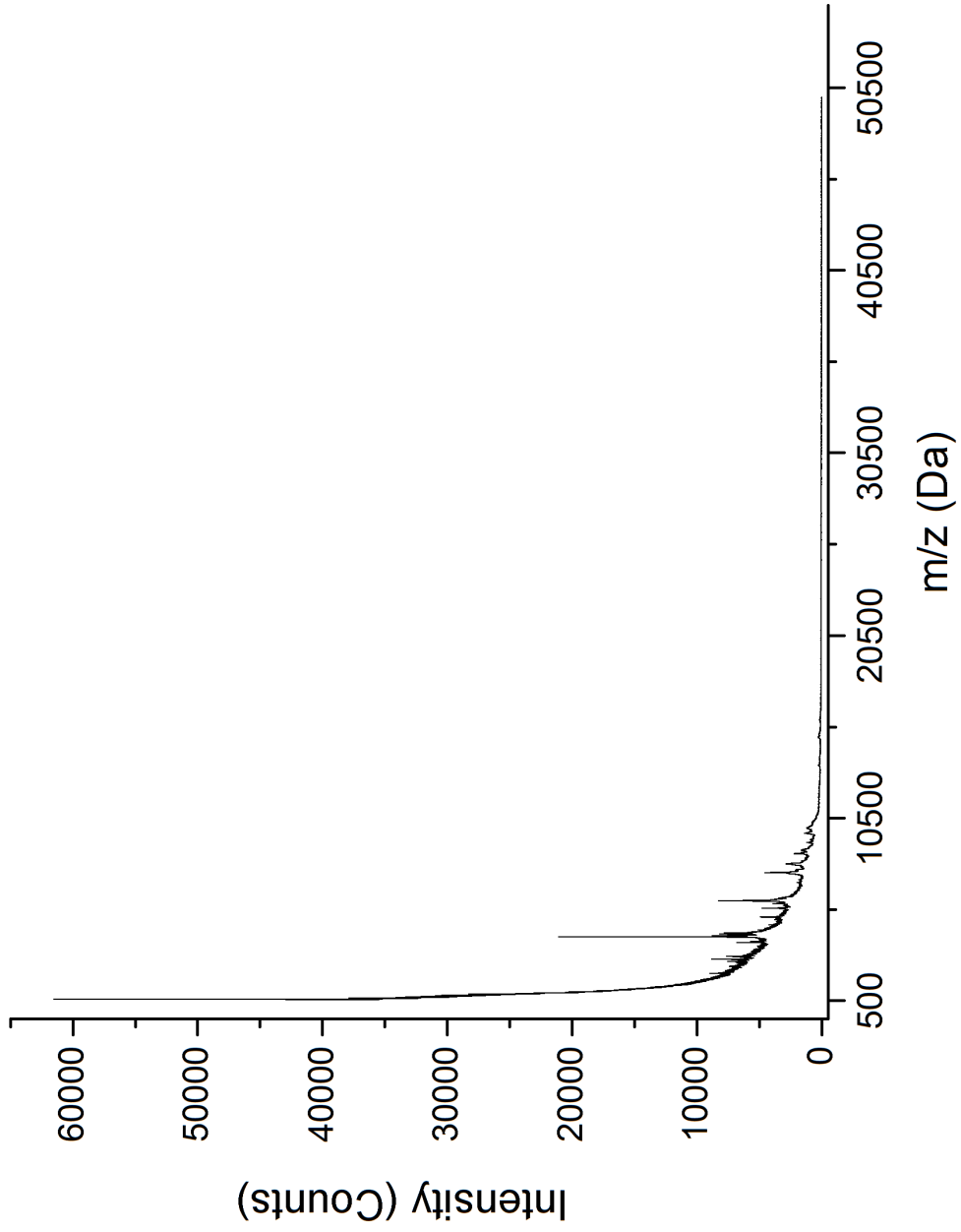


| Region | Spotsize    | Resolution | nr. Scans | Date                  |
|--------|-------------|------------|-----------|-----------------------|
| N 1s   | 250x1000 µm | 50 eV      | 15        | 7/29/2015 11:55:28 PM |

Composition Table

| XPS Line | Adj BE | Scans | Area  | Norm Area | Sigma | Atom % |
|----------|--------|-------|-------|-----------|-------|--------|
| P 2p     | 135.2  | 15    | 1438  | 5.6       | 1.3   | 0.17   |
| N 1s     | 401.3  | 15    | 6823  | 20.7      | 1.7   | 0.63   |
| Si 2s    | 151.7  | 5     | 637   | 30.4      | 1.0   | 0.93   |
| S 2p     | 170.5  | 5     | 999   | 27.4      | 1.8   | 0.83   |
| C 1s     | 287.0  | 5     | 56568 | 2777.4    | 1.0   | 84.55  |
| O 1s     | 533.6  | 5     | 21499 | 423.2     | 2.5   | 12.88  |

MALDI Spectrum



## 5.3 Proteins Identified by nLC-MS/MS

Proteins in the following tables are grouped by the following background colors:

- Unique proteins
- Sample 1: FBS
- Sample 2: 25 nm Diam. + 10% FBS
- Sample 3: 25 nm Diam. + 10% FBS (washed)
- Sample 4: 25 nm Diam. + DMEM + 10% FBS

The proteins of the following samples are listed from Table 36 till Table 45: Sample 1: FBS, Sample 2: 25 nm Diam. + 10% FBS, Sample 3: 25 nm Diam. + 10% FBS (washed), Sample 4: 25 nm Diam. + DMEM + 10% FBS, Sample 5: 25 nm Diam. + DMEM + 10% FBS (washed).

The -10lgP refers to the PEAKS Peptide Score, NpSpCk to the normalized spectral count, #Spec to the number of spectra assigned to the protein and IEP to the theoretic isoelectric point IEP (from [http://web.expasy.org/compute\\_pi/](http://web.expasy.org/compute_pi/)). Protein descriptions include FASTA headers that have the following meaning (from <http://www.uniprot.org/help/fasta-headers>): OS=Organism Name, GN=Gene Name, PE=Protein Existence (a numerical value describing the evidence for the existence of the protein), SV=Sequence Version (version number of the sequence).

Table 36 Proteins identified in Sample 1.

| Sample 1               | FBS  |        |       |                |            |      |
|------------------------|--|--------|-------|----------------|------------|------|
| Accession              | Description  | -10lgP | #Spec | Avg. Mass [Da] | NpSpCk [%] | IEP  |
| P12763 FETUA_BOVIN     | Spleen trypsin inhibitor I OS=Bos taurus PE=1 SV=2           | 130.98 | 115   | 38419          | 34.02      | 5.10 |
| P02769 ALBU_BOVIN      | Fibrinogen alpha chain OS=Bos taurus GN=FGA PE=1 SV=5        | 140.85 | 197   | 69294          | 32.32      | 5.60 |
| P01966 HBA_BOVIN       | Hemoglobin subunit alpha OS=Bos taurus GN=HBA PE=1 SV=2      | 255.96 | 7     | 15184          | 5.24       | 8.19 |
| P62894 CYC_BOVIN       | Actin aortic smooth muscle OS=Bos taurus GN=ACTA2 PE=1 SV=1  | 123.84 | 4     | 11704          | 3.88       | 9.52 |
| tr F1MD83 F1MD83_BOVIN | Platelet factor 4 OS=Bos taurus GN=PF4 PE=3 SV=1             | 222.08 | 4     | 12567          | 3.62       | 9.30 |
| P02081 HBBF_BOVIN      | Hemoglobin fetal subunit beta OS=Bos taurus PE=1 SV=1        | 158.63 | 4     | 15859          | 2.87       | 6.51 |
| tr G3X6N3 G3X6N3_BOVIN | Serotransferrin OS=Bos taurus GN=TF PE=4 SV=1                | 296.52 | 19    | 77666          | 2.78       | 7.13 |
| P04815 BPT2_BOVIN      | Serum albumin OS=Bos taurus GN=ALB PE=1 SV=4                 | 566.53 | 2     | 10843          | 2.10       | 9.00 |
| P81644 APOA2_BOVIN     | Actin alpha skeletal muscle OS=Bos taurus GN=ACTA1 PE=1 SV=1 | 123.84 | 2     | 11202          | 2.03       | 7.80 |
| P00978 AMBP_BOVIN      | Protein AMBP OS=Bos taurus GN=AMBP PE=1 SV=2                 | 225.76 | 7     | 39235          | 2.03       | 7.81 |
| tr F1MYN5 F1MYN5_BOVIN | Fibulin-1 OS=Bos taurus GN=FBLN1 PE=3 SV=2                   | 244.35 | 10    | 77486          | 1.47       | 4.94 |
| Q2UVX4 CO3_BOVIN       | Apolipoprotein A-II OS=Bos taurus GN=APOA2 PE=1 SV=2         | 164.08 | 19    | 187145         | 1.15       | 6.41 |

## Annex

|                        |   |        |   |        |      |      |
|------------------------|---|--------|---|--------|------|------|
| Q58D62 FETUB_BOVIN     | Actin alpha cardiac muscle 1<br>OS=Bos taurus GN=ACTC1 PE=2<br>SV=1                 | 123.84 | 3 | 42663  | 0.80 | 5.59 |
| P01030 CO4_BOVIN       | Complement C4 (Fragments)<br>OS=Bos taurus GN=C4 PE=1 SV=2                          | 178.98 | 5 | 101908 | 0.56 | 6.15 |
| P60712 ACTB_BOVIN      | Alpha-2-HS-glycoprotein OS=Bos<br>taurus GN=AHSG PE=1 SV=2                          | 546.82 | 2 | 41737  | 0.54 | 5.29 |
| P63258 ACTG_BOVIN      | Cytochrome c OS=Bos taurus<br>GN=CYCS PE=1 SV=2                                     | 214.48 | 2 | 41793  | 0.54 | 5.31 |
| Q5E9B5 ACTH_BOVIN      | Fetuin-B OS=Bos taurus<br>GN=FETUB PE=2 SV=1  | 174.79 | 2 | 41877  | 0.54 | 5.31 |
| tr F1MKC4 F1MKC4_BOVIN | Uncharacterized protein OS=Bos<br>taurus PE=3 SV=2                                  | 123.84 | 2 | 41934  | 0.54 | 5.74 |
| P62739 ACTA_BOVIN      | Actin cytoplasmic 1 OS=Bos taurus<br>GN=ACTB PE=1 SV=1                              | 123.84 | 2 | 42009  | 0.54 | 5.24 |
| Q3ZC07 ACTC_BOVIN      | Inter-alpha-trypsin inhibitor heavy<br>chain H4 OS=Bos taurus GN=ITIH4<br>PE=1 SV=1 | 110.4  | 2 | 42019  | 0.54 | 5.23 |
| P68138 ACTS_BOVIN      | Actin cytoplasmic 2 OS=Bos taurus<br>GN=ACTG1 PE=1 SV=1                             | 123.84 | 2 | 42051  | 0.54 | 5.23 |
| P00735 THRB_BOVIN      | Prothrombin OS=Bos taurus<br>GN=F2 PE=1 SV=2  | 185.07 | 3 | 70506  | 0.48 | 5.97 |
| tr A5PJE3 A5PJE3_BOVIN | Actin gamma-enteric smooth<br>muscle OS=Bos taurus GN=ACTG2<br>PE=2 SV=1            | 123.84 | 2 | 66998  | 0.34 | 6.57 |
| tr E1BH06 E1BH06_BOVIN | Uncharacterized protein OS=Bos<br>taurus GN=C4A PE=4 SV=2                           | 178.98 | 5 | 192764 | 0.29 | 7.20 |
| Q3T052 ITIH4_BOVIN     | Complement C3 OS=Bos taurus<br>GN=C3 PE=1 SV=2                                      | 283.87 | 2 | 101513 | 0.22 | 6.22 |

Table 37 Redundant proteins identified in Sample 1

| Redundant proteins     |   |        |  |  |  |  |
|------------------------|---|--------|--|--|--|--|
| Accession              | Description   | -10lgP |  |  |  |  |
| tr G3X7A5 G3X7A5_BOVIN | Complement C3 OS=Bos taurus GN=C3 PE=4 SV=1 (= Q2UVX4 CO3_BOVIN)  | 283.87 |  |  |  |  |
| tr F1MRD0 F1MRD0_BOVIN | Actin cytoplasmic 1 OS=Bos taurus GN=ACTB PE=3 SV=2   | 123.84 |  |  |  |  |
| tr G8JKX4 G8JKX4_BOVIN | Actin aortic smooth muscle OS=Bos taurus GN=ACTA2 PE=3 SV=1   | 123.84 |  |  |  |  |
| tr A5PJE3 A5PJE3_BOVIN | Fibrinogen alpha chain OS=Bos taurus GN=FGA PE=2 SV=1   | 140.85 |  |  |  |  |
| tr F1MMK9 F1MMK9_BOVIN | Protein AMBP OS=Bos taurus GN=AMBP PE=4 SV=2  | 225.76 |  |  |  |  |
| tr F1MMD7 F1MMD7_BOVIN | Inter-alpha-trypsin inhibitor heavy chain H4 OS=Bos taurus GN=ITIH4 PE=4 SV=2                                 | 110.40 |  |  |  |  |
| tr G3X7A8 G3X7A8_BOVIN | Uncharacterized protein OS=Bos taurus GN=PTI PE=4 SV=1 (= Spleen trypsin inhibitor I OS=Bos taurus PE=1 SV=2) | 130.98 |  |  |  |  |

Table 38 Proteins identified in Sample 2

| Sample 2           |   | 25 nm Diam. + 10% FBS |       |                |            |      |
|--------------------|---|-----------------------|-------|----------------|------------|------|
| Accession          | Description   | -10lgP                | #Spec | Avg. Mass [Da] | NpSpCk [%] | IEP  |
| P12763 FETUA_BOVIN | Alpha-2-HS-glycoprotein OS=Bos taurus GN=AHSG PE=1 SV=2 | 585.54                | 81    | 38419          | 38.32      | 5.10 |
| P02769 ALBU_BOVIN  | Serum albumin OS=Bos taurus GN=ALB PE=1 SV=4            | 555.86                | 86    | 69294          | 22.56      | 5.60 |
| P62894 CYC_BOVIN   | Cytochrome c OS=Bos taurus GN=CYCS PE=1 SV=2            | 199.6                 | 7     | 11704          | 10.87      | 9.52 |



## Annex

|                                |  |        |   |        |      |      |
|--------------------------------|--|--------|---|--------|------|------|
| tr F1MD83 F1MD83_BOVIN         | Platelet factor 4 OS=Bos taurus<br>GN=PF4 PE=3 SV=1        | 198.63 | 4 | 12567  | 5.78 | 9.30 |
| P82943 REG1_BOVIN              | Regakine-1 OS=Bos taurus PE=1<br>SV=2                      | 137.16 | 3 | 10281  | 5.30 | 8.80 |
| P04815 BPT2_BOVIN              | Spleen trypsin inhibitor I OS=Bos<br>taurus PE=1 SV=2      | 171.01 | 3 | 10843  | 5.03 | 9.00 |
| P01966 HBA_BOVIN               | Hemoglobin subunit alpha OS=Bos<br>taurus GN=HBA PE=1 SV=2 | 158.17 | 4 | 15184  | 4.79 | 8.07 |
| P00978 AMBP_BOVIN              | Protein AMBP OS=Bos taurus<br>GN=AMBP PE=1 SV=2            | 235.65 | 6 | 39235  | 2.78 | 7.81 |
| P17690 APOH_BOVIN              | Beta-2-glycoprotein 1 OS=Bos<br>taurus GN=APOH PE=1 SV=4   | 232.11 | 4 | 38252  | 1.90 | 8.53 |
| Q2UVX4 CO3_BOVIN               | Complement C3 OS=Bos taurus<br>GN=C3 PE=1 SV=2             | 223.10 | 9 | 187252 | 0.87 | 6.41 |
| tr F1MYN5 F1MYN5_BOVIN         | Fibulin-1 OS=Bos taurus<br>GN=FBLN1 PE=3 SV=2              | 135.96 | 3 | 77486  | 0.70 | 4.94 |
| Q29443 TRFE_BOVIN <sup>5</sup> | Serotransferrin OS=Bos taurus<br>GN=TF PE=2 SV=1           | 123.00 | 3 | 77753  | 0.70 | 7.13 |
| P06868 PLMN_BOVIN              | Plasminogen OS=Bos taurus<br>GN=PLG PE=1 SV=2              | 164.79 | 2 | 91216  | 0.40 | 6.75 |

Table 39 Redundant proteins identified in Sample 2

| Redundant proteins     |  |  |        |
|------------------------|--|--|--------|
| Accession              | Description  |  | -10lgP |
| tr G3X7A5 G3X7A5_BOVIN | Complement C3 OS=Bos taurus GN=C3 PE=4 SV=1            |  | 223.10 |
| tr F1MMK9 F1MMK9_BOVIN | Protein AMBP OS=Bos taurus GN=AMBP PE=4 SV=2           |  | 235.65 |
| tr G3X7A8 G3X7A8_BOVIN | Uncharacterized protein OS=Bos taurus GN=PTI PE=4 SV=1 |  | 171.01 |
| tr G3X6N3 G3X6N3_BOVIN | Serotransferrin OS=Bos taurus GN=TF PE=4 SV=1          |  | 123.00 |
| tr E1B726 E1B726_BOVIN | Plasminogen OS=Bos taurus GN=PLG PE=3 SV=2             |  | 164.79 |

Table 40 Proteins identified in Sample 3

| Sample 3           |   | 25 nm Diam. + 10% FBS (washed) |       |                |            |      |  |
|--------------------|---|--------------------------------|-------|----------------|------------|------|--|
| Accession          | Description   | -10lgP                         | #Spec | Avg. Mass [Da] | NpSpCk [%] | IEP  |  |
| P02769 ALBU_BOVIN  | Serum albumin OS=Bos taurus<br>GN=ALB PE=1 SV=4               | 487.21                         | 134   | 69294          | 16.64      | 5.60 |  |
| P12763 FETUA_BOVIN | Alpha-2-HS-glycoprotein OS=Bos<br>taurus GN=AHSG PE=1 SV=2    | 381.84                         | 69    | 38419          | 15.46      | 5.10 |  |
| P02081 HBBF_BOVIN  | Hemoglobin fetal subunit beta<br>OS=Bos taurus PE=1 SV=1      | 277.18                         | 16    | 15859          | 8.68       | 6.51 |  |
| P01966 HBA_BOVIN   | Hemoglobin subunit alpha<br>OS=Bos taurus GN=HBA PE=1<br>SV=2 | 270.20                         | 10    | 15184          | 5.67       | 8.07 |  |
| P62894 CYC_BOVIN   | Cytochrome c OS=Bos taurus<br>GN=CYCS PE=1 SV=2               | 187.31                         | 6     | 11704          | 4.41       | 9.52 |  |
| Q58D62 FETUB_BOVIN | Fetuin-B OS=Bos taurus<br>GN=FETUB PE=2 SV=1                  | 295.46                         | 18    | 42663          | 3.63       | 5.59 |  |
| P34955 A1AT_BOVIN  | Alpha-1-antiproteinase OS=Bos<br>taurus GN=SERPINA1 PE=1 SV=1 | 260.86                         | 15    | 46104          | 2.80       | 6.05 |  |

<sup>5</sup> Recognized as tr|G3X6N3|G3X6N3\_BOVIN in Sample 1.

## Annex

|                        |   |        |    |        |      |      |
|------------------------|---|--------|----|--------|------|------|
| Q2UVX4 CO3_BOVIN       | Complement C3 OS=Bos taurus<br>GN=C3 PE=1 SV=2                                      | 430.26 | 58 | 187252 | 2.67 | 6.41 |
| P17690 APOH_BOVIN      | Beta-2-glycoprotein 1 OS=Bos<br>taurus GN=APOH PE=1 SV=4                            | 235.89 | 10 | 38252  | 2.25 | 8.53 |
| Q3MHN5 VTDB_BOVIN      | Vitamin D-binding protein OS=Bos<br>taurus GN=GC PE=2 SV=1                          | 288.26 | 13 | 53342  | 2.10 | 5.36 |
| Q3SZ57 FETA_BOVIN      | Alpha-fetoprotein OS=Bos taurus<br>GN=AFP PE=2 SV=1                                 | 291.48 | 16 | 68588  | 2.01 | 5.92 |
| tr F1MC11 F1MC11_BOVIN | Pigment epithelium-derived<br>factor OS=Bos taurus<br>GN=SERPINF1 PE=1 SV=1         | 200.36 | 12 | 51911  | 1.99 | 5.08 |
| P06868 PLMN_BOVIN      | Plasminogen OS=Bos taurus<br>GN=PLG PE=1 SV=2                                       | 303.90 | 21 | 91216  | 1.98 | 7.68 |
| Q7SIH1 A2MG_BOVIN      | Alpha-2-macroglobulin OS=Bos<br>taurus GN=A2M PE=1 SV=2                             | 364.9  | 38 | 167575 | 1.95 | 5.71 |
| tr F1MNV4 F1MNV4_BOVIN | Inter-alpha-trypsin inhibitor heavy<br>chain H2 OS=Bos taurus GN=ITIH2<br>PE=4 SV=2 | 288.79 | 23 | 106156 | 1.86 | 7.93 |
| P81187 CFAB_BOVIN      | Complement factor B OS=Bos<br>taurus GN=CFB PE=1 SV=2                               | 305.89 | 17 | 85366  | 1.71 | 7.87 |
| Q29443 TRFE_BOVIN      | Serotransferrin OS=Bos taurus<br>GN=TF PE=2 SV=1                                    | 281.4  | 14 | 77753  | 1.55 | 6.75 |
| P81644 APOA2_BOVIN     | Apolipoprotein A-II OS=Bos taurus<br>GN=APOA2 PE=1 SV=2                             | 107.28 | 2  | 11202  | 1.54 | 7.80 |
| Q95121 PEDF_BOVIN      | Pigment epithelium-derived<br>factor OS=Bos taurus<br>GN=SERPINF1 PE=1 SV=1         | 213.31 | 8  | 46229  | 1.49 | 6.57 |
| tr G3N0V2 G3N0V2_BOVIN | Uncharacterized protein OS=Bos<br>taurus GN=KRT1 PE=3 SV=1                          | 222.15 | 10 | 63151  | 1.36 | 8.41 |
| tr Q17QC8 Q17QC8_BOVIN | Complement factor properdin<br>OS=Bos taurus GN=CFP PE=2 SV=1                       | 215.13 | 8  | 50750  | 1.36 | 8.32 |
| Q3SZV7 HEMO_BOVIN      | Hemopexin OS=Bos taurus<br>GN=HPX PE=2 SV=1   | 219.21 | 8  | 52209  | 1.32 | 7.90 |
| P01888 B2MG_BOVIN      | Beta-2-microglobulin OS=Bos<br>taurus GN=B2M PE=1 SV=2                              | 112.74 | 2  | 13677  | 1.26 | 7.79 |
| P15497 APOA1_BOVIN     | Apolipoprotein A-I OS=Bos taurus<br>GN=APOA1 PE=1 SV=3                              | 173.35 | 4  | 30276  | 1.14 | 5.71 |
| P02672 FIBA_BOVIN      | Fibrinogen alpha chain OS=Bos<br>taurus GN=FGA PE=1 SV=5                            | 185.1  | 7  | 67012  | 0.90 | 6.73 |
| Q03247 APOE_BOVIN      | Apolipoprotein E OS=Bos taurus<br>GN=APOE PE=2 SV=1                                 | 177.83 | 3  | 35980  | 0.72 | 5.55 |
| tr F1N1I6 F1N1I6_BOVIN | Gelsolin OS=Bos taurus GN=GSN<br>PE=4 SV=1  | 222.87 | 7  | 85687  | 0.70 | 5.86 |
| Q28178 TSP1_BOVIN      | Thrombospondin-1 OS=Bos taurus<br>GN=THBS1 PE=2 SV=2                                | 233.65 | 10 | 129534 | 0.66 | 4.74 |
| tr F1MMK9 F1MMK9_BOVIN | Protein AMBP OS=Bos taurus<br>GN=AMBP PE=4 SV=2                                     | 158.8  | 3  | 39294  | 0.66 | 8.07 |
| tr F1N4M7 F1N4M7_BOVIN | Uncharacterized protein OS=Bos<br>taurus GN=CFI PE=3 SV=2                           | 193.43 | 5  | 68905  | 0.62 | 8.07 |
| P60712 ACTB_BOVIN      | Actin cytoplasmic 1 OS=Bos<br>taurus GN=ACTB PE=1 SV=1                              | 178.24 | 3  | 41737  | 0.62 | 5.29 |
| P63258 ACTG_BOVIN      | Actin cytoplasmic 2 OS=Bos<br>taurus GN=ACTG1 PE=1 SV=1                             | 178.24 | 3  | 41793  | 0.62 | 5.31 |
| Q5E9B5 ACTH_BOVIN      | Actin gamma-enteric smooth<br>muscle OS=Bos taurus GN=ACTG2<br>PE=2 SV=1            | 178.24 | 3  | 41877  | 0.62 | 5.31 |
| P62739 ACTA_BOVIN      | Actin aortic smooth muscle<br>OS=Bos taurus GN=ACTA2 PE=1<br>SV=1                   | 178.24 | 3  | 42009  | 0.61 | 5.24 |
| Q3ZC07 ACTC_BOVIN      | Actin alpha cardiac muscle 1<br>OS=Bos taurus GN=ACTC1 PE=2<br>SV=1                 | 178.24 | 3  | 42019  | 0.61 | 5.23 |

## Annex

|                        |   |        |   |        |      |      |
|------------------------|---|--------|---|--------|------|------|
| P68138 ACTS_BOVIN      | Actin alpha skeletal muscle OS=Bos taurus GN=ACTA1 PE=1 SV=1                          | 178.24 | 3 | 42051  | 0.61 | 5.23 |
| Q3T052 ITIH4_BOVIN     | Inter-alpha-trypsin inhibitor heavy chain H4 OS=Bos taurus GN=ITIH4 PE=1 SV=1         | 186.6  | 7 | 101513 | 0.59 | 6.22 |
| tr Q1RMH5 Q1RMH5_BOVIN | C1QC protein (Fragment) OS=Bos taurus GN=C1QC PE=2 SV=1                               | 112.29 | 2 | 29023  | 0.59 | 8.80 |
| Q2KJF1 A1BG_BOVIN      | Alpha-1B-glycoprotein OS=Bos taurus GN=A1BG PE=1 SV=1                                 | 160.18 | 3 | 53554  | 0.48 | 5.30 |
| Q28085 CFAH_BOVIN      | Complement factor H OS=Bos taurus GN=CFH PE=1 SV=3                                    | 219.48 | 7 | 140374 | 0.43 | 6.43 |
| tr Q3SZH5 Q3SZH5_BOVIN | Angiotensinogen OS=Bos taurus GN=AGT PE=2 SV=1  | 132.92 | 2 | 45456  | 0.38 | 9.30 |
| tr E1BH06 E1BH06_BOVIN | Uncharacterized protein OS=Bos taurus GN=C4A PE=4 SV=2                                | 256.26 | 8 | 192764 | 0.36 | 7.20 |
| tr Q3SZZ9 Q3SZZ9_BOVIN | FGG protein OS=Bos taurus GN=FGG PE=2 SV=1  | 121.75 | 2 | 49167  | 0.35 | 5.56 |
| tr F1MGU7 F1MGU7_BOVIN | Fibrinogen gamma-B chain OS=Bos taurus GN=FGG PE=4 SV=1                               | 121.75 | 2 | 50232  | 0.34 | 5.44 |
| P02676 FIBB_BOVIN      | Fibrinogen beta chain OS=Bos taurus GN=FGB PE=1 SV=2                                  | 140.4  | 2 | 53340  | 0.32 | 8.45 |
| P56652 ITIH3_BOVIN     | Inter-alpha-trypsin inhibitor heavy chain H3 OS=Bos taurus GN=ITIH3 PE=1 SV=2         | 147.44 | 3 | 99551  | 0.26 | 5.59 |
| P02453 CO1A1_BOVIN     | Collagen alpha-1(I) chain OS=Bos taurus GN=COL1A1 PE=1 SV=3                           | 167.1  | 4 | 138939 | 0.25 | 5.60 |
| tr Q2KJC7 Q2KJC7_BOVIN | Periostin variant 7 OS=Bos taurus GN=POSTN PE=2 SV=1                                  | 119.17 | 2 | 86859  | 0.20 | 7.25 |
| Q29RQ1 CO7_BOVIN       | Complement component C7 OS=Bos taurus GN=C7 PE=2 SV=1                                 | 179.43 | 2 | 93090  | 0.18 | 6.91 |
| tr G5E6M0 G5E6M0_BOVIN | Uncharacterized protein OS=Bos taurus GN=POSTN PE=4 SV=1                              | 119.17 | 2 | 93194  | 0.18 | 7.02 |
| tr B8Y9T0 B8Y9T0_BOVIN | Cumulus cell-specific fibronectin 1 transcript variant OS=Bos taurus GN=FN1 PE=2 SV=1 | 144.45 | 3 | 249128 | 0.10 | 5.42 |
| tr B8Y9S9 B8Y9S9_BOVIN | Embryo-specific fibronectin 1 transcript variant OS=Bos taurus GN=FN1 PE=2 SV=1       | 144.45 | 3 | 262424 | 0.10 | 5.49 |
| P07589 FINC_BOVIN      | Fibronectin OS=Bos taurus GN=FN1 PE=1 SV=4  | 144.45 | 3 | 272151 | 0.09 | 5.32 |

Table 41 Redundant proteins identified in Sample 3

| Redundant proteins     |   |        |
|------------------------|---|--------|
| Accession              | Description   | -10lgP |
| tr G3X7A5 G3X7A5_BOVIN | Complement C3 OS=Bos taurus GN=C3 PE=4 SV=1                                   | 430.26 |
| tr A5PJE3 A5PJE3_BOVIN | Fibrinogen alpha chain OS=Bos taurus GN=FGA PE=2 SV=1                         | 185.10 |
| tr F1MRD0 F1MRD0_BOVIN | Actin cytoplasmic 1 OS=Bos taurus GN=ACTB PE=3 SV=2                           | 178.24 |
| tr G8JKX4 G8JKX4_BOVIN | Actin aortic smooth muscle OS=Bos taurus GN=ACTA2 PE=3 SV=1                   | 178.24 |
| tr F1MMD7 F1MMD7_BOVIN | Inter-alpha-trypsin inhibitor heavy chain H4 OS=Bos taurus GN=ITIH4 PE=4 SV=2 | 186.6  |
| tr F1N3A1 F1N3A1_BOVIN | Thrombospondin-1 OS=Bos taurus GN=THBS1 PE=4 SV=1                             | 233.65 |
| tr F1MAV0 F1MAV0_BOVIN | Fibrinogen beta chain OS=Bos taurus GN=FGB PE=4 SV=2                          | 140.4  |
| tr F1N045 F1N045_BOVIN | Complement component C7 OS=Bos taurus GN=C7 PE=4 SV=1                         | 179.43 |
| tr G5E5A9 G5E5A9_BOVIN | Fibronectin OS=Bos taurus GN=FN1 PE=4 SV=1                                    | 144.45 |

## Annex

In Sample 3, Protein AMBP was found only as tr|F1MMK9|F1MMK9\_BOVIN and P00978|AMBP\_BOVIN was not found.

Table 42 Proteins identified in Sample 4

| Sample 4               |  | 25 nm Diam. + DMEM + 10% FBS |       |                    |            |      |  |
|------------------------|--|------------------------------|-------|--------------------|------------|------|--|
| Accession              | Description  | -10lgP                       | #Spec | Avg. Mass [Da]     | NpSpCk [%] | IEP  |  |
| P02081 HBBF_BOVIN      | Hemoglobin fetal subunit beta OS=Bos taurus PE=1 SV=1                          | 332.43                       | 32    | 15859              | 10.93      | 6.51 |  |
| P01966 HBA_BOVIN       | Hemoglobin subunit alpha OS=Bos taurus GN=HBA PE=1 SV=2                        | 351.43                       | 30    | 15184              | 10.70      | 8.07 |  |
| P02769 ALBU_BOVIN      | Serum albumin OS=Bos taurus GN=ALB PE=1 SV=4                                   | 452.91                       | 119   | 69294              | 9.30       | 5.82 |  |
| P12763 FETUA_BOVIN     | Alpha-2-HS-glycoprotein OS=Bos taurus GN=AHSG PE=1 SV=2                        | 448.92                       | 63    | 38419              | 8.88       | 5.26 |  |
| P81644 APOA2_BOVIN     | Apolipoprotein A-II OS=Bos taurus GN=APOA2 PE=1 SV=2                           | 220.97                       | 10    | 11202              | 4.83       | 7.80 |  |
| P02672 FIBA_BOVIN      | Fibrinogen alpha chain OS=Bos taurus GN=FGA PE=1 SV=5                          | 467.83                       | 44    | 67012              | 3.56       | 6.73 |  |
| P60712 ACTB_BOVIN      | Actin cytoplasmic 1 OS=Bos taurus GN=ACTB PE=1 SV=1                            | 330.52                       | 24    | 41737              | 3.11       | 5.29 |  |
| P63258 ACTG_BOVIN      | Actin cytoplasmic 2 OS=Bos taurus GN=ACTG1 PE=1 SV=1                           | 330.52                       | 24    | 41793              | 3.11       | 5.31 |  |
| P15497 APOA1_BOVIN     | Apolipoprotein A-I OS=Bos taurus GN=APOA1 PE=1 SV=3                            | 303.18                       | 17    | 30276              | 3.04       | 5.71 |  |
| Q03247 APOE_BOVIN      | Apolipoprotein E OS=Bos taurus GN=APOE PE=2 SV=1                               | 294.17                       | 16    | 35980              | 2.41       | 5.55 |  |
| P62894 CYC_BOVIN       | Cytochrome c OS=Bos taurus GN=CYCS PE=1 SV=2                                   | 198.52                       | 5     | 11704              | 2.31       | 9.52 |  |
| Q3MHN5 VTDB_BOVIN      | Vitamin D-binding protein OS=Bos taurus GN=GC PE=2 SV=1                        | 298.22                       | 21    | 53342              | 2.13       | 5.36 |  |
| P82943 REG1_BOVIN      | Regakine-1 OS=Bos taurus PE=1 SV=2   | 192.90                       | 4     | 10281              | 2.11       | 8.80 |  |
| P13384 IBP2_BOVIN      | Insulin-like growth factor-binding protein 2 OS=Bos taurus GN=IGFBP2 PE=1 SV=2 | 271.77                       | 13    | 34015              | 2.07       | 7.13 |  |
| tr F1N4M7 F1N4M7_BOVIN | Uncharacterized protein OS=Bos taurus GN=CFI PE=3 SV=2                         | 280.25                       | 26    | 68905              | 2.04       | 8.07 |  |
| P00735 THRB_BOVIN      | Prothrombin OS=Bos taurus GN=F2 PE=1 SV=2                                      | 333.64                       | 26    | 70506              | 2.00       | 5.97 |  |
| tr F1N1I6 F1N1I6_BOVIN | Gelsolin OS=Bos taurus GN=GSN PE=4 SV=1  | 299.98                       | 25    | 85687              | 1.58       | 5.86 |  |
| P17690 APOH_BOVIN      | Beta-2-glycoprotein 1 OS=Bos taurus GN=APOH PE=1 SV=4                          | 225.86                       | 11    | 38252              | 1.56       | 8.53 |  |
| Q3T052 ITI4_BOVIN      | Inter-alpha-trypsin inhibitor heavy chain H4 OS=Bos taurus GN=ITI4 PE=1 SV=1   | 344.55                       | 29    | 10151 <sub>3</sub> | 1.55       | 6.22 |  |
| tr F1MD83 F1MD83_BOVIN | Platelet factor 4 OS=Bos taurus GN=PF4 PE=3 SV=1                               | 170.00                       | 3     | 12567              | 1.29       | 9.30 |  |
| Q28085 CFAH_BOVIN      | Complement factor H OS=Bos taurus GN=CFH PE=1 SV=3                             | 345.55                       | 32    | 14037 <sub>4</sub> | 1.23       | 6.43 |  |
| tr F1MYN5 F1MYN5_BOVIN | Fibulin-1 OS=Bos taurus GN=FBLN1 PE=3 SV=2                                     | 273.42                       | 17    | 77486              | 1.19       | 4.94 |  |
| Q7SIH1 A2MG_BOVIN      | Alpha-2-macroglobulin OS=Bos taurus GN=A2M PE=1 SV=2                           | 353.11                       | 35    | 16757 <sub>5</sub> | 1.13       | 5.71 |  |
| Q05718 IBP6_BOVIN      | Insulin-like growth factor-binding protein 6 OS=Bos taurus GN=IGFBP6 PE=2 SV=2 | 194.71                       | 5     | 24967              | 1.08       | 8.73 |  |
| Q58D62 FETUB_BOVIN     | Fetuin-B OS=Bos taurus GN=FETUB PE=2 SV=1                                      | 217.21                       | 8     | 42663              | 1.02       | 5.59 |  |

## Annex

|                        |  |        |    |        |      |      |
|------------------------|--|--------|----|--------|------|------|
| P19035 APOC3_BOVIN     | Apolipoprotein C-III OS=Bos taurus GN=APOC3 PE=1 SV=2                          | 121.37 | 2  | 10692  | 1.01 | 5.02 |
| tr Q3ZBS7 Q3ZBS7_BOVIN | Uncharacterized protein OS=Bos taurus GN=VTN PE=2 SV=1                         | 190.09 | 9  | 53575  | 0.91 | 5.92 |
| P00978 AMBP_BOVIN      | Protein AMBP OS=Bos taurus GN=AMBP PE=1 SV=2                                   | 247.95 | 6  | 39235  | 0.83 | 7.81 |
| Q3SZ57 FETA_BOVIN      | Alpha-fetoprotein OS=Bos taurus GN=AFP PE=2 SV=1                               | 224.19 | 10 | 68588  | 0.79 | 5.92 |
| Q2KIS7 TETN_BOVIN      | Tetranectin OS=Bos taurus GN=CLEC3B PE=2 SV=1                                  | 171.10 | 3  | 22144  | 0.73 | 5.47 |
| tr F1MNW4 F1MNW4_BOVIN | Inter-alpha-trypsin inhibitor heavy chain H2 OS=Bos taurus GN=ITIH2 PE=4 SV=2  | 245.76 | 14 | 106156 | 0.71 | 7.93 |
| Q95121 PEDF_BOVIN      | Pigment epithelium-derived factor OS=Bos taurus GN=SERPINF1 PE=1 SV=1          | 213.55 | 5  | 46229  | 0.59 | 6.57 |
| Q5E9F7 COF1_BOVIN      | Cofilin-1 OS=Bos taurus GN=CFL1 PE=2 SV=3                                      | 115.20 | 2  | 18519  | 0.58 | 8.16 |
| Q05716 IBP4_BOVIN      | Insulin-like growth factor-binding protein 4 OS=Bos taurus GN=IGFBP4 PE=2 SV=1 | 160.30 | 3  | 27890  | 0.58 | 7.10 |
| P07456 IGF2_BOVIN      | Insulin-like growth factor II OS=Bos taurus GN=IGF2 PE=1 SV=4                  | 149.26 | 2  | 19682  | 0.55 | 9.11 |
| tr Q08DQ6 Q08DQ6_BOVIN | Uncharacterized protein OS=Bos taurus GN=ZYX PE=2 SV=1                         | 204.62 | 6  | 60101  | 0.54 | 6.33 |
| P41361 ANT3_BOVIN      | Antithrombin-III OS=Bos taurus GN=SERPINC1 PE=1 SV=2                           | 137.51 | 5  | 52347  | 0.52 | 7.01 |
| P98140 FA12_BOVIN      | Coagulation factor XII OS=Bos taurus GN=F12 PE=1 SV=2                          | 196.11 | 6  | 67160  | 0.48 | 7.91 |
| Q9XSJ4 ENOA_BOVIN      | Alpha-enolase OS=Bos taurus GN=ENO1 PE=1 SV=4                                  | 155.63 | 4  | 47326  | 0.46 | 6.37 |
| Q28178 TSP1_BOVIN      | Thrombospondin-1 OS=Bos taurus GN=THBS1 PE=2 SV=2                              | 231.92 | 10 | 129534 | 0.42 | 4.74 |
| tr F1N045 F1N045_BOVIN | Complement component C7 OS=Bos taurus GN=C7 PE=4 SV=1                          | 213.04 | 7  | 92990  | 0.41 | 7.09 |
| Q2UVX4 CO3_BOVIN       | Complement C3 OS=Bos taurus GN=C3 PE=1 SV=2                                    | 276.74 | 14 | 187252 | 0.40 | 6.41 |
| tr E1BH06 E1BH06_BOVIN | Uncharacterized protein OS=Bos taurus GN=C4A PE=4 SV=2                         | 268.54 | 13 | 192764 | 0.37 | 7.20 |
| tr E1BLA8 E1BLA8_BOVIN | Uncharacterized protein OS=Bos taurus GN=GOLM1 PE=4 SV=1                       | 87.97  | 3  | 45536  | 0.36 | 4.82 |
| P34955 A1AT_BOVIN      | Alpha-1-antitrypsin OS=Bos taurus GN=SERPINA1 PE=1 SV=1                        | 165.54 | 3  | 46104  | 0.35 | 6.05 |
| tr Q2HJB6 Q2HJB6_BOVIN | Procollagen C-endopeptidase enhancer OS=Bos taurus GN=PCOLCE PE=2 SV=1         | 134.44 | 3  | 48211  | 0.34 | 8.13 |
| P17697 CLUS_BOVIN      | Clusterin OS=Bos taurus GN=CLU PE=1 SV=1                                       | 201.43 | 3  | 51114  | 0.32 | 5.73 |
| P81187 CFAB_BOVIN      | Complement factor B OS=Bos taurus GN=CFB PE=1 SV=2                             | 187.48 | 5  | 85366  | 0.32 | 7.87 |
| P06868 PLMN_BOVIN      | Plasminogen OS=Bos taurus GN=PLG PE=1 SV=2                                     | 196.50 | 5  | 91216  | 0.30 | 7.68 |
| Q5E9B1 LDHB_BOVIN      | L-lactate dehydrogenase B chain OS=Bos taurus GN=LDHB PE=2 SV=4                | 91.83  | 2  | 36724  | 0.29 | 6.02 |
| Q0VCM5 ITIH1_BOVIN     | Inter-alpha-trypsin inhibitor heavy chain H1 OS=Bos taurus GN=ITIH1 PE=2 SV=1  | 155.24 | 5  | 101237 | 0.27 | 6.98 |
| tr F1MMP5 F1MMP5_BOVIN | Inter-alpha-trypsin inhibitor heavy chain H1 OS=Bos taurus GN=ITIH1 PE=4 SV=1  | 155.24 | 5  | 101238 | 0.27 | 6.73 |
| Q3MHN2 CO9_BOVIN       | Complement component C9 OS=Bos taurus GN=C9 PE=2 SV=1                          | 135.13 | 3  | 61998  | 0.26 | 5.66 |

## Annex

|                        |   |        |   |            |      |      |
|------------------------|---|--------|---|------------|------|------|
| tr Q2KJC7 Q2KJC7_BOVIN | Periostin variant 7 OS=Bos taurus<br>GN=POSTN PE=2 SV=1                                     | 146.68 | 4 | 86859      | 0.25 | 7.25 |
| tr G5E6M0 G5E6M0_BOVIN | Uncharacterized protein OS=Bos<br>taurus GN=POSTN PE=4 SV=1                                 | 146.68 | 4 | 93194      | 0.23 | 7.02 |
| tr E1BI98 E1BI98_BOVIN | Uncharacterized protein OS=Bos<br>taurus GN=COL6A1 PE=4 SV=1                                | 127.01 | 4 | 10867<br>1 | 0.20 | 5.24 |
| tr A6QP30 A6QP30_BOVIN | CPN2 protein OS=Bos taurus<br>GN=CPN2 PE=2 SV=1   | 131.03 | 2 | 60040      | 0.18 | 5.76 |
| Q5E9Z2 HABP2_BOVIN     | Hyaluronan-binding protein 2<br>OS=Bos taurus GN=HABP2 PE=2<br>SV=1                         | 115.30 | 2 | 62441      | 0.17 | 6.32 |
| tr F1MDH3 F1MDH3_BOVIN | Uncharacterized protein<br>(Fragment) OS=Bos taurus<br>GN=TLN1 PE=4 SV=2                    | 240.93 | 8 | 27081<br>3 | 0.16 | 5.81 |
| tr E1BA44 E1BA44_BOVIN | Uncharacterized protein OS=Bos<br>taurus GN=LTBP4 PE=4 SV=2                                 | 130.26 | 2 | 17297<br>9 | 0.06 | 5.71 |
| tr G3MZT8 G3MZT8_BOVIN | Uncharacterized protein OS=Bos<br>taurus GN=LTBP4 PE=4 SV=1                                 | 130.26 | 2 | 17610<br>9 | 0.06 | 5.68 |
| tr B8Y9T0 B8Y9T0_BOVIN | Cumulus cell-specific fibronectin<br>1 transcript variant OS=Bos<br>taurus GN=FN1 PE=2 SV=1 | 139.20 | 2 | 24912<br>8 | 0.04 | 5.42 |
| tr B8Y9S9 B8Y9S9_BOVIN | Embryo-specific fibronectin 1<br>transcript variant OS=Bos taurus<br>GN=FN1 PE=2 SV=1       | 139.20 | 2 | 26242<br>4 | 0.04 | 5.49 |
| P07589 FINC_BOVIN      | Fibronectin OS=Bos taurus<br>GN=FN1 PE=1 SV=4   | 139.20 | 2 | 27215<br>1 | 0.04 | 5.32 |
| tr F1N169 F1N169_BOVIN | Uncharacterized protein OS=Bos<br>taurus GN=FLNA PE=4 SV=2                                  | 121.47 | 2 | 28117<br>1 | 0.04 | 5.80 |

Table 43 Redundant proteins identified in Sample 4

| Redundant proteins     |  |  |        |
|------------------------|--|--|--------|
| Accession              | Description  |  | -10lgP |
| tr A5PJE3 A5PJE3_BOVIN | Fibrinogen alpha chain OS=Bos taurus<br>GN=FGA PE=2 SV=1                             |  | 467.83 |
| tr F1MMK9 F1MMK9_BOVIN | Protein AMBP OS=Bos taurus<br>GN=AMBP PE=4 SV=2                                      |  | 247.95 |
| tr F1MMD7 F1MMD7_BOVIN | Inter-alpha-trypsin inhibitor heavy chain<br>H4 OS=Bos taurus GN=ITIH4 PE=4<br>SV=2  |  | 344.55 |
| tr G3X7A5 G3X7A5_BOVIN | Complement C3 OS=Bos taurus<br>GN=C3 PE=4 SV=1                                       |  | 276.74 |
| tr F1N3A1 F1N3A1_BOVIN | Thrombospondin-1 OS=Bos taurus<br>GN=THBS1 PE=4 SV=1                                 |  | 231.92 |
| tr G5E5A9 G5E5A9_BOVIN | Fibronectin OS=Bos taurus<br>GN=FN1 PE=4 SV=1  |  | 139.20 |
| tr F1MUK3 F1MUK3_BOVIN | Insulin-like growth factor-binding protein<br>6 OS=Bos taurus GN=IGFBP6<br>PE=4 SV=1 |  | 194.71 |
| tr F1MSZ6 F1MSZ6_BOVIN | Antithrombin-III OS=Bos taurus<br>GN=SERPINC1 PE=3 SV=1                              |  | 137.51 |
| tr F1MTT3 F1MTT3_BOVIN | Coagulation factor XII OS=Bos taurus<br>GN=F12 PE=3 SV=1                             |  | 196.11 |
| tr F1MB08 F1MB08_BOVIN | Alpha-enolase OS=Bos taurus<br>GN=ENO1 PE=3 SV=1                                     |  | 155.63 |

In Sample 4, Complement C3 was found only as Q2UVX4|CO3\_BOVIN and tr|G3X7A5|G3X7A5\_BOVIN was not found. For Complement component C7, tr|F1N045|F1N045\_BOVIN was found, but Q29RQ1|CO7\_BOVIN was not.

## Annex

Table 44 Proteins identified in Sample 4

| Sample 5               | 25 nm Diam. + DMEM + 10% FBS (washed)  |        |       |                |      |            |      |
|------------------------|--|--------|-------|----------------|------|------------|------|
| Accession              | Description  | -10lgP | #Spec | Avg. Mass [Da] | Mass | NpSpCk [%] | IEP  |
| P02081 HBBF_BOVIN      | Hemoglobin fetal subunit beta OS=Bos taurus PE=1 SV=1                          | 511.77 | 88    | 15859          |      | 6.20       | 6.51 |
| P15497 APOA1_BOVIN     | Apolipoprotein A-I OS=Bos taurus GN=APOA1 PE=1 SV=3                            | 550.35 | 136   | 30276          |      | 5.02       | 5.71 |
| P01966 HBA_BOVIN       | Hemoglobin subunit alpha OS=Bos taurus GN=HBA PE=1 SV=2                        | 472.91 | 64    | 15184          |      | 4.71       | 8.07 |
| Q03247 APOE_BOVIN      | Apolipoprotein E OS=Bos taurus GN=APOE PE=2 SV=1                               | 496.07 | 83    | 35980          |      | 2.58       | 5.55 |
| tr F1N1I6 F1N1I6_BOVIN | Gelsolin OS=Bos taurus GN=GSN PE=4 SV=1  | 749.20 | 179   | 85687          |      | 2.33       | 5.86 |
| P02769 ALBU_BOVIN      | Serum albumin OS=Bos taurus GN=ALB PE=1 SV=4                                   | 616.74 | 130   | 69294          |      | 2.10       | 5.82 |
| P81644 APOA2_BOVIN     | Apolipoprotein A-II OS=Bos taurus GN=APOA2 PE=1 SV=2                           | 347.09 | 19    | 11202          |      | 1.90       | 7.80 |
| tr A5PJE3 A5PJE3_BOVIN | Fibrinogen alpha chain OS=Bos taurus GN=FGA PE=2 SV=1 (only in one DB)         | 622.07 | 113   | 66998          |      | 1.88       | 6.57 |
| P60712 ACTB_BOVIN      | Actin, cytoplasmic 1 OS=Bos taurus GN=ACTB PE=1 SV=1                           | 579.09 | 66    | 41737          |      | 1.77       | 5.29 |
| P63258 ACTG_BOVIN      | Actin, cytoplasmic 2 OS=Bos taurus GN=ACTG1 PE=1 SV=1                          | 579.09 | 66    | 41793          |      | 1.76       | 5.31 |
| Q3T052 ITIH4_BOVIN     | Inter-alpha-trypsin inhibitor heavy chain H4 OS=Bos taurus GN=ITIH4 PE=1 SV=1  | 669.45 | 153   | 101513         |      | 1.68       | 6.22 |
| P13384 IBP2_BOVIN      | Insulin-like growth factor-binding protein 2 OS=Bos taurus GN=IGFBP2 PE=1 SV=2 | 468.94 | 46    | 34015          |      | 1.51       | 7.13 |
| Q95121 PEDF_BOVIN      | Pigment epithelium-derived factor OS=Bos taurus GN=SERPINF1 PE=1 SV=1          | 551.73 | 62    | 46229          |      | 1.50       | 6.57 |
| P00735 THRB_BOVIN      | Prothrombin OS=Bos taurus GN=F2 PE=1 SV=2                                      | 555.07 | 93    | 70506          |      | 1.47       | 5.97 |
| tr F1MD83 F1MD83_BOVIN | Platelet factor 4 OS=Bos taurus GN=PF4 PE=3 SV=1                               | 356.07 | 16    | 12567          |      | 1.42       | 9.30 |
| tr F1N4M7 F1N4M7_BOVIN | Uncharacterized protein OS=Bos taurus GN=CFI PE=3 SV=2                         | 529.42 | 83    | 68905          |      | 1.35       | 8.07 |
| P12763 FETUA_BOVIN     | Alpha-2-HS-glycoprotein OS=Bos taurus GN=AHSG PE=1 SV=2                        | 455.90 | 46    | 38419          |      | 1.34       | 5.26 |
| P67983 MT1A_BOVIN      | Metallothionein-1A OS=Bos taurus GN=MT1A PE=1 SV=1                             | 160.39 | 7     | 5951           |      | 1.31       | 8.38 |
| P55943 MT2H_BOVIN      | Metallothionein-II, hippocampal OS=Bos taurus PE=1 SV=1                        | 152.27 | 7     | 5956           |      | 1.31       | 8.38 |
| P58280 MT1_BOVIN       | Metallothionein-1 OS=Bos taurus GN=MT1 PE=1 SV=1                               | 160.39 | 7     | 5992           |      | 1.31       | 8.50 |
| P68301 MT2_BOVIN       | Metallothionein-2 OS=Bos taurus GN=MT2 PE=1 SV=1                               | 160.39 | 7     | 6028           |      | 1.30       | 8.23 |
| P55942 MT1H_BOVIN      | Metallothionein-I, hippocampal OS=Bos taurus PE=1 SV=1                         | 152.27 | 7     | 6086           |      | 1.29       | 8.23 |
| tr F1MC45 F1MC45_BOVIN | Complement factor H (Fragment) OS=Bos taurus GN=CFH PE=4 SV=2                  | 567.98 | 101   | 96593          |      | 1.17       | 5.98 |
| Q28085 CFAH_BOVIN      | Complement factor H OS=Bos taurus GN=CFH PE=1 SV=3                             | 638.17 | 145   | 140374         |      | 1.15       | 6.43 |
| Q3ZC07 ACTC_BOVIN      | Actin, alpha cardiac muscle 1 OS=Bos taurus GN=ACTC1 PE=2 SV=1                 | 457.48 | 43    | 42019          |      | 1.14       | 5.23 |

## Annex

|                        |  |        |     |        |      |      |
|------------------------|--|--------|-----|--------|------|------|
| P68138 ACTS_BOVIN      | Actin, alpha skeletal muscle<br>OS=Bos taurus GN=ACTA1 PE=1<br>SV=1                  | 457.48 | 43  | 42051  | 1.14 | 5.23 |
| Q9N2I2 IPSP_BOVIN      | Plasma serine protease inhibitor<br>OS=Bos taurus GN=SERPINA5<br>PE=1 SV=1           | 495.08 | 46  | 45297  | 1.13 | 9.40 |
| tr F1N5M2 F1N5M2_BOVIN | Vitamin D-binding protein OS=Bos<br>taurus GN=GC PE=4 SV=2                           | 517.54 | 54  | 53356  | 1.13 | 5.42 |
| tr Q3ZBS7 Q3ZBS7_BOVIN | Uncharacterized protein OS=Bos<br>taurus GN=VTN PE=2 SV=1                            | 443.82 | 51  | 53575  | 1.06 | 5.92 |
| Q2KIS7 TETN_BOVIN      | Tetranectin OS=Bos taurus<br>GN=CLEC3B PE=2 SV=1                                     | 388.09 | 21  | 22144  | 1.06 | 5.47 |
| Q7SIH1 A2MG_BOVIN      | Alpha-2-macroglobulin OS=Bos<br>taurus GN=A2M PE=1 SV=2                              | 691.13 | 151 | 167575 | 1.01 | 5.71 |
| Q2UVX4 CO3_BOVIN       | Complement C3 OS=Bos taurus<br>GN=C3 PE=1 SV=2                                       | 646.65 | 167 | 187252 | 1.00 | 6.41 |
| P34955 A1AT_BOVIN      | Alpha-1-antiproteinase OS=Bos<br>taurus GN=SERPINA1 PE=1 SV=1                        | 437.05 | 38  | 46104  | 0.92 | 6.05 |
| P17690 APOH_BOVIN      | Beta-2-glycoprotein 1 OS=Bos<br>taurus GN=APOH PE=1 SV=4                             | 432.72 | 30  | 38252  | 0.88 | 8.53 |
| P19035 APOC3_BOVIN     | Apolipoprotein C-III OS=Bos<br>taurus GN=APOC3 PE=1 SV=2                             | 260.96 | 8   | 10692  | 0.84 | 5.02 |
| tr F1MNV4 F1MNV4_BOVIN | Inter-alpha-trypsin inhibitor heavy<br>chain H2 OS=Bos taurus GN=ITIH2<br>PE=4 SV=2  | 583.01 | 77  | 106156 | 0.81 | 7.93 |
| Q58D62 FETUB_BOVIN     | Fetuin-B OS=Bos taurus<br>GN=FETUB PE=2 SV=1   | 397.86 | 29  | 42663  | 0.76 | 5.59 |
| tr F1MMK9 F1MMK9_BOVIN | Protein AMBP OS=Bos taurus<br>GN=AMBP PE=4 SV=2                                      | 330.35 | 26  | 39294  | 0.74 | 8.07 |
| P10096 G3P_BOVIN       | Glyceraldehyde-3-phosphate<br>dehydrogenase OS=Bos taurus<br>GN=GAPDH PE=1 SV=4      | 369.55 | 23  | 35868  | 0.72 | 8.51 |
| O46375 TTHY_BOVIN      | Transthyretin OS=Bos taurus<br>GN=TTR PE=1 SV=1                                      | 269.94 | 10  | 15727  | 0.71 | 5.90 |
| Q5E9F5 TAGL2_BOVIN     | Transgelin-2 OS=Bos taurus<br>GN=TAGLN2 PE=2 SV=3                                    | 322.38 | 14  | 22426  | 0.70 | 8.40 |
| Q5E9F7 COF1_BOVIN      | Cofilin-1 OS=Bos taurus GN=CFL1<br>PE=2 SV=3   | 308.24 | 11  | 18519  | 0.66 | 8.16 |
| Q3SYV4 CAP1_BOVIN      | Adenylyl cyclase-associated<br>protein 1 OS=Bos taurus GN=CAP1<br>PE=2 SV=3          | 486.15 | 29  | 51273  | 0.63 | 7.16 |
| Q05718 IBP6_BOVIN      | Insulin-like growth factor-binding<br>protein 6 OS=Bos taurus<br>GN=IGFBP6 PE=2 SV=2 | 311.95 | 14  | 24967  | 0.63 | 8.73 |
| tr F1MDH3 F1MDH3_BOVIN | Uncharacterized protein<br>(Fragment) OS=Bos taurus<br>GN=TLN1 PE=4 SV=2             | 678.92 | 151 | 270813 | 0.62 | 5.81 |
| tr Q2HJB6 Q2HJB6_BOVIN | Procollagen C-endopeptidase<br>enhancer OS=Bos taurus<br>GN=PCOLCE PE=2 SV=1         | 362.77 | 25  | 48211  | 0.58 | 8.13 |
| Q28178 TSP1_BOVIN      | Thrombospondin-1 OS=Bos taurus<br>GN=THBS1 PE=2 SV=2                                 | 499.22 | 67  | 129534 | 0.58 | 4.74 |
| P06868 PLMN_BOVIN      | Plasminogen OS=Bos taurus<br>GN=PLG PE=1 SV=2  | 463.47 | 46  | 91216  | 0.56 | 7.68 |
| tr F1MLW0 F1MLW0_BOVIN | Non-muscle caldesmon OS=Bos<br>taurus GN=CALD1 PE=4 SV=2                             | 417.13 | 31  | 62076  | 0.56 | 6.24 |
| tr G5E6M0 G5E6M0_BOVIN | Uncharacterized protein OS=Bos<br>taurus GN=POSTN PE=4 SV=1                          | 416.12 | 45  | 93194  | 0.54 | 7.02 |
| tr E1BH06 E1BH06_BOVIN | Uncharacterized protein OS=Bos<br>taurus GN=C4A PE=4 SV=2                            | 560.73 | 93  | 192764 | 0.54 | 7.20 |
| Q29RQ1 CO7_BOVIN       | Complement component C7<br>OS=Bos taurus GN=C7 PE=2 SV=1                             | 468.28 | 44  | 93090  | 0.53 | 6.91 |
| Q9XSJ4 ENOA_BOVIN      | Alpha-enolase OS=Bos taurus<br>GN=ENO1 PE=1 SV=4                                     | 359.10 | 22  | 47326  | 0.52 | 6.37 |



## Annex

|                        |  |        |    |        |      |      |
|------------------------|--|--------|----|--------|------|------|
| Q05716 IBP4_BOVIN      | Insulin-like growth factor-binding protein 4 OS=Bos taurus GN=IGFBP4 PE=2 SV=1 | 341.39 | 12 | 27890  | 0.48 | 7.10 |
| Q8SPP7 PGRP1_BOVIN     | Peptidoglycan recognition protein 1 OS=Bos taurus GN=PGLYRP1 PE=1 SV=1         | 267.64 | 9  | 21063  | 0.48 | 9.59 |
| P81187 CFAB_BOVIN      | Complement factor B OS=Bos taurus GN=CFB PE=1 SV=2                             | 418.08 | 36 | 85366  | 0.47 | 7.87 |
| P01044 KNG1_BOVIN      | Kininogen-1 OS=Bos taurus GN=KNG1 PE=1 SV=1                                    | 408.45 | 29 | 68890  | 0.47 | 6.14 |
| tr F1MMP5 F1MMP5_BOVIN | Inter-alpha-trypsin inhibitor heavy chain H1 OS=Bos taurus GN=ITIH1 PE=4 SV=1  | 417.43 | 42 | 101238 | 0.46 | 6.73 |
| P17697 CLUS_BOVIN      | Clusterin OS=Bos taurus GN=CLU PE=1 SV=1                                       | 324.16 | 20 | 51114  | 0.44 | 5.73 |
| tr F1MVK1 F1MVK1_BOVIN | Uncharacterized protein (Fragment) OS=Bos taurus PE=4 SV=2                     | 529.65 | 68 | 173973 | 0.44 | 6.47 |
| P82943 REG1_BOVIN      | Regakine-1 OS=Bos taurus PE=1 SV=2   | 240.91 | 4  | 10281  | 0.43 | 8.80 |
| Q3MHN2 CO9_BOVIN       | Complement component C9 OS=Bos taurus GN=C9 PE=2 SV=1                          | 353.45 | 24 | 61998  | 0.43 | 5.66 |
| tr F1MKS5 F1MKS5_BOVIN | Histidine-rich glycoprotein OS=Bos taurus GN=HRG PE=4 SV=2                     | 341.03 | 23 | 60744  | 0.42 | 7.11 |
| P04815 BPT2_BOVIN      | Spleen trypsin inhibitor I OS=Bos taurus PE=1 SV=2                             | 172.81 | 4  | 10843  | 0.41 | 9.00 |
| P01035 CYTC_BOVIN      | Cystatin-C OS=Bos taurus GN=CST3 PE=1 SV=2                                     | 215.71 | 6  | 16265  | 0.41 | 9.23 |
| P28800 A2AP_BOVIN      | Alpha-2-antiplasmin OS=Bos taurus GN=SERPINF2 PE=1 SV=2                        | 383.29 | 20 | 54711  | 0.41 | 5.45 |
| tr A5D984 A5D984_BOVIN | Pyruvate kinase OS=Bos taurus GN=PKM2 PE=2 SV=1                                | 353.90 | 21 | 57949  | 0.40 | 7.96 |
| tr F1MSZ6 F1MSZ6_BOVIN | Antithrombin-III OS=Bos taurus GN=SERPINC1 PE=3 SV=1                           | 330.62 | 19 | 52440  | 0.40 | 6.38 |
| Q3TOA3 CFAD_BOVIN      | Complement factor D OS=Bos taurus GN=CFD PE=2 SV=1                             | 322.06 | 10 | 27878  | 0.40 | 7.64 |
| P60661 MYL6_BOVIN      | Myosin light polypeptide 6 OS=Bos taurus GN=MYL6 PE=2 SV=2                     | 222.46 | 6  | 16930  | 0.40 | 4.56 |
| P60661-2 MYL6_BOVIN    | Isoform Smooth muscle of Myosin light polypeptide 6 OS=Bos taurus GN=MYL6      | 222.46 | 6  | 16961  | 0.40 | 4.56 |
| Q3MHL4 SAHH_BOVIN      | Adenosylhomocysteinase OS=Bos taurus GN=AHCY PE=2 SV=3                         | 294.03 | 16 | 47638  | 0.38 | 5.88 |
| tr F1MYN5 F1MYN5_BOVIN | Fibulin-1 OS=Bos taurus GN=FBLN1 PE=3 SV=2                                     | 405.53 | 26 | 77486  | 0.37 | 4.94 |
| P98140 FA12_BOVIN      | Coagulation factor XII OS=Bos taurus GN=F12 PE=1 SV=2                          | 376.61 | 20 | 67160  | 0.33 | 7.91 |
| tr E1BI98 E1BI98_BOVIN | Uncharacterized protein OS=Bos taurus GN=COL6A1 PE=4 SV=1                      | 376.63 | 32 | 108671 | 0.33 | 5.24 |
| P01888 B2MG_BOVIN      | Beta-2-microglobulin OS=Bos taurus GN=B2M PE=1 SV=2                            | 156.95 | 4  | 13677  | 0.33 | 7.79 |
| Q3MHM5 TBB4B_BOVIN     | Tubulin beta-4B chain OS=Bos taurus GN=TUBB4B PE=2 SV=1                        | 297.18 | 14 | 49831  | 0.31 | 4.79 |
| tr E1BJK2 E1BJK2_BOVIN | Uncharacterized protein OS=Bos taurus GN=TUBB1 PE=3 SV=1                       | 259.69 | 14 | 49987  | 0.31 | 4.99 |
| Q5E9B1 LDHB_BOVIN      | L-lactate dehydrogenase B chain OS=Bos taurus GN=LDHB PE=2 SV=4                | 263.58 | 10 | 36724  | 0.30 | 6.02 |
| tr G5E604 G5E604_BOVIN | Uncharacterized protein (Fragment) OS=Bos taurus PE=4 SV=1                     | 142.38 | 3  | 11058  | 0.30 | 8.02 |

## Annex

|                        |   |        |    |        |      |       |
|------------------------|---|--------|----|--------|------|-------|
| tr Q08DQ6 Q08DQ6_BOVIN | Uncharacterized protein OS=Bos taurus GN=ZYX PE=2 SV=1                          | 299.31 | 16 | 60101  | 0.30 | 6.33  |
| tr F1MAV0 F1MAV0_BOVIN | Fibrinogen beta chain OS=Bos taurus GN=FGB PE=4 SV=2                            | 319.82 | 15 | 56441  | 0.30 | 8.50  |
| P62894 CYC_BOVIN       | Cytochrome c OS=Bos taurus GN=CYCS PE=1 SV=2                                    | 135.78 | 3  | 11704  | 0.29 | 9.52  |
| tr F1MM32 F1MM32_BOVIN | Sulfhydryl oxidase OS=Bos taurus GN=QSOX1 PE=3 SV=2                             | 312.74 | 16 | 63006  | 0.28 | 9.32  |
| P20959 IBP3_BOVIN      | Insulin-like growth factor-binding protein 3 OS=Bos taurus GN=IGFBP3 PE=1 SV=3  | 202.23 | 8  | 31570  | 0.28 | 9.03  |
| Q3SZ57 FETA_BOVIN      | Alpha-fetoprotein OS=Bos taurus GN=AFP PE=2 SV=1                                | 251.56 | 17 | 68588  | 0.28 | 5.92  |
| tr A5D7L1 A5D7L1_BOVIN | CLEC11A protein OS=Bos taurus GN=CLEC11A PE=2 SV=1                              | 234.37 | 8  | 35615  | 0.25 | 5.44  |
| tr Q3SZZ9 Q3SZZ9_BOVIN | FGG protein OS=Bos taurus GN=FGG PE=2 SV=1                                      | 316.07 | 11 | 49167  | 0.25 | 5.56  |
| tr F1MGU7 F1MGU7_BOVIN | Fibrinogen gamma-B chain OS=Bos taurus GN=FGG PE=4 SV=1                         | 316.07 | 11 | 50232  | 0.24 | 5.44  |
| tr Q2TBQ1 Q2TBQ1_BOVIN | Coagulation factor XIII, B polypeptide OS=Bos taurus GN=F13B PE=2 SV=1          | 301.61 | 16 | 75167  | 0.24 | 6.34  |
| tr E1BMJ0 E1BMJ0_BOVIN | Uncharacterized protein OS=Bos taurus GN=SERPING1 PE=3 SV=2                     | 275.90 | 11 | 51711  | 0.24 | 6.20  |
| Q32PJ2 APOA4_BOVIN     | Apolipoprotein A-IV OS=Bos taurus GN=APOA4 PE=2 SV=1                            | 266.36 | 9  | 43018  | 0.23 | 5.30  |
| Q5E9Z2 HABP2_BOVIN     | Hyaluronan-binding protein 2 OS=Bos taurus GN=HABP2 PE=2 SV=1                   | 290.69 | 13 | 62441  | 0.23 | 6.32  |
| P81947 TBA1B_BOVIN     | Tubulin alpha-1B chain OS=Bos taurus PE=1 SV=2                                  | 285.90 | 10 | 50152  | 0.22 | 4.94  |
| tr A6QPP2 A6QPP2_BOVIN | SERPIND1 protein OS=Bos taurus GN=SERPIND1 PE=2 SV=1                            | 292.04 | 11 | 55207  | 0.22 | 6.37  |
| Q2HJ86 TBA1D_BOVIN     | Tubulin alpha-1D chain OS=Bos taurus GN=TUBA1D PE=1 SV=1                        | 285.90 | 10 | 50283  | 0.22 | 4.91  |
| tr A8YXZ2 A8YXZ2_BOVIN | C8G protein OS=Bos taurus GN=C8G PE=2 SV=1                                      | 172.50 | 5  | 25288  | 0.22 | 11.06 |
| Q2TA49 VASP_BOVIN      | Vasodilator-stimulated phosphoprotein OS=Bos taurus GN=VASP PE=2 SV=3           | 263.04 | 8  | 40463  | 0.22 | 8.78  |
| Q0VCP3 OLFL3_BOVIN     | Olfactomedin-like protein 3 OS=Bos taurus GN=OLFML3 PE=2 SV=1                   | 234.89 | 9  | 45886  | 0.22 | 6.23  |
| tr B8Y9S9 B8Y9S9_BOVIN | Embryo-specific fibronectin 1 transcript variant OS=Bos taurus GN=FN1 PE=2 SV=1 | 477.86 | 51 | 262424 | 0.22 | 5.49  |
| tr F1MW79 F1MW79_BOVIN | Uncharacterized protein OS=Bos taurus GN=LOC101908952 PE=4 SV=2                 | 199.54 | 6  | 30881  | 0.22 | 6.24  |
| Q3MHY1 CSR1_BOVIN      | Cysteine and glycine-rich protein 1 OS=Bos taurus GN=CSR1 PE=2 SV=3             | 162.38 | 4  | 20612  | 0.22 | 8.91  |
| P07589 FINC_BOVIN      | Fibronectin OS=Bos taurus GN=FN1 PE=1 SV=4                                      | 477.86 | 51 | 272151 | 0.21 | 5.32  |
| Q2KIG3 CBPB2_BOVIN     | Carboxypeptidase B2 OS=Bos taurus GN=CPB2 PE=1 SV=1                             | 229.26 | 9  | 48822  | 0.21 | 8.76  |
| tr F1MW44 F1MW44_BOVIN | Coagulation factor XIII A chain OS=Bos taurus GN=F13A1 PE=3 SV=1                | 316.37 | 15 | 82675  | 0.20 | 5.75  |
| Q28107 FA5_BOVIN       | Coagulation factor V OS=Bos taurus GN=F5 PE=1 SV=1                              | 451.40 | 45 | 248981 | 0.20 | 5.53  |

## Annex

|                        |   |        |    |        |      |      |
|------------------------|---|--------|----|--------|------|------|
| P68103 EF1A1_BOVIN     | Elongation factor 1-alpha 1<br>OS=Bos taurus GN=EEF1A1 PE=1 SV=1                                  | 277.55 | 9  | 50141  | 0.20 | 9.10 |
| tr E1B9F6 E1B9F6_BOVIN | Elongation factor 1-alpha OS=Bos taurus GN=EEF1A1 PE=3 SV=2                                       | 277.55 | 9  | 50170  | 0.20 | 9.15 |
| Q3T149 HSPB1_BOVIN     | Heat shock protein beta-1 OS=Bos taurus GN=HSPB1 PE=2 SV=1  | 245.24 | 4  | 22393  | 0.20 | 5.98 |
| tr Q58DP6 Q58DP6_BOVIN | Ribonuclease 4 OS=Bos taurus GN=RNASE4 PE=2 SV=1  | 191.16 | 3  | 16938  | 0.20 | 9.18 |
| Q3SZK8 NHRF1_BOVIN     | Na(+)/H(+) exchange regulatory cofactor NHE-RF1 OS=Bos taurus GN=SLC9A3R1 PE=2 SV=1               | 266.88 | 7  | 39603  | 0.20 | 5.29 |
| Q3SZV7 HEMO_BOVIN      | Hemopexin OS=Bos taurus GN=HPX PE=2 SV=1  | 244.39 | 9  | 52209  | 0.19 | 7.90 |
| Q32LP0 URP2_BOVIN      | Fermitin family homolog 3 OS=Bos taurus GN=FERMT3 PE=2 SV=1                                       | 360.08 | 13 | 75783  | 0.19 | 6.20 |
| Q2KJ63 KLKB1_BOVIN     | Plasma kallikrein OS=Bos taurus GN=KLKB1 PE=2 SV=1  | 293.85 | 12 | 70994  | 0.19 | 8.64 |
| tr E1BIK4 E1BIK4_BOVIN | Uncharacterized protein OS=Bos taurus GN=PPBP PE=3 SV=1   | 146.63 | 2  | 12912  | 0.17 | 9.39 |
| tr E1BCW0 E1BCW0_BOVIN | Uncharacterized protein (Fragment) OS=Bos taurus GN=HGFAC PE=3 SV=2                               | 168.41 | 5  | 32745  | 0.17 | 8.65 |
| Q2KIV9 C1QB_BOVIN      | Complement C1q subcomponent subunit B OS=Bos taurus GN=C1QB PE=1 SV=1                             | 195.65 | 4  | 26399  | 0.17 | 9.53 |
| P00741 FA9_BOVIN       | Coagulation factor IX (Fragment) OS=Bos taurus GN=F9 PE=1 SV=1                                    | 216.94 | 7  | 46785  | 0.17 | 5.63 |
| tr A7MB82 A7MB82_BOVIN | C1QTNF3 protein OS=Bos taurus GN=C1QTNF3 PE=2 SV=1  | 152.08 | 4  | 26810  | 0.17 | 6.10 |
| tr E1BB91 E1BB91_BOVIN | Uncharacterized protein OS=Bos taurus GN=COL6A3 PE=4 SV=1   | 430.61 | 50 | 342408 | 0.16 | 6.11 |
| tr F1N7Y8 F1N7Y8_BOVIN | Dermokine OS=Bos taurus GN=DMKN PE=4 SV=2   | 199.76 | 7  | 48040  | 0.16 | 6.31 |
| Q0P569 NUCB1_BOVIN     | Nucleobindin-1 OS=Bos taurus GN=NUCB1 PE=2 SV=1   | 239.41 | 8  | 54982  | 0.16 | 5.11 |
| Q2KIT0 HP20_BOVIN      | Protein HP-20 homolog OS=Bos taurus PE=2 SV=1   | 222.34 | 3  | 20646  | 0.16 | 8.85 |
| A6QQF6 SBSN_BOVIN      | Suprabasin OS=Bos taurus GN=SBSN PE=2 SV=1  | 182.69 | 8  | 56854  | 0.16 | 6.74 |
| tr F1N169 F1N169_BOVIN | Uncharacterized protein OS=Bos taurus GN=FLNA PE=4 SV=2   | 465.31 | 39 | 281171 | 0.16 | 5.80 |
| Q3SYR5 APOC4_BOVIN     | Apolipoprotein C-IV OS=Bos taurus GN=APOC4 PE=2 SV=1  | 156.07 | 2  | 14438  | 0.15 | 8.75 |
| A2VE23 DMKN_BOVIN      | Dermokine OS=Bos taurus GN=DMKN PE=2 SV=1   | 199.76 | 7  | 50549  | 0.15 | 6.64 |
| tr F1MBS3 F1MBS3_BOVIN | Transforming growth factor-beta-induced protein ig-h3 (Fragment) OS=Bos taurus GN=TGFBI PE=4 SV=2 | 262.11 | 10 | 72252  | 0.15 | 6.70 |
| tr Q1RMH5 Q1RMH5_BOVIN | C1QC protein (Fragment) OS=Bos taurus GN=C1QC PE=2 SV=1   | 183.98 | 4  | 29023  | 0.15 | 8.80 |
| tr F1N102 F1N102_BOVIN | Uncharacterized protein OS=Bos taurus GN=C8B PE=4 SV=2  | 257.42 | 9  | 66658  | 0.15 | 8.38 |
| Q3B7M5 LASP1_BOVIN     | LIM and SH3 domain protein 1 OS=Bos taurus GN=LASP1 PE=2 SV=1                                     | 183.40 | 4  | 29677  | 0.15 | 6.61 |
| tr F1MFL4 F1MFL4_BOVIN | Coagulation factor IX OS=Bos taurus GN=F9 PE=3 SV=1   | 216.94 | 7  | 52046  | 0.15 | 5.63 |
| P56652 ITI3_BOVIN      | Inter-alpha-trypsin inhibitor heavy chain H3 OS=Bos taurus GN=ITI3 PE=1 SV=2                      | 268.21 | 13 | 99551  | 0.15 | 5.59 |

## Annex

|                        |  |        |    |        |      |      |
|------------------------|--|--------|----|--------|------|------|
| O02675 DPYL2_BOVIN     | Dihydropyrimidinase-related protein 2 OS=Bos taurus GN=DPYSL2 PE=1 SV=1                | 248.93 | 8  | 62278  | 0.14 | 5.95 |
| Q5E9C0 RSU1_BOVIN      | Ras suppressor protein 1 OS=Bos taurus GN=RSU1 PE=2 SV=1                               | 167.44 | 4  | 31537  | 0.14 | 8.56 |
| tr F1MRZ8 F1MRZ8_BOVIN | Uncharacterized protein OS=Bos taurus GN=PLEK PE=4 SV=2                                | 190.04 | 5  | 40057  | 0.14 | 8.64 |
| Q3T054 RAN_BOVIN       | GTP-binding nuclear protein Ran OS=Bos taurus GN=RAN PE=2 SV=3                         | 107.24 | 3  | 24423  | 0.14 | 7.01 |
| O62644 LECT2_BOVIN     | Leukocyte cell-derived chemotaxin-2 OS=Bos taurus GN=LECT2 PE=1 SV=1                   | 144.36 | 2  | 16320  | 0.14 | 9.25 |
| P35445 COMP_BOVIN      | Cartilage oligomeric matrix protein OS=Bos taurus GN=COMP PE=1 SV=2                    | 284.77 | 10 | 82362  | 0.14 | 4.37 |
| tr F1MX87 F1MX87_BOVIN | Uncharacterized protein OS=Bos taurus GN=C8A PE=4 SV=1                                 | 241.11 | 8  | 66277  | 0.13 | 6.23 |
| tr F1MQ37 F1MQ37_BOVIN | Uncharacterized protein OS=Bos taurus GN=MYH9 PE=4 SV=2                                | 373.09 | 27 | 227101 | 0.13 | 5.50 |
| Q3Y5Z3 ADIPO_BOVIN     | Adiponectin OS=Bos taurus GN=ADIPOQ PE=1 SV=1  | 146.12 | 3  | 26133  | 0.13 | 5.44 |
| Q27965 HS71B_BOVIN     | Heat shock 70 kDa protein 1B OS=Bos taurus GN=HSPA1B PE=2 SV=1                         | 269.45 | 8  | 70229  | 0.13 | 5.67 |
| Q27975 HS71A_BOVIN     | Heat shock 70 kDa protein 1A OS=Bos taurus GN=HSPA1A PE=1 SV=2                         | 269.45 | 8  | 70259  | 0.13 | 5.67 |
| Q3SZP2 MARE2_BOVIN     | Microtubule-associated protein RP/EB family member 2 OS=Bos taurus GN=MAPRE2 PE=2 SV=1 | 217.14 | 4  | 36988  | 0.12 | 5.36 |
| tr A7E3W4 A7E3W4_BOVIN | Transketolase OS=Bos taurus GN=TKT PE=2 SV=1   | 243.90 | 7  | 64875  | 0.12 | 6.71 |
| tr A7Z014 A7Z014_BOVIN | Transketolase OS=Bos taurus GN=TKT PE=2 SV=1   | 243.90 | 7  | 67798  | 0.12 | 7.20 |
| P31976 EZRI_BOVIN      | Ezrin OS=Bos taurus GN=EZR PE=1 SV=2   | 211.72 | 7  | 68760  | 0.11 | 6.06 |
| P07456 IGF2_BOVIN      | Insulin-like growth factor II OS=Bos taurus GN=IGF2 PE=1 SV=4                          | 122.48 | 2  | 19682  | 0.11 | 9.11 |
| Q3SZV3 EF1G_BOVIN      | Elongation factor 1-gamma OS=Bos taurus GN=EEF1G PE=2 SV=1                             | 182.08 | 5  | 50378  | 0.11 | 6.15 |
| Q92176 COR1A_BOVIN     | Coronin-1A OS=Bos taurus GN=CORO1A PE=1 SV=3   | 162.81 | 5  | 50979  | 0.11 | 6.25 |
| Q76LV2 HS90A_BOVIN     | Heat shock protein HSP 90-alpha OS=Bos taurus GN=HSP90AA1 PE=1 SV=3                    | 229.20 | 8  | 84731  | 0.11 | 4.92 |
| Q3SWW8 TSP4_BOVIN      | Thrombospondin-4 OS=Bos taurus GN=THBS4 PE=2 SV=1                                      | 292.57 | 10 | 105974 | 0.11 | 4.44 |
| P02453 CO1A1_BOVIN     | Collagen alpha-1(I) chain OS=Bos taurus GN=COL1A1 PE=1 SV=3                            | 299.98 | 13 | 138939 | 0.10 | 5.60 |
| tr F1N2L9 F1N2L9_BOVIN | 4-trimethylaminobutyraldehyde dehydrogenase OS=Bos taurus GN=ALDH9A1 PE=3 SV=2         | 188.97 | 5  | 53991  | 0.10 | 5.84 |
| Q9BGI3 PRDX2_BOVIN     | Peroxiredoxin-2 OS=Bos taurus GN=PRDX2 PE=2 SV=1                                       | 114.67 | 2  | 21946  | 0.10 | 5.37 |
| tr E1BLA8 E1BLA8_BOVIN | Uncharacterized protein OS=Bos taurus GN=GOLM1 PE=4 SV=1                               | 220.21 | 4  | 45536  | 0.10 | 4.82 |
| tr A6H7E3 A6H7E3_BOVIN | PDZ and LIM domain 1 OS=Bos taurus GN=PDLIM1 PE=2 SV=1                                 | 141.37 | 3  | 35821  | 0.09 | 6.76 |
| tr A5D7E1 A5D7E1_BOVIN | MGC139254 protein OS=Bos taurus GN=MGC139254 PE=2 SV=1                                 | 180.49 | 5  | 60931  | 0.09 | 6.12 |

## Annex

|                        |  |        |    |        |      |      |
|------------------------|--|--------|----|--------|------|------|
| O77834 PRDX6_BOVIN     | Peroxiredoxin-6 OS=Bos taurus<br>GN=PRDX6 PE=1 SV=3  | 130.58 | 2  | 25067  | 0.09 | 6.00 |
| P37141 GPX3_BOVIN      | Glutathione peroxidase 3 OS=Bos<br>taurus GN=GPX3 PE=2 SV=2                                  | 118.42 | 2  | 25663  | 0.09 | 6.84 |
| tr F1N468 F1N468_BOVIN | Uncharacterized protein OS=Bos<br>taurus GN=ADK PE=4 SV=2                                    | 162.91 | 3  | 38532  | 0.09 | 5.85 |
| P00745 PROC_BOVIN      | Vitamin K-dependent protein C<br>(Fragment) OS=Bos taurus<br>GN=PROC PE=1 SV=1               | 191.67 | 4  | 51416  | 0.09 | 5.80 |
| Q5E9B7 CLIC1_BOVIN     | Chloride intracellular channel<br>protein 1 OS=Bos taurus<br>GN=CLIC1 PE=2 SV=3              | 133.87 | 2  | 26992  | 0.08 | 5.17 |
| Q5EAD2 SERA_BOVIN      | D-3-phosphoglycerate<br>dehydrogenase OS=Bos taurus<br>GN=PHGDH PE=2 SV=3                    | 152.17 | 4  | 56452  | 0.08 | 6.47 |
| P24591 IBP1_BOVIN      | Insulin-like growth factor-binding<br>protein 1 OS=Bos taurus<br>GN=IGFBP1 PE=2 SV=2         | 83.63  | 2  | 28794  | 0.08 | 6.33 |
| tr A5PJT7 A5PJT7_BOVIN | ECM1 protein OS=Bos taurus<br>GN=ECM1 PE=2 SV=1  | 128.04 | 4  | 57637  | 0.08 | 7.22 |
| Q5KR47-2 TPM3_BOVIN    | Isoform 2 of Tropomyosin alpha-3<br>chain OS=Bos taurus GN=TPM3                              | 116.28 | 2  | 29033  | 0.08 | 4.68 |
| tr E1B9H5 E1B9H5_BOVIN | Uncharacterized protein OS=Bos<br>taurus GN=TGFBR3 PE=4 SV=2                                 | 244.24 | 6  | 89803  | 0.07 | 5.78 |
| tr F1MJK3 F1MJK3_BOVIN | Uncharacterized protein OS=Bos<br>taurus GN=LOC506828 PE=4 SV=2                              | 321.42 | 11 | 165610 | 0.07 | 6.76 |
| tr F1MI18 F1MI18_BOVIN | Uncharacterized protein OS=Bos<br>taurus GN=LOC506828 PE=4 SV=2                              | 321.42 | 11 | 165758 | 0.07 | 7.34 |
| Q05717 IBP5_BOVIN      | Insulin-like growth factor-binding<br>protein 5 OS=Bos taurus<br>GN=IGFBP5 PE=2 SV=2         | 108.17 | 2  | 30314  | 0.07 | 8.72 |
| tr F1MI46 F1MI46_BOVIN | Osteopontin OS=Bos taurus<br>GN=SPP1 PE=4 SV=1   | 122.18 | 2  | 30727  | 0.07 | 4.44 |
| A2I7M9 SPA32_BOVIN     | Serpin A3-2 OS=Bos taurus<br>GN=SERPINA3-2 PE=3 SV=1   | 106.84 | 3  | 46237  | 0.07 | 5.67 |
| Q9TTE1 SPA31_BOVIN     | Serpin A3-1 OS=Bos taurus<br>GN=SERPINA3-1 PE=1 SV=3   | 106.84 | 3  | 46237  | 0.07 | 5.67 |
| tr G8JKW7 G8JKW7_BOVIN | Uncharacterized protein OS=Bos<br>taurus GN=SERPINA3 PE=3 SV=1                               | 106.84 | 3  | 46344  | 0.07 | 6.29 |
| P31096 OSTP_BOVIN      | Osteopontin OS=Bos taurus<br>GN=SPP1 PE=1 SV=2   | 122.18 | 2  | 30904  | 0.07 | 4.49 |
| A2I7N1 SPA35_BOVIN     | Serpin A3-5 OS=Bos taurus<br>GN=SERPINA3-5 PE=3 SV=1   | 106.84 | 3  | 46397  | 0.07 | 6.48 |
| P33072 LYOX_BOVIN      | Protein-lysine 6-oxidase OS=Bos<br>taurus GN=LOX PE=1 SV=3                                   | 182.17 | 3  | 47123  | 0.07 | 8.49 |
| Q5KR47 TPM3_BOVIN      | Tropomyosin alpha-3 chain<br>OS=Bos taurus GN=TPM3 PE=2<br>SV=1                              | 116.28 | 2  | 32819  | 0.07 | 4.68 |
| tr A6QR15 A6QR15_BOVIN | LOC535277 protein OS=Bos<br>taurus GN=LOC535277 PE=2 SV=1                                    | 116.28 | 2  | 32824  | 0.07 | 4.70 |
| Q76LV1 HS90B_BOVIN     | Heat shock protein HSP 90-beta<br>OS=Bos taurus GN=HSP90AB1<br>PE=2 SV=3                     | 227.03 | 5  | 83253  | 0.07 | 4.96 |
| Q2HJ49 MOES_BOVIN      | Moesin OS=Bos taurus GN=MSN<br>PE=2 SV=3   | 145.73 | 4  | 67975  | 0.07 | 5.90 |
| Q2HJ60 ROA2_BOVIN      | Heterogeneous nuclear<br>ribonucleoproteins A2/B1 OS=Bos<br>taurus GN=HNRNPA2B1 PE=2<br>SV=1 | 101.15 | 2  | 36006  | 0.06 | 8.67 |
| Q3SZB7 F16P1_BOVIN     | Fructose-1,6-bisphosphatase 1<br>OS=Bos taurus GN=FBP1 PE=2<br>SV=3                          | 152.07 | 2  | 36728  | 0.06 | 6.54 |
| Q5E9A3 PCBP1_BOVIN     | Poly(rC)-binding protein 1 OS=Bos<br>taurus GN=PCBP1 PE=2 SV=1                               | 105.52 | 2  | 37498  | 0.06 | 6.66 |

## Annex

|                        |   |        |    |        |      |      |
|------------------------|---|--------|----|--------|------|------|
| tr F1MY85 F1MY85_BOVIN | Complement C5a anaphylatoxin<br>OS=Bos taurus GN=C5 PE=4 SV=2                             | 267.45 | 10 | 189045 | 0.06 | 6.06 |
| Q3ZC42 ADHX_BOVIN      | Alcohol dehydrogenase class-3<br>OS=Bos taurus GN=ADH5 PE=2<br>SV=1                       | 125.58 | 2  | 39677  | 0.06 | 7.46 |
| Q5EA61 KCRB_BOVIN      | Creatine kinase B-type OS=Bos<br>taurus GN=CKB PE=1 SV=1                                  | 92.33  | 2  | 42719  | 0.05 | 5.47 |
| P02465 CO1A2_BOVIN     | Collagen alpha-2(I) chain OS=Bos<br>taurus GN=COL1A2 PE=1 SV=2                            | 233.33 | 6  | 129064 | 0.05 | 9.23 |
| Q2KJH4 WDR1_BOVIN      | WD repeat-containing protein 1<br>OS=Bos taurus GN=WDR1 PE=2<br>SV=3                      | 191.90 | 3  | 66258  | 0.05 | 6.24 |
| tr F1MTP5 F1MTP5_BOVIN | WD repeat-containing protein 1<br>OS=Bos taurus GN=WDR1 PE=4<br>SV=2                      | 191.90 | 3  | 66277  | 0.05 | 6.29 |
| Q2KJH6 SERPH_BOVIN     | Serpin H1 OS=Bos taurus<br>GN=SERPINH1 PE=2 SV=1  | 126.89 | 2  | 46507  | 0.05 | 9.01 |
| Q5NTB3 FA11_BOVIN      | Coagulation factor XI OS=Bos<br>taurus GN=F11 PE=1 SV=1                                   | 187.07 | 3  | 69872  | 0.05 | 7.81 |
| tr A5PK77 A5PK77_BOVIN | SERPINA11 protein OS=Bos taurus<br>GN=SERPINA11 PE=2 SV=1                                 | 150.61 | 2  | 46844  | 0.05 | 6.64 |
| A6H7G2 DBNL_BOVIN      | Drebrin-like protein OS=Bos<br>taurus GN=DBNL PE=2 SV=1                                   | 128.10 | 2  | 47723  | 0.05 | 4.95 |
| Q0VCX1 C1S_BOVIN       | Complement C1s subcomponent<br>OS=Bos taurus GN=C1S PE=2 SV=2                             | 141.97 | 3  | 76609  | 0.04 | 4.97 |
| Q3SWY2 ILK_BOVIN       | Integrin-linked protein kinase<br>OS=Bos taurus GN=ILK PE=2 SV=1                          | 116.57 | 2  | 51447  | 0.04 | 4.97 |
| tr G5E505 G5E505_BOVIN | Integrin-linked protein kinase<br>OS=Bos taurus GN=ILK PE=4 SV=1                          | 116.57 | 2  | 51494  | 0.04 | 7.66 |
| tr F1MJ12 F1MJ12_BOVIN | Complement C1s subcomponent<br>OS=Bos taurus GN=C1S PE=3 SV=1                             | 141.97 | 3  | 77382  | 0.04 | 4.98 |
| tr Q3ZCI4 Q3ZCI4_BOVIN | 6-phosphogluconate<br>dehydrogenase, decarboxylating<br>OS=Bos taurus GN=PGD PE=2<br>SV=2 | 107.27 | 2  | 53077  | 0.04 | 6.65 |
| tr A5D9E9 A5D9E9_BOVIN | Complement component 1, r<br>subcomponent OS=Bos taurus<br>GN=C1R PE=1 SV=1               | 144.59 | 3  | 80213  | 0.04 | 5.86 |
| Q9XTA3 MYOC_BOVIN      | Myocilin OS=Bos taurus<br>GN=MYOC PE=2 SV=1   | 115.95 | 2  | 54886  | 0.04 | 5.47 |
| tr Q3SX06 Q3SX06_BOVIN | Myocilin OS=Bos taurus<br>GN=MYOC PE=2 SV=1   | 115.95 | 2  | 54888  | 0.04 | 5.33 |
| tr E1BA44 E1BA44_BOVIN | Uncharacterized protein OS=Bos<br>taurus GN=LTBP4 PE=4 SV=2                               | 238.84 | 6  | 172979 | 0.04 | 5.71 |
| Q3MHL7 TCPZ_BOVIN      | T-complex protein 1 subunit zeta<br>OS=Bos taurus GN=CCT6A PE=1<br>SV=3                   | 110.85 | 2  | 57956  | 0.04 | 6.32 |
| tr F1MXR3 F1MXR3_BOVIN | Uncharacterized protein OS=Bos<br>taurus GN=ADAMTSL4 PE=4 SV=1                            | 219.28 | 4  | 116311 | 0.04 | 8.55 |
| tr G3MZT8 G3MZT8_BOVIN | Uncharacterized protein OS=Bos<br>taurus GN=LTBP4 PE=4 SV=1                               | 238.84 | 6  | 176109 | 0.04 | 5.68 |
| tr F1MGX0 F1MGX0_BOVIN | T-complex protein 1 subunit zeta<br>OS=Bos taurus GN=CCT6A PE=3<br>SV=2                   | 110.85 | 2  | 58838  | 0.04 | 8.20 |
| Q24K22 HGFL_BOVIN      | Hepatocyte growth factor-like<br>protein OS=Bos taurus GN=MST1<br>PE=2 SV=1               | 127.21 | 2  | 79973  | 0.03 | 8.41 |
| Q95M18 ENPL_BOVIN      | Endoplasmin OS=Bos taurus<br>GN=HSP90B1 PE=2 SV=1   | 119.48 | 2  | 92427  | 0.02 | 4.76 |
| Q3SYU2 EF2_BOVIN       | Elongation factor 2 OS=Bos taurus<br>GN=EEF2 PE=2 SV=3                                    | 107.79 | 2  | 95368  | 0.02 | 6.41 |
| tr F1N6W9 F1N6W9_BOVIN | Uncharacterized protein OS=Bos<br>taurus GN=COL18A1 PE=4 SV=2                             | 153.41 | 3  | 153879 | 0.02 | 5.20 |

## Annex

|                        |  |        |   |        |      |      |
|------------------------|--|--------|---|--------|------|------|
| Q29RU4 CO6_BOVIN       | Complement component C6<br>OS=Bos taurus GN=C6 PE=2 SV=1                   | 133.75 | 2 | 104541 | 0.02 | 6.73 |
| tr F1N0K0 F1N0K0_BOVIN | Collagen alpha-1(XI) chain OS=Bos<br>taurus GN=COL11A1 PE=4 SV=2           | 150.29 | 3 | 182353 | 0.02 | 5.62 |
| tr F1N789 F1N789_BOVIN | Uncharacterized protein OS=Bos<br>taurus GN=VCL PE=4 SV=1                  | 154.65 | 2 | 123864 | 0.02 | 5.58 |
| tr G3MZI7 G3MZI7_BOVIN | Uncharacterized protein<br>(Fragment) OS=Bos taurus<br>GN=COL5A1 PE=4 SV=1 | 188.43 | 3 | 199437 | 0.02 | 5.13 |
| tr F1MSR8 F1MSR8_BOVIN | Collagen alpha-1(II) chain OS=Bos<br>taurus GN=COL2A1 PE=4 SV=2            | 176.60 | 2 | 134427 | 0.02 | 8.66 |
| P02459 CO2A1_BOVIN     | Collagen alpha-1(II) chain OS=Bos<br>taurus GN=COL2A1 PE=1 SV=4            | 176.60 | 2 | 141829 | 0.02 | 6.82 |
| tr F1MPK6 F1MPK6_BOVIN | Uncharacterized protein<br>(Fragment) OS=Bos taurus<br>GN=TNXB PE=4 SV=2   | 247.07 | 6 | 439314 | 0.02 | 4.92 |
| tr F1N0R5 F1N0R5_BOVIN | von Willebrand factor OS=Bos<br>taurus GN=VWF PE=4 SV=2                    | 171.68 | 3 | 307677 | 0.01 | 5.39 |
| tr E1BNR0 E1BNR0_BOVIN | Uncharacterized protein OS=Bos<br>taurus GN=APOB PE=4 SV=2                 | 138.96 | 5 | 515764 | 0.01 | 6.32 |
| tr F1MER7 F1MER7_BOVIN | Uncharacterized protein<br>(Fragment) OS=Bos taurus<br>GN=HSPG2 PE=4 SV=1  | 201.52 | 4 | 466033 | 0.01 | 6.00 |

Table 45 Redundant proteins identified in Sample 5

| Accession              | Description   | -10lgP |
|------------------------|---|--------|
| tr G3X7A8 G3X7A8_BOVIN | Uncharacterized protein OS=Bos taurus GN=PTI PE=4 SV=1                            | 172.81 |
| tr G5E5A9 G5E5A9_BOVIN | Fibronectin OS=Bos taurus GN=FN1 PE=4 SV=1  | 477.86 |
| tr F1N3A1 F1N3A1_BOVIN | Thrombospondin-1 OS=Bos taurus GN=THBS1 PE=4 SV=1                                 | 499.22 |
| tr F1MUK3 F1MUK3_BOVIN | Insulin-like growth factor-binding protein 6 OS=Bos taurus GN=IGFBP6<br>PE=4 SV=1 | 311.95 |
| tr F1MTT3 F1MTT3_BOVIN | Coagulation factor XII OS=Bos taurus GN=F12 PE=3 SV=1                             | 376.61 |
| tr F1MB08 F1MB08_BOVIN | Alpha-enolase OS=Bos taurus GN=ENO1 PE=3 SV=1                                     | 359.10 |
| tr Q17QH0 Q17QH0_BOVIN | Metallothionein OS=Bos taurus GN=MT1E PE=2 SV=1                                   | 152.27 |
| tr A6QLB7 A6QLB7_BOVIN | Adenylyl cyclase-associated protein OS=Bos taurus GN=CAP1 PE=2 SV=1               | 486.15 |
| tr E1BA13 E1BA13_BOVIN | Uncharacterized protein OS=Bos taurus PE=3 SV=1 (= CYC_BOVIN)                     | 135.78 |
| tr F1N3Q7 F1N3Q7_BOVIN | Apolipoprotein A-IV OS=Bos taurus GN=APOA4 PE=3 SV=1                              | 266.36 |
| tr F2Z4C1 F2Z4C1_BOVIN | Uncharacterized protein OS=Bos taurus GN=TUBA1A PE=3 SV=1 (= P81947 TBA1B_BOVIN)  | 285.90 |
| tr E1BEL7 E1BEL7_BOVIN | Heat shock protein beta-1 OS=Bos taurus GN=HSPB1 PE=3 SV=2                        | 245.24 |
| tr F1MG05 F1MG05_BOVIN | Elongation factor 1-gamma OS=Bos taurus GN=EEF1G PE=4 SV=1                        | 182.08 |
| tr G3X8D7 G3X8D7_BOVIN | Glutathione peroxidase OS=Bos taurus GN=GPX3 PE=3 SV=1                            | 118.42 |
| tr A5D7S7 A5D7S7_BOVIN | LOX protein OS=Bos taurus GN=LOX PE=2 SV=1  | 182.17 |
| tr F1MUT4 F1MUT4_BOVIN | Coagulation factor XI OS=Bos taurus GN=F11 PE=3 SV=1                              | 187.07 |
| tr E1BDW7 E1BDW7_BOVIN | Hepatocyte growth factor-like protein OS=Bos taurus GN=MST1 PE=3 SV=2             | 127.21 |
| tr F1MM86 F1MM86_BOVIN | Complement component C6 OS=Bos taurus GN=C6 PE=4 SV=1                             | 133.75 |

In Sample 5, the following proteins were found in only one database:

- Fibrinogen alpha chain (tr|A5PJE3|A5PJE3\_BOVIN). Not found: P02672|FIBA\_BOVIN
- Protein AMBP (tr|F1MMK9|F1MMK9\_BOVIN). Not found: P00978|AMBP\_BOVIN
- Antithrombin-III (tr|F1MSZ6|F1MSZ6\_BOVIN). Not found: P41361|ANT3\_BOVIN

## 5.4ND Modification

The following antibody was used: Fluorescein (FITC) AffiniPure Goat Anti-Mouse IgG (H+L) (Jackson ImmunoResearch Inc., USA). The following specifications applied:

Target: Mouse

Host: Goat

Antibody Format: Whole IgG

Specificity: IgG (H+L)

Minimal Cross Reactivity: Human, Bovine, Horse, Rabbit, Swine Serum Proteins

Conjugate: Fluorescein (FITC)

Product Category: Whole IgG Affinity-Purified Antibodies

Clonality: Polyclonal



## 6. List of Figures

|  |    |
|--|----|
| Figure 1 (a) Lattice structure of the NV center. (b, c) Three-dimensional electron density of the $^3A_2$ electronic ground state and the $^3E$ excited state. Reprinted with permission from <sup>[5]</sup> .....   | 8  |
| Figure 2 (a) Simplified energy diagram of the NV <sup>-</sup> center: After excitation with a green laser (532 nm in the equipment of the group) fluorescence in the red spectral region is emitted <sup>[5]</sup> . $ g\rangle$ marks the electronic ground state, $ e\rangle$ the electronic excited state, and $ s\rangle$ the metastable singlet state. Wiggly arrows indicate the radiative transition, and black arrows indicate strong and weak nonradiative decay via the singlet state <sup>[5]</sup> . As the process is strongly spin-preserving and there are differing cross-over rates depending on the spin state (The three spin sublevels are shown in the yellow box: $m_s = 0$ and $m_s = \pm 1$ at zero and nonzero magnetic field B. D is the zero-field splitting and $2\gamma B$ is the Zeeman splitting, where $\gamma$ is the electron gyromagnetic ratio.), an optical contrast between $m_s = 0$ and $m_s = \pm 1$ states of approximately 30% is achieved: The spin state can be read out by fluorescence (basis of the “Optically Detected Magnetic Resonance”, ODMR) <sup>[5]</sup> . (b) The photoluminescence spectrum (used for the quantification of diamond in this work) with the NV <sup>0</sup> zero phonon line (575 nm), the NV <sup>-</sup> zero phonon line (638 nm), and NV <sup>-</sup> vibrational side bands (630–800 nm). (c) The optical contrast between the spin states is for 2- $\mu$ s laser pulse that disappears after some time (due to the repumping of the electron to $m_s = 0$ via the $ s\rangle$ singlet state). ) <sup>[5]</sup> . (d,e) Electron paramagnetic resonance (EPR) spectrum of a single NV center at zero and nonzero magnetic field (measured using ODMR). Reprinted with permission from <sup>[5]</sup> ..... | 10 |
| Figure 3 Comparison of 70 nm Adámas Diamonds with 75 nm Microdiamant Diamonds based on the Size Distribution by Number. ....   | 25 |
| Figure 4 Comparison of 120 nm Adámas Diamonds with 125 nm Microdiamant Diamonds based on the Size Distribution by Number. ....   | 25 |
| Figure 5 25 nm NDs on glow discharged plain carbon coated 400 mesh copper grids at different spots. ....   | 27 |
| Figure 6 25 nm NDs on holey carbon coated grids. The big dark diamond in the middle of the picture marks de center where SAED was done.....  | 27 |
| Figure 7 Hexagonal structure of the diamond 111 plane. This points to 111 texturation of the NDs..   | 27 |
| Figure 8 Schematic image of the implications of a flat, flake-like shape of the NDs with an assumed 111 texturation (with the NV <sup>-</sup> -center’s main axis along the (111) crystal axis). The blue arrow marks the NV <sup>-</sup> -center while the red arrows represent external spins of interest (e.g. ROS). ....   | 28 |

## List of Figures

|   |    |
|---|----|
| Figure 9 XPS spectrum of the NDs of 25 nm size (Microdiamant AG). Exemplarily shown for the measurement at the first spot. The complete measurement information including the peak fittings for the elements for this spot as well as for the other three spots measured can be found in the annex.   | 31 |
| Figure 10 Precipitation with NDs of 25 nm median size after 24 hours. From left to right: ND in DI water, ND in 10% FBS, ND in pure FBS, ND in DMEM (without FBS), ND in DMEM with 10% FBS. ....  | 32 |
| Figure 11 Blue: Measurements with disposable sizing cuvettes. Orange: Measurements with disposable folded capillary cells. The error bar corresponds to the standard deviation. ....  | 34 |
| Figure 12 XPS spectrum for the NDs of 25 nm of median size (Microdiamant AG) in DMEM with 10% FBS. ....   | 36 |
| Figure 13 XPS spectrum NDs of 25 nm of median size (Microdiamant AG) in DMEM (without FBS) - Spot A. ....   | 37 |
| Figure 14 XPS spectrum NDs of 25 nm of median size (Microdiamant AG) in DMEM (without FBS) - Spot B. ....   | 38 |
| Figure 15 XPS spectrum of NDs of 25 nm of median size (Microdiamant AG) in YMB (Spot A) .....   | 39 |
| Figure 16 Aggregates with 25 nm NDs (Microdiamant AG) in DMEM with 10% FBS (The same sample is shown at different spots.). In the upper left part (in both images), the edges of the hole on the grid are visible. ....   | 41 |
| Figure 17 Aggregates with 25 nm NDs (Microdiamant AG) in DMEM with 10% FBS. The image on the right shows the same spot with a higher magnification. The arrow points at the proteins that forms a layer of approximately 2-3 nm thickness. "Clusters" of NDs are formed with proteins (acting as a "glue") around. ....   | 41 |
| Figure 18 25 nm ND (Microdiamant AG) aggregation with "yeast medium base without amino acids" .....   | 42 |
| Figure 19 MALDI-TOF-MS Fingerprint of the protein corona. ....  | 43 |
| Figure 20 Overview of the number of proteins found .....  | 44 |
| Figure 21 Left: Confocal microscopy images of 70 nm FNDs conjugated with FITC-labelled antibodies. Huge aggregations formed in the drying process are visible. The picture is split into 4, showing the FITC-signal in green in the top left, the differential interference contrast (DIC) in the top right and the FND signal in the bottom left. The sizes are is 224.7 $\mu\text{m}$ x 224.7 $\mu\text{m}$ . Right: Salt crystals with NDs that are formed in DMEM if not sufficiently spin coated (similar results are obtained for NDs in PBS). As a result, the droplet was spin-coated 2x for 30 seconds for the samples in PBS and DMEM, which solved the issue. .... | 49 |
| Figure 22 NDs of 70 nm (Adámas) with antibodies (in DI water). Contrast and brightness were increased by to improve visibility. ....  | 50 |

## List of Figures

|  |    |
|--|----|
| Figure 23 NDs of 70 nm (Adámas) with antibodies in PBS. Contrast and brightness were increased to improve visibility. ....   | 50 |
| Figure 24 NDs of 70 nm (Adámas) with antibodies in FBS. Contrast and brightness were increased to improve visibility. ....   | 51 |
| Figure 25 NDs of 70 nm (Adámas) with antibodies in 10% FBS. Contrast and brightness were increased to improve visibility. ....   | 51 |
| Figure 26 NDs of 70 nm (Adámas) with antibodies in DMEM with 10% FBS. Contrast and brightness were increased to improve visibility. ....   | 51 |
| Figure 27 NDs of 70 nm (Adámas) with antibodies in indicatorless DMEM with 10% FBS. Contrast and brightness were increased to improve visibility.....  | 52 |
| Figure 28 Fluorescence spectrum obtained for standard solutions with NDs in DI water. Between 550 – 850 nm, the fluorescence of the NV <sup>-</sup> -center as well as the Raman peak of water can be seen. The right shows the second order diffraction of the 532 nm laser limiting the acquisition time. .... | 53 |
| Figure 29 Extract of the spectrum from Figure 28 showing the area between 550 – 900 nm. ....   | 54 |
| Figure 30 Fluorescence spectrum of the NV <sup>-</sup> - center obtained after subtracting the water spectrum. ....  | 54 |
| Figure 31 Fluorescence of the cell lysates between 500 – 900 nm.....   | 57 |

## 7. List of Tables

|  |    |
|--|----|
| Table 1 NDs from Microdiamant AG .....   | 14 |
| Table 2 FNDs from Adámas Technologies .....  | 14 |
| Table 3 DLS settings for size measurements .....   | 15 |
| Table 4 DLS Measurements with Different Diamond Concentrations .....   | 23 |
| Table 5 DLS Measurements of the Diamond Slurries with a Concentration of 10 µg/mL .....  | 24 |
| Table 6 Zeta potentials measured for the ND suspensions with a concentration of 10 µg/mL .....   | 26 |
| Table 7 Zeta potentials measured for the ND suspensions with a concentration of 1 µg/mL .....  | 26 |
| Table 8 Crystallite sizes and lattice parameters obtained by XRD .....   | 28 |
| Table 9 XPS results for NDs of 25 nm of median size (Microdiamant AG) – Spot 1. For more details see the annex.....                              | 29 |
| Table 10 XPS results for NDs of 25 nm of median size (Microdiamant AG) – Spot 2. For more details see the annex.....                             | 29 |
| Table 11 XPS results for NDs of 25 nm of median size (Microdiamant AG) – Spot 3. For more details see the annex.....                             | 29 |
| Table 12 Summary of the peak fitting of carbon (1s) of all the 3 spots measured (NDs of 25 nm of median size, Microdiamant AG).....              | 30 |
| Table 13 Summary of the peak fitting of oxygen (1s) of all the 3 spots measured (NDs of 25 nm of median size, Microdiamant AG).....              | 30 |
| Table 14 DLS measurements related to aggregation in DMEM medium (using disposable sizing cuvettes).....  | 33 |
| Table 15 DLS measurements related to aggregation in DMEM medium (disposable folded capillary cells).....   | 33 |
| Table 16 Zeta potential measurements related to aggregation in DMEM medium .....   | 34 |
| Table 17 DLS measurements aiming at mitigating the aggregation behavior for practical use. ....  | 35 |
| Table 18 DLS measurements of ND aggregation in YMB .....   | 35 |
| Table 19 Element ratios for DMEM and YMB.....  | 36 |
| Table 20 XPS results for NDs of 25 nm of median size (Microdiamant AG) in DMEM with 10% FBS ...  | 36 |
| Table 21 Atomic ratios for NDs of 25 nm of median size (Microdiamant AG) in DMEM with 10% FBS without carbon and oxygen taken into account. .... | 37 |
| Table 22 XPS results for NDs of 25 nm of median size (Microdiamant AG) in DMEM without FBS .....   | 38 |
| Table 23 Atomic ratios for NDs of 25 nm of median size (Microdiamant AG) in DMEM without FBS without carbon and oxygen taken into account. ....  | 38 |

## List of Tables

|   |     |
|---|-----|
| Table 24 XPS results for NDs of 25 nm of median size (Microdiamant AG) in YMB – Spot A .....  | 40  |
| Table 25 XPS results for NDs of 25 nm of median size (Microdiamant AG) in YMB – Spot B .....  | 40  |
| Table 26 XPS results for NDs of 25 nm of median size (Microdiamant AG) in YMB – Spot C .....  | 40  |
| Table 27 Overview of the number of proteins found .....   | 43  |
| Table 28 Most abundant proteins (*Ca-binding) .....   | 47  |
| Table 29 Overview of the magnitude of co-localization .....   | 49  |
| Table 30 Water blanks and ND standards (in DI water) measured with 0.2 s exposure time and 200 accumulations. ....  | 55  |
| Table 31 Water blanks and ND standards (in DI water) measured with 0.2 s exposure time and 500 accumulations. ....  | 56  |
| Table 32 Stability of the signal of cell lysate (spiked with ND). Parameters: 200 spectra accumulated, 0.2 seconds exposure time and an accumulate cycle time of 0.23374 s. ....                                      | 56  |
| Table 33 Stability of the signal of cell lysate (spiked with ND). Measurements were performed 5 times. Parameters: 750 spectra accumulated, 0.2 seconds exposure time and an accumulate cycle time of 0.23374 s. .... | 56  |
| Table 34 DMEM medium composition.....   | 63  |
| Table 35 Yeast medium base without amino acids (Formedium), YMB .....   | 64  |
| Table 36 Proteins identified in Sample 1.....   | 87  |
| Table 37 Redundant proteins identified in Sample 1.....   | 88  |
| Table 38 Proteins identified in Sample 2.....   | 88  |
| Table 39 Redundant proteins identified in Sample 2.....   | 89  |
| Table 40 Proteins identified in Sample 3.....   | 89  |
| Table 41 Redundant proteins identified in Sample 3.....   | 91  |
| Table 42 Proteins identified in Sample 4.....   | 92  |
| Table 43 Redundant proteins identified in Sample 4.....   | 94  |
| Table 44 Proteins identified in Sample 4.....   | 95  |
| Table 45 Redundant proteins identified in Sample 5.....   | 103 |

## 8. Acknowledgements

I would like to thank Prof. Lendl and Prof. Schirhagl for their supervision and encouraging to pursue my own ideas within the project. Also, I would like to thank all members of the group for the great working atmosphere: I would like to thank Simon R. Hemelaar and Mayeul Chipaux explicitly for the great discussions and close collaboration. Finally, thanks to Sona Guluzade and Melissa M. Rodriguez for the great cooperation.

Thanks to Prof. Browne for making measurements at his spectroscopy instruments possible. Furthermore I'd like to thank Marc Stuart for the excellent TEM training and Joop de Vries for his support with the XPS measurements.

I would like to thank Hjalmar Permentier and Marcel de Vries for the great discussions and help regarding the proteomics and mass spectroscopy.

Last but not least I would like to thank the Federation of Austrian Industries in Carinthia (Industriellenvereinigung Kärnten) for their financial support that made this work in Groningen possible.